

SYNTHESIS, MODIFICATION AND CHARACTERIZATION OF
SODALITES

116 212

A THESIS SUBMITTED TO
THE GRADUATE SCHOOL OF NATURAL AND APPLIED SCIENCES
OF
THE MIDDLE EAST TECHNICAL UNIVERSITY

BY

AYBAR CAN ACAR

IN PARTIAL FULFILLMENT OF THE REQUIREMENTS FOR THE DEGREE OF

MASTER OF SCIENCE

IN

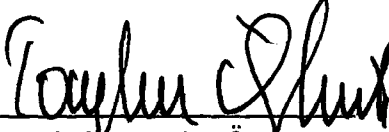
THE DEPARTMENT OF CHEMICAL ENGINEERING

July 2001


116212

T.C. YÜKSEKÖĞRETİM KURULU
DOKÜMANTASYON MERKEZİ


Approval of the Graduate School of Natural and Applied Sciences.



Prof. Dr. Tayfur Öztürk
Director

I certify that this thesis satisfies all the requirements as a thesis for the degree of Master of Science.


Prof. Dr. Timur Doğu
Head of Department

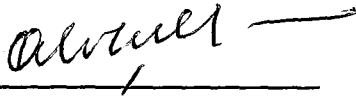
This is to certify that we have read this thesis and that in our opinion it is fully adequate, in scope and quality, as a thesis for the degree of Master of Science.


Prof. Dr. Hayrettin Yücel
Co-Supervisor

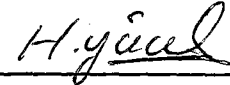

Prof. Dr. Ali Çulfaz
Supervisor

Examining Committee Members


Prof. Dr. Ali Çulfaz



Prof. Dr. Hayrettin Yücel




Prof. Dr. Güniz Gürüz



Prof. Dr. Müjgan Çulfaz



Prof. Dr. Timur Doğu



ABSTRACT

SYNTHESIS, MODIFICATION AND CHARACTERIZATION OF SODALITES

Acar, Aybar Can

M.Sc., Department of Chemical Engineering

Supervisor: Prof. Dr. Ali Çulfaz

Co-Supervisor: Prof. Dr. Hayrettin Yücel

July 2001, 118 pages

Aluminosilicate sodalites of three different types, chlorosodalite, basic sodalite and oxalate sodalite, have been synthesized in their sodium forms using hydrothermal synthesis. The syntheses were investigated in terms of their relative rates of crystallization and final crystallinities using powder X-ray diffraction. It was seen that the template species used in the synthesis determines both the rate and extent of crystallization. In this respect chloride ions seem to be the most effective templates.

These sodalites were subsequently loaded with silver by aqueous ion exchange. The exchange was studied primarily by monitoring the solution phase. Rate of exchange and equilibrium behavior have been established over the temperature range of 25 - 80°C for all three types. High selectivity toward silver over sodium was observed, with little dependence on temperature. It was seen that the occluded anion in sodalite affects the ion exchange rates and equilibria such that the amount of occlusion is inversely related to the selectivity towards silver and the rates are directly affected by cage sizes.

Both sodium and silver sodalites were characterized by powder diffraction and crystallographic data for silver sodalites have been derived using Rietveld refinement. Electron micrographs of sodalites have been used for investigations of crystallite morphology and size which were seen to be in the nanoscopic. Chemical and thermal analyses of the samples were performed in order to identify chemical composition and temperature stability. It was seen that the produced sodium sodalites essentially have an Al/Si ratio of unity and are stable up to 800 °C. Silver sodalites have been observed to manifest various optical properties including photochromic, barochromic, thermochromic and fluorescent behavior.

Keywords: chlorosodalite, basic sodalite, oxalate sodalite, hydrothermal synthesis, silver ion exchange

ÖZ

SODALİT SENTEZİ, MODİFİKASYONU VE KARAKTERİZASYONU

Acar, Aybar Can

Yüksek Lisans, Kimya Mühendisliği Bölümü

Tez Yöneticisi: Prof. Dr. Ali Çulfaz

Ortak Tez Yöneticisi: Prof. Dr. Hayrettin Yücel

Temmuz 2001, 118 sayfa

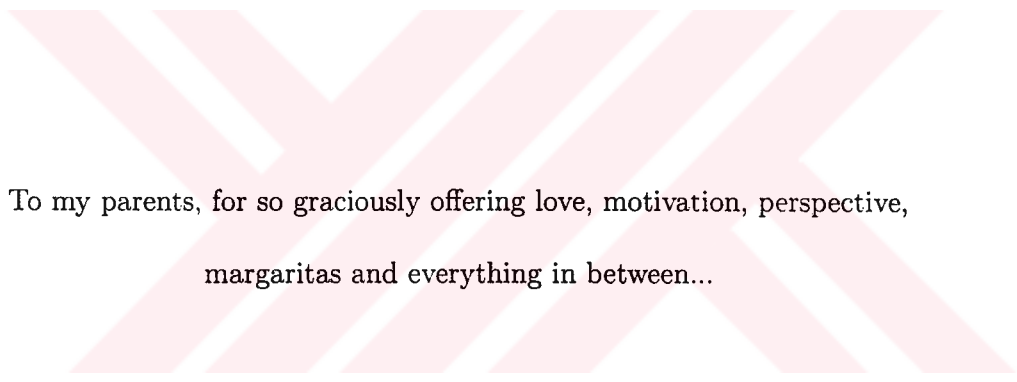
Hidrotermal sentez yöntemleri kullanılarak klorosodalit, hidroksisodalit ve oksalat sodalit olmak üzere üç çeşit sodalitin üretimi gerçekleştirilmiştir. Bu malzemelerin sentezi X-ışını kırınımı yöntemiyle görece kristalizasyon hızları ve nihayi kristaliniteleri açısından incelenmiştir. Kristalizasyon hızını ve miktarını sentezde kullanılan şablon bileşiğin belirlediği görülmüştür. Bu anlamda klorür iyonlarının en etkili şablonlar oldukları görülmektedir.

Üretilen sodalitelere çözeltide iyon değişimi yöntemiyle gümüş yüklenmiştir. İyon değişimi çözeltideki gümüş oranı izlenerek incelenmiştir. İyon değişim hızı ve iyon değişiminin 25 - 80 °C arasındaki denge davranışı bulunmuştur. Sodal-

itin gümüşe karşı sodyuma nazaran yüksek seçicilik gösterdiği ve bu seçiciliğin sıcaklığa fazla bağımlı olmadığı farkedilmiştir. Sodaliti dolduran anyonun iyon değişim hızlarını ve dengelerini etkilediği, seçiciliğin kafesin doluluk oranı arttıkça azaldığı, değişim hızının ise kafes boyları ile doğrudan alakalı olduğu görülmüştür.

Üretilen sodyum ve gümüş sodalitler X-ışını kırınımıyla karakterize edilmiş ve gümüş sodalitlerin kristal yapıları Rietveld yöntemi kullanılarak çözülmüştür. Kristal boyutu ve morfolojisini incelemek üzere sodalitlerin elektron mikrografları kullanılmış ve kristalitlerin nanoskopik olduğu görülmüştür. Örneklerin ısı kararlılıkları ve kimyasal bileşimlerinin anlaşılması için termal ve kimyasal analizler uygulanmıştır. Üretilen sodyum sodalitlerin Al/Si oranlarının bire eşit olduğu ve 800C'a kadar kararlı oldukları görülmüştür. Gümüş sodalitlerin fotokromik, barokromik, termokromik ve floresans olmak üzere çeşitli optik özellikler gösterdikleri göze çarpmaktadır.

Anahtar Kelimeler: klorosodalit, hidroksisodalit, oksalat sodalit, hidrotermal sentez, gümüş iyon değişimi



To my parents, for so graciously offering love, motivation, perspective,
margaritas and everything in between...

ACKNOWLEDGMENTS

I am deeply indebted to my supervisor Prof. Dr. Ali ulfaz for his insightful guidance and untiring diligence without which this thesis would not be possible. I would also like to thank my co-supervisor Prof. Dr. Hayrettin Yücel for the advice and material he has offered during my study.

I would like to thank Dr. Halil Kalıpçılar for his invaluable help and orientation during the beginning of my research. I am grateful for the technical assistance provided by Kerime Güney and Mihrican Aıkgöz for the chemical and thermogravimetric analyses. I would also like to thank Assoc. Prof. Suna Balcı from Gazi University who arranged for the electron microscopy.

Finally I would like to express my heartfelt gratitude to Prof. Dr. Güniz Gürüz for introducing me to the chemical engineering profession and guiding me throughout my education of four years in this fine department, a time which I will always cherish...

TABLE OF CONTENTS

ABSTRACT	iii
ÖZ	v
DEDICATON	vii
ACKNOWLEDGMENTS	viii
TABLE OF CONTENTS	ix
LIST OF TABLES	xii
LIST OF FIGURES	xiv
LIST OF SYMBOLS	xvi
CHAPTER	
1 INTRODUCTION	1
1.1 Introduction to Zeolites and Sodalite	1
1.2 Aims and Scope of the Research	4
2 THEORETICAL BACKGROUND	5
2.1 Sodalite Structure and Synthesis	5
2.1.1 Structure of the Sodalite Framework	6
2.1.2 Variants of Sodalite Based on Occluded Species	8
2.1.3 Synthesis of Sodalite	12
2.2 Ion Exchange	14
2.2.1 Ion Exchange Basics and Ion Exchange in Zeolites	14
2.2.2 Na-Ag Ion Exchange on Sodalite	17
2.3 X-ray Diffraction Analysis	19
2.3.1 The Basics of X-ray Diffraction	19

3	EXPERIMENTAL	22
3.1	Synthesis	22
3.1.1	Batch Composition Selection	22
3.1.2	Batch Preparation	24
3.1.3	Crystallization	25
3.1.4	Recovery of the Solid Product	26
3.2	Ion Exchange	26
3.2.1	Ion Exchange	26
3.3	Characterization of Solids	28
3.3.1	Characterization by XRD	28
3.3.2	Structure Determination by XRD Powder Diffraction	29
3.3.3	Other Methods	31
4	RESULTS	33
4.1	Syntheses of Sodium Sodalites	33
4.1.1	Synthesis of Sodium Chlorosodalite	33
4.1.1.1	Crystallization	33
4.1.1.2	Characterization	35
4.1.2	Synthesis of Sodium Basic Sodalite	39
4.1.2.1	Crystallization	39
4.1.2.2	Characterization	44
4.1.3	Synthesis of Sodium Oxalate Sodalite	46
4.1.3.1	Crystallization	46
4.1.3.2	Characterization	48
4.2	Modification of Sodalites	50
4.2.1	Ion Exchange Rates	50
4.2.2	Ion Exchange Equilibria	52
4.3	Characterization of Solids	58
4.3.0.1	XRD Structure Determination of Silver Sodalites	58
4.3.0.2	Microscopic Analyses	63

5	DISCUSSIONS	64
5.1	The Effect of Guest Species on Nucleation and Crystallization	64
5.2	Ion Exchange Behavior of Sodalite with respect to Guest Species	69
5.3	Optical Properties Observed in Silver Sodalites	70
6	CONCLUSION	73
	REFERENCES	74
	APPENDICES	78
A	Synthesis Calculations	78
A.1	Synthesis Details	78
A.2	Yield Calculations	80
A.3	Miscellaneous Analysis Results for Sodium Sodalites	81
	A.3.0.3 Thermal Gravimetric Analysis	82
	A.3.0.4 Scanning Electron Micrographs	85
B	Ion Exchange Calculations	88
B.1	Estimation of Mean Ionic Activities	88
B.2	Silver Determination in Solution	89
B.3	Experimental Data and Intermediate Calculations	90
B.4	Kielland Plots for Sodalite	97
B.5	Miscellaneous Analysis Results for Silver Sodalites	99
	B.5.0.5 Thermal Gravimetric Analysis	99
	B.5.0.6 Scanning Electron Micrographs	102
C	X-Ray Diffraction and Structure Determination Calculations	105
C.1	Crystallinity Measurements	105
C.2	High Temperature Decomposition of Sodalites	110
C.3	XRD Structure Determination	113
	C.3.0.7 Calculation of Framework Oxygen Locations using Cell Edge	113
C.4	PDF Files	116
C.5	Peak Listings	118

LIST OF TABLES

2.1	Formulae and Unit Cell Edges of Sodalite Variants	10
3.1	Batch Compositions used in Synthesis	24
3.2	Hydrothermal Synthesis Conditions	25
3.3	XRD Scan Conditions	28
3.4	Conditions used in TGA Analyses	32
4.1	Yield and Conversion Results for Sodium Chlorosodalite	37
4.2	Yield and Conversion Results for Sodium Basic Sodalite	42
4.3	Yield and Conversion Results for Sodium Oxalate Sodalite	48
4.4	Formulae of Sodium and Silver Sodalites	50
4.5	Cation Exchange Capacities of Sodalites	52
4.6	Equilibrium Constants and Standard Free Energies for Sodium-Silver Ion Exchange in Sodalite	53
4.7	Framework Data for Silver Sodalites	60
A.1	List of Samples Produced	78
A.2	Chemical Composition of Sodium Chlorosodalite	81
A.3	Chemical Composition of Sodium Basic Sodalite	81
A.4	Chemical Composition of Sodium Oxalate Sodalite	81
B.1	Values of Debye-Hückel Parameters at Relevant Temperatures	88
B.2	Calculated Mean Ionic Activity Coefficients	89
B.3	Experimental Data and Intermediate Calculations for Chlorosodalite Isotherm at 25°C	92
B.4	Experimental Data and Intermediate Calculations for Chlorosodalite Isotherm at 50°C	92
B.5	Experimental Data and Intermediate Calculations for Chlorosodalite Isotherm at 80°C	93
B.6	Experimental Data and Intermediate Calculations for Basic Sodalite Isotherm at 25°C	93
B.7	Experimental Data and Intermediate Calculations for Basic Sodalite Isotherm at 50°C	94
B.8	Experimental Data and Intermediate Calculations for Basic Sodalite Isotherm at 80°C	94
B.9	Experimental Data and Intermediate Calculations for Oxalate Sodalite Isotherm at 25°C	95

B.10 Experimental Data and Intermediate Calculations for Oxalate Sodalite Isotherm at 50°C	95
B.11 Experimental Data and Intermediate Calculations for Oxalate Sodalite Isotherm at 80°C	96
B.12 Integration Results for Kielland Plots	97
C.1 Variation of Framework Oxygen Locations with Cell Edge	114
C.2 Peak Listing for Silver Chlorosodalite	118
C.3 Peak Listing for Silver Basic Sodalite	119



LIST OF FIGURES

2.1	The Outline of the Sodalite Framework.	6
2.2	Ball and Stick Models of the β -cage	7
2.3	Ball and Stick Model of Na,Cl-SOD Unit Cell (proj. [101])	11
2.4	Sample XRD Powder Pattern with Perfect Peaks and no Noise	20
4.1	Crystallization of Sodium Chlorosodalite over Time	38
4.2	Comparison of the Synthesized Sodium Chlorosodalite with Reference Pattern	40
4.3	SEM Picture of Sodium Chlorosodalite at x6000 Magnification	41
4.4	Comparison of XRD Scans of Sodium Basic Sodalite at 95 and 130°C	41
4.5	Crystallization of Sodium Basic Sodalite over Time	43
4.6	Comparison of the Synthesized Sodium Basic Sodalite with Reference Pattern	45
4.7	SEM Picture of Sodium Basic Sodalite at x6000 Magnification	46
4.8	Comparison of XRD Scans of Sodium Oxalate Sodalite at 130 and 170°C	47
4.9	SEM Picture of Sodium Oxalate Sodalite at x6000 Magnification	49
4.10	Sodium-Silver Ion Exchange Rates of Sodalites at 25°C	51
4.11	Na-Ag Ion Exchange Isotherms for Sodalites at 25°C	54
4.12	Na-Ag Ion Exchange Isotherms for Sodalites at 50°C	55
4.13	Na-Ag Ion Exchange Isotherms for Sodalites at 80°C	56
4.14	Kielland Plots for Sodalites at 25°C	57
4.15	Comparison of XRD Scan of Silver Chlorosodalites to Calculated Pattern	61
4.16	Comparison of XRD Scan of Silver Basic Sodalite to Calculated Pattern	62
5.1	High Temperature Conversion of Oxalate Sodalite to Basic Sodalite	68
5.2	Variation of Sodalite Na-Ag Exchange Equilibrium Constants with Temperature	71
A.1	Flowchart of Synthesis Procedure	79
A.2	TGA Scan of Sodium Chlorosodalite	82
A.3	TGA Scan of Sodium Basic Sodalite	83
A.4	TGA Scan of Sodium Oxalate Sodalite	84
A.5	SEM Images of Sodium Chlorosodalite	85
A.6	SEM Images of Sodium Basic Sodalite	86
A.7	SEM Images of Sodium Oxalate Sodalite	87

B.1	Kielland Plots for Sodalites at 25°C	97
B.2	Kielland Plots for Sodalites at 50°C	98
B.3	Kielland Plots for Sodalites at 80°C	98
B.4	TGA Scan of Silver Chlorosodalite	99
B.5	TGA Scan of Silver Basic Sodalite	100
B.6	TGA Scan of Silver Oxalate Sodalite	101
B.7	SEM Images of Silver Chlorosodalite	102
B.8	SEM Images of Silver Basic Sodalite	103
B.9	SEM Images of Silver Oxalate Sodalite	104
C.1	XRD Patterns of Crystallinity References for Chlorosodalite	106
C.2	Crystallinity Index versus Integrated Peak Intensities for Chlorosodalite	107
C.3	XRD Patterns of Crystallinity References for Basic Sodalite	108
C.4	Crystallinity Index versus Integrated Peak Intensities for Basic Sodalite	109
C.5	High Temperature Decomposition Behavior of Chlorosodalite	110
C.6	High Temperature Decomposition Behavior of Basic Sodalite	111
C.7	High Temperature Decomposition Behavior of Oxalate Sodalite	112
C.8	Flowchart for Crystal Structure Determination Procedure	115
C.9	PDF File for Sodium Chlorosodalite	116
C.10	PDF File for Sodium Basic Sodalite	117

LIST OF SYMBOLS

a	Unit cell edge (Å); Debye-Hückel parameter	α	Separation factor
A_S	Fractional equivalent concentration of silver in the solution phase	β	Debye-Hückel ionic radius parameter
A_Z	Fractional equivalent concentration of silver in the zeolite phase	$\gamma_{\pm iX}$	Mean ionic activity coefficient of species i
c	XRD pattern scaling factor	λ	X-ray wavelength (Å)
d	Interatomic plane spacing (/AA)	μ	Ionic strength of solution (mol/L)
F(hkl)	Structure factor for plane hkl	2θ	Bragg angle, degrees
ΔG°	Standard free energy of exchange (kJ/mol)		
K_a	Thermodynamic equilibrium constant		
K_N^A	Rational selectivity		
$K_N'^A$	Corrected rational selectivity		
N_S	Fractional equivalent concentration of sodium in the solution phase		
N_Z	Fractional equivalent concentration of sodium in the zeolite phase		
R_{wp}	Rietveld refinement goodness of fit		
w_i	weighting factor at point i of XRD pattern		
$Y_i(\text{calc})$	Calculated XRD pattern intensity at point i		
$Y_i(\text{obs})$	Observed XRD pattern intensity at point i		
Z_i, z_i	Charge of cation i		

CHAPTER 1

INTRODUCTION

1.1 Introduction to Zeolites and Sodalite

Zeolites are defined as aluminosilicate framework minerals of alkali and alkaline earth elements. They are formed of SiO_4 and AlO_4 tetrahedra linked through shared oxygens. The open framework structures thus formed in zeolites contain nanoscopic channels and cavities in which cations and water molecules may reside. The existence of these channel and cavity structures within zeolite crystals provide a host of unique and useful features to be exploited by today's scientists and engineers.

Zeolites are hence used in a variety of applications involving primarily separations. The physical aspects of the cavities may be employed in sieving or adsorbing certain molecules based upon size, and the cation holding zeolites may be employed as ion exchangers and water softeners. Also, the structure restricting

characteristics of zeolites are useful in engineering catalysts which provide high selectivity by sieving the desired reactants and/or products.

The strict definition of zeolites dictates that the aluminosilicate framework may contain cations to balance the negative charge of the framework and occluded water exclusively. There are however certain variants which contain anions within the cavities with the additional cations to negate the charge of the anion itself. Such materials have been called *feldspathoids*. These materials therefore have whole salts included within their structure.

Sodalite is one such material. The natural form of sodalite contains sodium cations and chloride anions, hence sodium chloride salts occluded within its structure. Another form of sodalitic framework mineral contains polysulfides and is called *nosean*. Although not existent in natural reserves a true zeolite which is the analogue of sodalite can be synthesized artificially and is called *hydroxysodalite* or *basic sodalite*. Hydroxysodalite, accordingly, ideally only contains sodium cations and hydration.

The difference of sodalite from the scores of zeolites being synthesized and exploited commercially today is that its cavities are relatively small and are uniform¹. This aspect of sodalite renders it all but useless in terms of the conventional applications of zeolites since the size and variety of the cavities provide means for the diffusion of species within the crystal which allows effects like sieving and catalysis to take place.

¹ Most zeolites such as zeolite A have two or more types of cavities which coexist within a unit cell whereas sodalite has only one type of cavity, namely the β -Cage

However, it is the same set of properties that make sodalite a valuable host material for applications where the guest species have to be immobilized within an inert framework. One example of such an application is waste storage and disposal, where leaching of the stored chemical from the holding medium is undesirable, especially if the waste in question is radioactive.

Another set of applications for sodalite involves trapping optically or electronically active chemical structures within the cavities. When hosted by the restrictive framework of sodalite such chemicals are utilized in ways not possible in their bulk forms.

The application of interest for this research thesis is based on trapping compounds of silver such as silver halides into the sodalite framework. Where this is accomplished, the light sensitive aspects of silver compounds may be still exploited, however with certain advantages.

First of all, since each cage will contain a single molecule of the compound, the resolution apparent in sodalite based optical recording media will be significantly higher than emulsion-based media, where grain sizes are the controlling dimensional constraint. Additionally, it will not be possible for the compounds to diffuse from cage to cage, therefore longevity of the recording medium and spatial certainty at the nanometer level is accomplished. Finally, compounds which are hazardous in bulk form but have promising optical properties, such as silver oxalate, can be utilized since their exposure to the environment is prevented when hosted by sodalite.

Therefore, sodalite as a hosting material is researched in terms of its synthesis and modification along with the characterization of the obtained products.

1.2 Aims and Scope of the Research

The research which is the embodiment of this thesis can be divided into three sections, synthesis, modification and characterization.

The syntheses of three forms of sodalite; sodium chloride sodalite, hydroxysodalite and sodium oxalate are to be carried out with the conventional hydrothermal methods. The crystallization rates and extents of the products are to be evaluated with respect to crystallization times and temperatures along with the phase purities.

These sodalites are to be further modified by replacing the sodium cations within the structure with silver cations, using aqueous ion exchange. The equilibrium characteristics of sodalite for the sodium-silver exchange is to be determined. The rate of exchange is also to be studied.

The solid products, both as synthesized and modified, are to be characterized in terms of their crystallinities, morphologies, chemical make-up, thermal behavior and crystallographic properties.

CHAPTER 2

THEORETICAL BACKGROUND

2.1 Sodalite Structure and Synthesis

Sodalite is a naturally occurring mineral as well as an artificial product. The natural forms of sodalite which contain occluded polysulphide¹ have been used over the centuries as pigments due to their long lasting blue-green color, the pigment being called *ultramarine*. Appropriately, the first synthesis of sodalite was done by J. B. Guimet in the beginning of the 19th century in order to obtain the previously very expensive ultramarine pigment artificially[1].

As zeolite technology started booming after the 1950's ([2] p.1) sodalite synthesis was studied but was far overshadowed by the efforts on zeolites like zeolite A, faujasite and the ZSM series sieves.

It would be worthwhile to examine the structural aspects of sodalite and the methods by which its synthesis is possible.

¹ Polysulphide containing sodalite analogues are called by various names, such as Nosean and Lazurite. However the historically valuable pigment ultramarine is obtained from the gem *Lapis Lazuli*, which is the mixture of (Calcium,Sodium Sulfate)Sodalite and Pyrite, originally found exclusively in Afghanistan and later mined in Colorado.

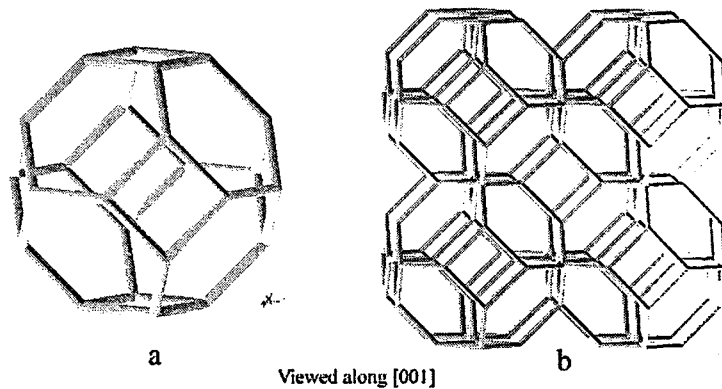


Figure 2.1: The Outline of the Sodalite Framework.
 (a) Single β -cage (b) β -cages stacked

2.1.1 Structure of the Sodalite Framework

Geologically speaking sodalite is a tectosilicate of the feldspathoid group[3]. In chemical terms sodalite is an framework aluminosilicate of perfectly periodic array of space filling polyhedra. The polyhedra are cubo-octahedrons called β -cages. The outline of the β -cage along with how these polyhedra are stacked can be seen in Fig. 2.1².

Each β -cage is composed of SiO_4 and AlO_4 tetrahedra connected to each other through shared oxygen atoms. The β -cages in the sodalite structure can be of different sizes. This size variation is due to the fact that sodalite 'tailors' itself to the possible guest species and also predictably due to temperature differences. The mechanism by which this resizing occurs is interesting.

When analyzing the structure of β -cages it is assumed that the metal-to-oxygen bonds are constant in length and this is shown to be true within observable limits [4]. But if the bond lengths are assumed constant the size of the cages

² Note that when eight β -cages are stacked as shown the intermediate cavity is also a β -cage

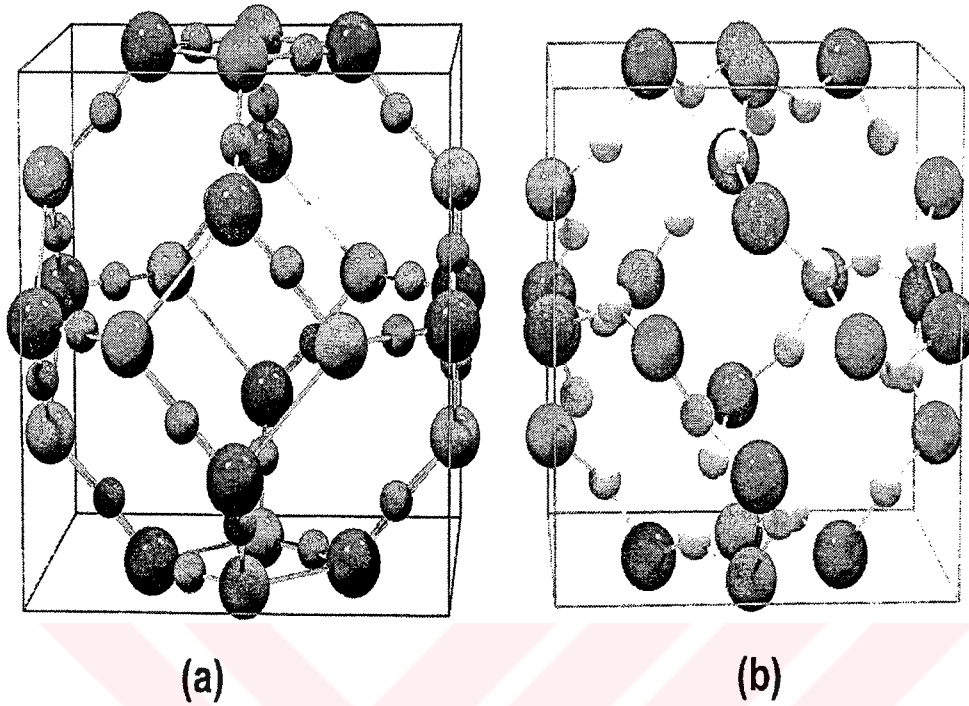


Figure 2.2: Ball and Stick Models of the β -cage
 (a) Ideal (b) Semi-collapsed

should also be constant. The answer lies in the fact that the β -cages are actually semi-collapsed. By this it is meant that the metal atoms do not connect over straight lines as shown in the outlines. The T-O-T angles are such that the β -cage in reality is 'crumpled'. Figure 2.2 illustrates the collapsed structure in contrast to the to ideal β -cage.

It is due to this collapsibility that the size of the β -cage, hence the unit cell edge, can not be easily established for a given temperature. However, a range can be given. Hassan and Grundy have calculated this range as lying between 8.141 and 9.317 Å[4]. The sodalite crystal can be defined with a primitive cubic unit cell, with space group space group is $P\bar{4}3n$

The general chemical formula of the sodalite cage may be given as $M_6[SiAlO_4]_6 \cdot nH_2O$. As can be seen from this formula the aluminosilicate framework itself is negatively charged with a charge of -6 and this is balanced by six univalent cations distributed within the structure.

The charge of the framework is variable and dependent on the Si/Al ratio of the crystal. By *Lowenstein's Principle* the minimum possible ratio is unity. Since AlO_4 tetrahedra may only connect to SiO_4 tetrahedra, there must be at least equal amounts of silicon and aluminium atoms within a framework [5]. However, the converse is not true. The Si/Al ratio for sodalite may approach infinity, resulting in a framework of the form $[SiO_2]_{12}$. Such purely siliceous forms are termed *silica sodalites*.

Silica sodalites belong to the group of clathrasils and their frameworks are electrically neutral. Due to this neutrality, silica sodalites, like other silica zeolites, lack the inter-framework cations and thus are incapable of certain chemical interactions such as ion exchange and most catalytic operations.

2.1.2 Variants of Sodalite Based on Occluded Species

Thus far the term sodalite has been used as an ambiguous descriptor for the framework explained above. The sodalite framework may host various guests and the properties of the final material are significantly dependent upon these guests or lack thereof.

The three primary classes of sodalite, classified with respect to their inclusions and framework charges are:

Basic Sodalite $M_6[\text{SiAlO}_4]_6 \cdot n\text{H}_2\text{O}$

Salt Occluded Sodalite $M_{6+x}[\text{SiAlO}_4]_6 A_x \cdot n\text{H}_2\text{O}$

Silica Sodalite $[\text{SiO}_2]_{12}$

where M denotes a univalent cation and A denotes a univalent anion.

Of these silica sodalite and basic sodalite have already been treated in the above section. Basic sodalite is a true zeolite in that it contains only cations and water within the framework. Basic and silica sodalites are exclusively artificial forms and neither form has ever been found in natural reserves.

The remaining type is the salt occluded sodalite class. This is the natural form of sodalite as a feldspathoid. Starting with basic sodalite, if anions were introduced into the framework each anion would locate itself within a β -cage and increase the negative charge of the cage by an amount equal to its charge. Therefore to balance the structure, additional cations would have to be introduced into the framework. In total since an anion and its respective cations are added to the framework, it is said that the framework now includes a salt.

For univalent anions and cations, each cage will hold the anion and an extra cation. For bivalent anions every other cage will hold an anion and every cage will hold a cation and so forth. A salt occluded sodalite for which every cage holds an anion would hence have the formula $M_8[\text{SiAlO}_4]_6 A_2 \cdot n\text{H}_2\text{O}$ as each formula unit describes two cages.

As a representative example sodium chloride sodalite, which is the primary form of natural sodalite, may be examined. In accordance with the above, the formula for this mineral is $\text{Na}_8[\text{SiAlO}_4]_6\text{Cl}_2$. In sodium chloride sodalite, hereafter referred to as Na,Cl-SOD, each cage holds one chloride anion at the center of symmetry of the cage. There are four sodium cations in the cage and these cations are fourfold coordinated to the chloride and three closest oxygens in the framework. The sodium cations hence occupy positions at the entrance of the hexagonal entrances of the cage. The positioning is detailed in Fig 2.3.

The distance of the cations from the anion, the distance of the cations from the framework and the size of the total unit cell all depend on the nature of the ions. Table 2.1 gives a summary of various sodalites.

Table 2.1: Formulae and Unit Cell Edges of Sodalite Variants

Type	Formula	U.C. Edge (Å)
Na,Cl-SOD	$\text{Na}_8[\text{SiAlO}_4]_6\text{Cl}_2$	8.882
Na,Br-SOD	$\text{Na}_8[\text{SiAlO}_4]_6\text{Br}_2$	8.931
Na,I-SOD	$\text{Na}_8[\text{SiAlO}_4]_6\text{I}_2$	9.008
Na,OH-SOD	$\text{Na}_8[\text{SiAlO}_4]_6\text{OH}_2$	8.734
Ag,Cl-SOD	$\text{Ag}_8[\text{SiAlO}_4]_6\text{Cl}_2$	8.871
Ag,Br-SOD	$\text{Ag}_8[\text{SiAlO}_4]_6\text{Br}_2$	8.911
Ag,I-SOD	$\text{Ag}_8[\text{SiAlO}_4]_6\text{I}_2$	8.952
Li,F-SOD	$\text{Li}_8[\text{SiAlO}_4]_6\text{F}_2$	8.141
Li,Cl-SOD	$\text{Li}_8[\text{SiAlO}_4]_6\text{Cl}_2$	8.447
Basic SOD	$\text{Na}_6[\text{SiAlO}_4]_6 \cdot 8\text{H}_2\text{O}$	8.848
Basic SOD(dehyd)	$\text{Na}_6[\text{SiAlO}_4]_6$	9.122

Compiled from [4, 6, 7, 8]

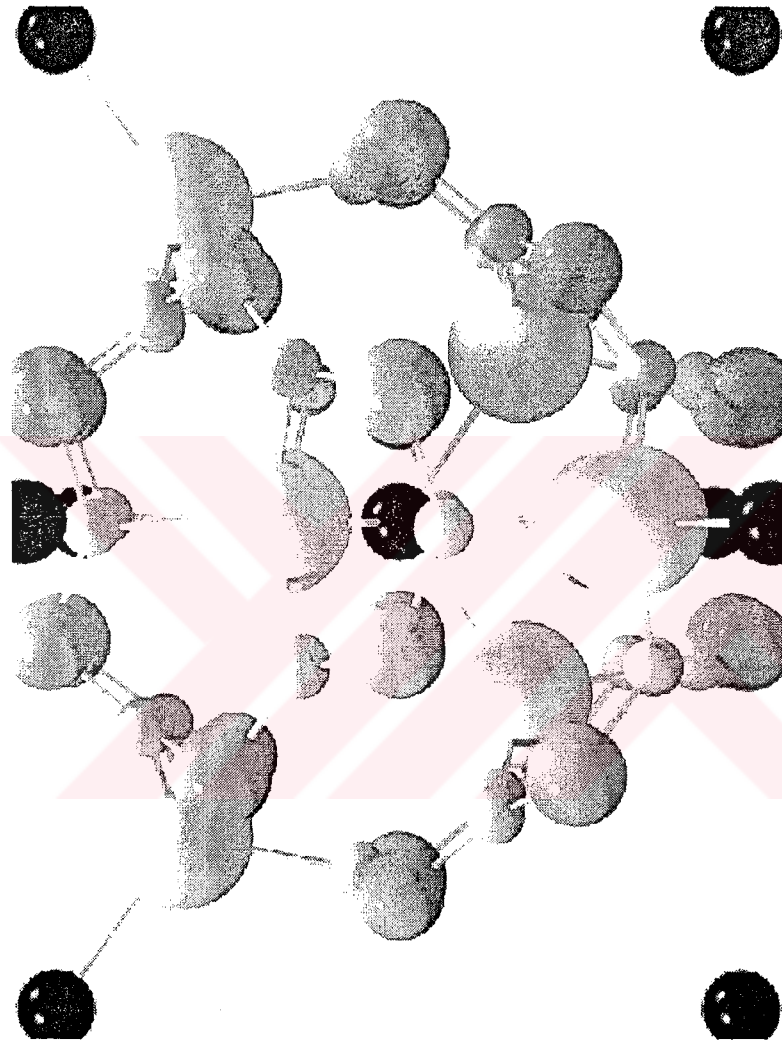


Figure 2.3: Ball and Stick Model of Na,Cl-SOD Unit Cell (proj. [101])
The black balls represent chloride ions and the large white balls are sodium ions

2.1.3 Synthesis of Sodalite

The synthesis of sodalite was initially performed using a solid state synthesis method where artificial ultramarine was synthesized by heating in a closed-fire clay furnace, a finely ground mixture of China clay, soda ash, coal or wood, charcoal, silica and sulfur[1].

Later, especially during the last half of the 20th century several groups have been issued patents detailing the synthesis sodalite by various solid state methods in order to obtain end products for use as cathode ray tube coatings and waste retention materials [9, 10, 11, 12].

Solid state synthesis methods, due to their high temperature and/or high pressure operating conditions, are generally less specific about the product obtained. As was reported by several of the above works, there are invariably some phase impurities, non-sodalitic phases which form. For the purposes of applications such as those above, the phase purity has high tolerance and accompanying phases are more or less inconsequential. However, for this study solid state synthesis was not considered due to its resource intensive nature and said shortcomings.

The second way of synthesis is the hydrothermal method. Hydrothermal synthesis enables one to establish the outcome of the synthesis more specifically, and can be carried out under low temperatures. Hydrothermal syntheses of sodalite are reported in the literature with a multitude of variations.

According to Breck ([2] p.269) initial syntheses of basic sodalite were carried out by Barrer and White. Barrer and Cole [13] detail this synthesis as a straightforward addition of kaolinite to a hot aqueous sodium hydroxide solution

and subsequent crystallization under autogenous pressure at 80°C which results in basic sodalite. In this work, by adding incremental amounts of different salts (NaCl, NaBr, NaClO₃⁻, NaClO₄⁻) they have thereby obtained halosodalites.

Sodalites vary in their chemical nature primarily according to the Si/Al ratio. Naturally occurring sodalites have an Si/Al ratio of unity. As dictated by the Lowenstein Principle this is the lowest possible ratio for any aluminosilicate framework. This extreme seems to be the preferred chemical composition of the system. Synthesis has been reported to be highly dependent on the amount of aluminium and this is usually the limiting reagent [14]. Pure silica sodalites have been produced by utilizing organic templates [15] and accordingly any Si/Al ratio from unity to infinity is possible for sodalite synthesis. However, as the aluminium content in the material decreases so does the framework charge.

The charge in the framework is important for the activity of the final material. Cation exchange capacity and most chemical aspects of the sodalite are directly dependent on the framework charge, and hence the aluminium content. All the sodalites produced in this study have been prepared with a Si/Al ratio of unity.

In hydrothermal synthesis, especially when done at low temperatures and accordingly low pressures, the crystallite sizes are generally small. Nanometer sized sodalite crystals have been synthesized by Schoeman et al. [16] by using highly dilute batches.

Millimeter sized crystals have been achieved by Tsuyoshi et al. [17] by employing temperatures in the excess of 600°C in gold lined autoclaves and have used both spontaneous and seeded nucleation. Buhl and Löns [18] have likewise

achieved crystals of nitrite sodalites with a size of a tenth of a millimeter, using silver lined autoclaves at up to 500°C, albeit with some cancrinite impurities.

Use of such extreme conditions seems compulsory to achieve large crystals. However, when smaller crystals prove no problem, as is the case with this study, sodalite may be produced much easily. Breck ([2] p.270) gives ternary ($\text{Na}_2\text{O} - \text{Al}_2\text{O}_3 - \text{SiO}_2$) compositional diagrams for the synthesis of basic sodalite at 100°C in which basic sodalite crystallizes in a large range compositions. Alternatively, a rather generalized 'recipe' for the synthesis of various sodalites are given by Stein in the International Zeolite Association's Verified Syntheses Compilation [19] which is performed at 95°C and produces crystals between 50-500nm.

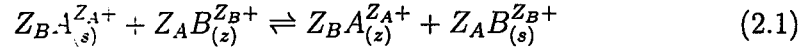
2.2 Ion Exchange

2.2.1 Ion Exchange Basics and Ion Exchange in Zeolites

Ion exchange is defined as a reversible chemical reaction wherein an ion from solution is exchanged for a similarly charged ion attached to an immobile solid particle.

These solid ion exchange particles are either inorganic materials such as clays and zeolites or synthetically produced organic resins. The resins are predominant in today's industry, however zeolites continue to hold attention since their greater stability allows them to be used in less hospitable environments. Additionally, apart from the separations point of view, the exchanged forms of zeolites themselves also attract interest as novel materials.

Ion exchange proceeds with the general reaction given below:



where A and B are competing cations, Z_A and Z_B are their respective charges and subscripts (z) and (s) denote the solid (i.e. zeolite) and solution phases respectively.

The ion exchange equilibrium is evaluated over an ion exchange isotherm, which is a plot of the zeolite vs. solution concentrations of one of the competing ions at constant temperature and total normality. For convenience in observing closure and for ease of expression, fractional equivalent concentrations are generally used in literature [20]. Ion exchange isotherms are therefore constructed by plotting the fractional equivalent concentration of the entering cation in solution against the fractional equivalent concentration of the same cation in the zeolite. The fractional equivalent concentration of the cation A^{Z_A+} is:

$$A_s = \frac{Z_A m_A}{Z_A m_A + Z_B m_B} \quad (2.2)$$

where $m_{A,B}$ are the concentrations of the ions in (mol/L). The fractional equivalent concentration of the same ion in the zeolite would be represented in terms of the cation exchange capacity of the zeolite:

$$A_z = \frac{Z_A M_A}{Q} \quad (2.3)$$

where M_A is the concentration of A^{Z_A+} in (mol/kg) and Q is the cation exchange capacity of the zeolite in number of charges per kg. The fractional equivalent

concentrations at each phase are dependent on each other due to the material balance, such that;

$$A_s + B_s = 1 \quad (2.4)$$

$$A_z + B_z = 1 \quad (2.5)$$

Therefore, isotherms may be plotted using the concentrations of a single ion only. The separation factor may be evaluated using the following equation:

$$\alpha = \frac{Z_A A_z B_s}{Z_B B_z A_s} \quad (2.6)$$

Note that α is dependent on concentration as well as temperature for real systems.

The conditions for selectivity with respect to α are:

$\alpha > (Z_A/Z_B)$: zeolite selective to A^{Z_A+}

$\alpha = (Z_A/Z_B)$: no preference

$\alpha < (Z_A/Z_B)$: zeolite selective to B^{Z_B+}

The rational selectivity coefficient ([2] pp. 532 - 533) is defined as:

$$K_B^A \equiv \frac{A_z^{Z_B} B_s^{Z_A}}{B_z^{Z_A} A_s^{Z_B}} \quad (2.7)$$

This coefficient is further elaborated to contain the mean ionic activity coefficients, yielding the corrected selectivity coefficient:

$$K_B'^A \equiv K_B^A \frac{[\gamma_{\pm BX}^{(Z_B+1)}]^{Z_A}}{[\gamma_{\pm AX}^{(Z_A+1)}]^{Z_B}} \quad (2.8)$$

where $\gamma_{\pm AX}$ and $\gamma_{\pm BX}$ are the mean ionic activity coefficients of the electrolytes.

X being the common anion in solution.

The thermodynamic equilibrium constant K_a is related to $K'_B{}^A$ through the relation:

$$K_a \equiv K'_B{}^A \frac{f_{A(z)}^{Z_B}}{f_{B(z)}^{Z_A}} \quad (2.9)$$

where $f_{A(z)}$ and $f_{B(z)}$ are the activity coefficients of the ions in the zeolite. In order to evaluate this activity correction the Gibbs-Duhem equation is employed. With the assumptions that total solution concentration is smaller than 1 M and that water activity terms are negligible, Dyer et al. [20] report that the evaluation of the Gibbs-Duhem equation yields:

$$\log K_a = (Z_B - Z_A) + \int_0^1 \log K'_B{}^A dA_Z \quad (2.10)$$

Thus, the thermodynamic equilibrium constant may be evaluated. This usually done by plotting $\log K'_B{}^A$ against A_Z and integrating the area under the curve. Such plots are called *Kielland* plots. From there on the standard free energy of exchange may be calculated by:

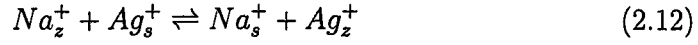
$$\Delta G^\circ = -(RT \ln K_a) \quad (2.11)$$

This being the general treatment, several simplifications may be used for the case of this study.

2.2.2 Na-Ag Ion Exchange on Sodalite

First of all, since sodium and silver are the cations of interest the exchange becomes a uni-univalent exchange. For the remainder of the text cation 'A' from

above will be redesignated as 'A' for Ag, and cation 'B' as 'N' for Na. As both sodium and silver are +1 charged the scheme given in the preceding section simplifies dramatically. The reaction 2.1 simplifies as:



Therefore the fractional equivalent concentrations in equations 2.2, 2.3, 2.4 and 2.5 become respectively:

$$A_s = \frac{m_A}{m_A + m_N} \quad (2.13)$$

$$A_z = \frac{M_A}{Q} \quad (2.14)$$

$$A_s + N_s = 1 \quad (2.15)$$

$$A_z + N_z = 1 \quad (2.16)$$

The corrected selectivity coefficient defined in equation 2.8 becomes:

$$K_B'^A \equiv K_B^A \frac{[\gamma_{\pm BX}]^2}{[\gamma_{\pm AX}]^2} \quad (2.17)$$

In this case, since the exponents of the ionic activities are the same, the system becomes almost independent of ionic strength. The ratio of activities itself can be assumed to be equal to unity ([2] p.535). This has been verified by calculation using the modified Debye-Hückel relation [21] in Appendix B.1. Consequently, the corrected selectivity coefficient is necessarily equal to the selectivity (Eqn. 2.7 which itself becomes:

$$K_N^A = \frac{A_z N_s}{N_z A_s} \quad (2.18)$$

Hence the thermodynamic equilibrium constant may be evaluated using:

$$\log K_a = \int_0^1 \log K_N^A dA_z \quad (2.19)$$

The treatment of ion exchange equilibria on sodalite thus becomes possible without engaging in complicated calculations.

2.3 X-ray Diffraction Analysis

Powder X-ray diffraction is used to investigate the crystallographic structures of the solid products produced and to identify crystalline phases which are otherwise equivalent in terms of chemical composition and physical properties.

2.3.1 The Basics of X-ray Diffraction

Interatomic distances in crystalline materials are on the order of 1 Å. In order to analyze such distances X-ray radiation is used since the wavelength is compatible. The analysis itself is done by monitoring the interference of photons scattered from different atomic planes. The beam is directed at an angle to the surface of a powder sample. The photons scattered from two points on a crystal lattice and arriving at an observation point lying at relative infinity will manifest interference according to their path differences, thereby affecting the total intensity recorded at the observation point. By varying the angle of incidence for the beam one may capture scattered photons from necessarily all the two-atom combinations within a crystal, or rather between all atomic planes since the structure is a repeating one.

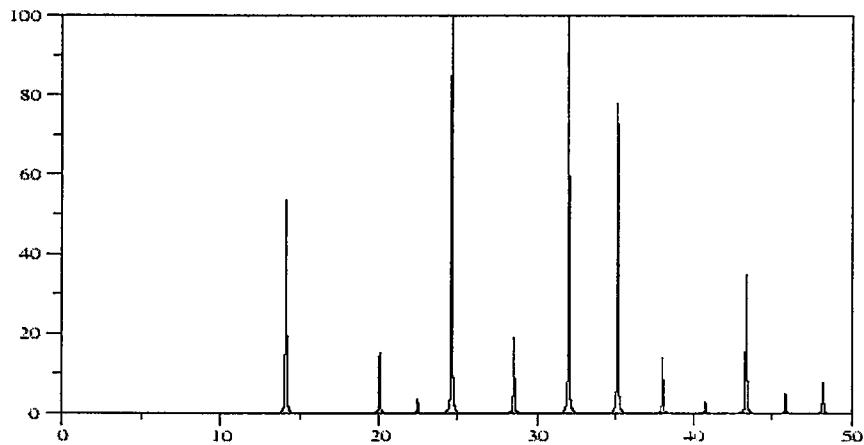


Figure 2.4: Sample XRD Powder Pattern with Perfect Peaks and no Noise

The relation that relates the interatomic distance between two scattering atoms to the angle of incidence is the *Bragg Equation*:

$$2d_{hkl} \sin \theta = n\lambda \quad (2.20)$$

which relates the distance between two planes of index $[hkl]$ to the angle of incidence as a function of beam wavelength λ .

The XRD diffraction pattern for a crystal, which is the plot of the intensity observed against the Bragg angle (2θ) usually acts as an unambiguous 'fingerprint' of the material and can therefore be compared to previously available XRD patterns. An idealized representative XRD pattern is given in Figure 2.4.

Real powder patterns generally incorporate noise and some background and the peaks are too broad to be attributed a single angle. Usually the background is fitted with a curve and purged from the pattern to compare the intensities of the peaks with common reference. Noise may be filtered by smoothing the data.

The peaks are attributed angles with tolerance, or the top of the peak is taken as the reference.

The peak intensities in sharp patterns may be evaluated directly from the height of the peak. When the peaks are broad, the area of the peaks are used as the intensity, in which case the area under the peak is evaluated.



CHAPTER 3

EXPERIMENTAL

3.1 Synthesis

In this study the sodium and silver forms of basic sodalite, chlorosodalite and oxalate sodalite have been studied. The syntheses of the sodium forms of these three sodalites have been carried out hydrothermally. Since only sodalites with a Si/Al ratio of unity have been produced, the synthesis is carried out in aqueous media and without any templates other than the salt desired in the final product (i.e. no organic templates have been used). A flowchart describing the whole synthesis operation starting from batch preparation to product recovery is available in Appendix A.

3.1.1 Batch Composition Selection

Several factors have been considered while selecting the composition of the batch to be used as the raw material. The sodium content of the batch was established using previous studies [2, 13]. When one examines the batch compositions pro-

vided by these works, it becomes clear that the sodium content to be used in sodalite production is significantly higher than what is needed stoichiometrically regarding the final chemical makeup of the product. The higher sodium concentration in the batch seems to increase selectivity towards sodalite with respect to other possible forms such as zeolite A, X or Y. This can be seen clearly from the eloquent compositional diagrams provided by Breck[2].

The final elements in the batch are the salt and water contents. These are closely related after a manner since in sodalite production it seems that the actual concentration of the salt within the batch is as important as its ratio to the framework metals. A study by Barrer and Cole [13] suggests that the maximum salt imbibition into sodalite for most sodium halides requires that the salt concentration be above 2 M at all times during synthesis. Since in the production of salt occluded sodalites we do not want partially imbibed specimens, the salt and water content is adjusted such that salt concentration is initially 5 M in the batch and hence does not fall below 2 M even after full conversion to sodalite.

After all these considerations the default batch composition for sodalite synthesis experiments is fixed as:



where SDA represents the structure directing agent, which is the salt used with respect to the sodalite variant desired. Table 3.1 summarizes the compositions used for the three different types produced. Point of note is the high water content

Table 3.1: Batch Compositions used in Synthesis

Sodalite Type	Batch Composition
Sodium chlorosodalite	$10Na_2O : 1Al_2O_3 : 2SiO_2 : 5NaCl : 67H_2O$
Sodium basic sodalite	$10Na_2O : Al_2O_3 : 2SiO_2 : 15NaOH : 67H_2O$
Sodium oxalate sodalite	$10Na_2O : 1Al_2O_3 : 2SiO_2 : 5Na_2(C_2O_2) : 150H_2O$

used for sodium oxalate sodalite. The reason for this is the low solubility sodium oxalate.

Since the crystallization process receives its components from the solution phase, there has to be sufficient amount of sodium oxalate to draw upon. This measure, however, brings the salt concentration to below the 2 M mark. This drawback was remedied to some extent by the utilization of higher temperatures and longer times for the crystallization of sodium oxalate sodalite.

3.1.2 Batch Preparation

The raw materials used were reagent grade sodium hydroxide pellets (Merck 106462), aluminium hydroxide (Merck 101091), Sodium Chloride (Merck 106400), sodium oxalate (Aldrich 223433) and ammonium stabilized colloidal silica (DuPont LUDOX AS-40).

The gel was prepared in several stages. Initially the desired amount of sodium hydroxide was dissolved in deionized water. After the sodium hydroxide was completely dissolved, the water lost due to the heat of reaction was made up before the desired amount of aluminium hydroxide was added. The mixture was heated gently and stirred until a clear sodium aluminate solution was obtained. This operation usually lasts about one to one and a half hours and is performed on a heated magnetic stirrer. The salt to be used was added to this solution and

dissolved completely. At this point the water lost during heating was made up once more.

Finally the colloidal silica was added to the sodium aluminate and salt solution. Gelation occurs immediately upon mixing and the mixture will usually thicken considerably, to an almost snow-like consistency. One other point of note is that, if ammonium stabilized silica is used, there will be a noticeable odor of ammonia which will be released as the colloidal silica encounters the highly basic environment. As the gel is stirred vigorously it will loosen gradually into a creamy and finally milk-like viscosity, which takes about 30 to 45 minutes, at which point it is charged into teflon lined steel autoclaves and sealed. For synthesis operations where the temperature does not exceed 100°C, screw-capped polypropylene bottles have been used instead of autoclaves.

3.1.3 Crystallization

The autoclaves were kept in the oven for times ranging from two hours to one week at temperatures from 75 to 170°C. Table 3.2 details the temperature and time ranges used for individual sodalite types.

Table 3.2: Hydrothermal Synthesis Conditions

Sodalite Type	Temperature (°C)	Time (h)
Sodium chlorosodalite	75 - 95	2 - 48
Sodium basic sodalite	90 - 130	4 - 60
Sodium oxalate sodalite	90 - 170	6 - 168

3.1.4 Recovery of the Solid Product

After crystallization the contents of the autoclaves were centrifuged for 10 minutes at 6000 rpm to ensure the sedimentation of all solid product. The liquid portion is decanted and the sediment was diluted with warm deionized water at 60°C at a ratio of about 100 ml for every gram of solid. This mixture is stirred for 30 minutes at 500 rpm on a magnetic stirrer and subsequently centrifuged to separate the solids. This cycle of dilution with fresh water, stirring and centrifugation was continued until the pH of the decanted liquid fell below 8. This is important to ensure that no sodium hydroxide or salt is left on the crystals. The use of warm water is especially important in the washing of basic sodalite in order to extract the hydroxide trapped within the cages. The obtained solids were air dried and later equilibrated at desiccators containing ammonium chloride solutions.

3.2 Ion Exchange

3.2.1 Ion Exchange

The produced sodium sodalites were subsequently modified in order to obtain silver loaded forms. The silver loading was done by aqueous ion exchange whereby the sodium cations in the framework was replaced by silver from the solution phase.

The exchange was carried batchwise in sealed polypropylene containers. Two primary aspects of the exchange, rate and equilibrium behavior, were studied during the experiments. For all the experiments the initial concentration of the solution was 0.1 N Ag^+ . The stock solution was prepared by dissolving reagent

grade silver nitrate (Aldrich 209139) in deionized water and calibration with respect to a 0.1 N Ag⁺ standard (Aldrich 319430). The concentration precision of the stock solutions were within ± 0.003 N and the individual variations were taken into consideration during subsequent calculations. Three distinct temperatures, 25, 50 and 80°C, have been investigated regarding ion exchange behavior.

For equilibrium experiments the solid to liquid ratio was varied in order to locate different points on the isotherm for a given temperature. The ratios were varied between 2 and 40 mg sodalite per ml of stock solution. The sealed vessels of different solid to liquid ratios were left at the desired temperature for at least 48 hours under mild continuous or intermittent agitation and then the liquid phase was sampled for silver and/or sodium determination. The determination of silver in the liquid phase was done with precipitation titrimetry using potassium thiocyanate as the titrant and iron(III)nitrate as indicator. The use of this method, which was derived from the Volhard Method [22], enables the immediate evaluation of silver content in the solution as opposed to the delayed evaluation that can be done with instrumental methods such as atomic absorption spectrometry, which in turn introduces several unknowns due to the fact that silver may be involved in side reactions during the time the sample waits for analysis. The details of the analysis method can be found in Appendix B.2.

3.3 Characterization of Solids

3.3.1 Characterization by XRD

The characterization of solid products was performed using several techniques.

The primary characterization method was X-ray powder diffraction. A Philips PW1840 diffractometer was used to scan the sodium and silver sodalites used.

The scan conditions used throughout the study are given in Table 3.3.

Table 3.3: XRD Scan Conditions

Anode	Cu
Filter	Ni
Radiation	CuK α (1.5405 Å)
Tube Potential	30 kV
Tube Current	24 mA
Step Size	0.01°
Scan Speed	0.05°/s
Intensity Range	10000 counts
Time Constant	1
Slit	0.2

The XRD method was used for three different analyses. Initially the patterns obtained from the produced samples are compared against peak listings (or Powder Diffraction Files) which are given in literature (see Appendix C.4). This is done in order to find out if the products are indeed sodalite, and if they are the form of sodalite that is desired. The observed patterns are compared to the diffraction files after their backgrounds have been fitted and removed from the signal. No noise smoothing was done on the patterns.

The crystallinities of the products were also evaluated using XRD. In order to quantify the degree of crystallinity, an internal reference was generated. This was done by scanning the most crystalline sample of each type successively mixing it with more and more of an amorphous sodium aluminosilicate zeolite precursor

(Zeolex). The pure sample is given a crystallinity index of 1, the same sample with 20% amorphous material is given an index of 0.8 and so forth. It was seen from the scans that the sum of heights for the five most intense peaks ($d = 3.626, 2.093, 2.374, 2.564, 6.281 \text{ \AA}$ in order of intensity) of sodalite for each sample was linearly dependent on this crystallinity index. The calibration graph for this experiment can be found in Appendix C.1.

Finally the thermal decomposition of sodalites were investigated by XRD. Samples of all three sodium sodalites were heated for two hours at temperatures of 400, 700, 900 and 1000°C. The resulting powders were scanned in order to evaluate changes in the pattern, such as diminishing crystallinity, increase in amorphous background and possibly the emergence of other phases due to conversion at high temperatures.

3.3.2 Structure Determination by XRD Powder Diffraction

The structures for silver sodalites, for which there is no available reference in the literature, were solved using freely available software packages. The packages have been obtained from the *Collaborative Computational Project Number 14: Single Crystal and Powder Diffraction* [23].

Two packages have been used for the structure refinements. Both packages work on the Rietveld refinement method for powder patterns. The patterns were initially fitted with *CelRef* [24], which only requires the powder pattern and space group data for the crystals in order to refine for the cell edge. This information was used to generate an initial model for the silver sodalite in question. This model was used in the primary software package, *PowderCell* [25], to generate

the simulated pattern which was then fitted, using Rietveld refinement, to the observed pattern.

In the generation of the initial model by CelRef, generally all the peaks aren't included into the model. An initial guess is made for the cell edge. This initial guess is the cell edge of the sodium counterpart of the sodalite. With this cell edge, and with the space group known, peak locations are generated for a general crystal with that symmetry and unit cell size. This is compared to the observed pattern. Initially only peaks of the observed pattern which fall within a tolerance level of $\pm 0.1^\circ$ to the simulated pattern are used¹. Note that CelRef does not take into consideration the peak intensities, only the peak locations.

With the limited set of peaks, a cell edge is refined for the crystal in question. This cell edge is used to generate the atomic locations for the framework atoms (i.e., the Si, Al and O atoms). With the new framework model, the cations (i.e., Ag) are placed in their 'initial guess' positions, which are initially again the locations of sodiums in the counterpart sodium sodalite. This now complete model is loaded into PowderCell along with the respective experimental pattern and Rietveld refinement is done.

During the refinement, the cell edge, cation positions, zero-shift, intensity scaling, and the Full Width at Half Maximum (FWHM) characteristics of the peaks are iterated upon to obtain a good fit. The background for the observed pattern is also constantly fitted with a 7th degree polynomial and added to the calculated pattern at each iteration.

The iteration seeks to minimize the objective function given by[26]:

¹ This will generally be about 6 or 7 of the 15 observable peaks

$$S_P = \sum w_i [Y_i(obs) - \frac{1}{c} Y_i(calc)]^2 \quad (3.2)$$

in which $Y_i(obs)$ and $Y_i(calc)$ are the intensities of the observed and calculated patterns at each step (i.e. at each data point). c is the scaling factor and w_i is the weight associated with each data point which is evaluated using counting statistics:

$$w_i = [Y_i(obs)]^{-1/2} \quad (3.3)$$

In accordance, the goodness of fit is evaluated by:

$$R_{wp} = \left\{ \frac{\sum w_i [Y_i(obs) - Y_i(calc)]^2}{\sum w_i Y_i^2(obs)} \right\}^{1/2} \quad (3.4)$$

When this fit is complete a new model is at hand, with a new cell edge. This cell edge then is used in CelRef to check for consistency in peak locations. If new peaks are within the tolerance level they are included into the calculation and a new model is generated and used in refinement with PowderCell. This cycle continues until at least 13 peaks have been included into the model and the goodness of fit is no longer improving.

3.3.3 Other Methods

In order to assess the morphologies and crystal sizes in the powders produced, microscopy was employed. Initial observations with an optical microscope revealed particle sizes below $1\mu\text{m}$ which is at the resolution limit of the microscope. Therefore, scanning electron microscopy was utilized and micrographs of both sodium

and silver sodalite powders were taken in magnifications of 200, 500, 2000 and 6000 times.

The hydration behavior and possible decomposition of sodalites has been investigated by Thermal Gravimetric Analysis. The conditions used in the TGA analyses are given in Table 3.4.

Table 3.4: Conditions used in TGA Analyses

Temperature Range	30 - 900°C
Heating Rate	10°C/min
Sample Mass	25 - 30mg
Purge Gas	N ₂
Purge Gas Flowrate	100 cc/min

Additionally the chemical compositions of the sodium sodalites synthesized were found using wet chemical analysis. The contents of Al₂O₃, Na₂O and SiO₂ were measured.

CHAPTER 4

RESULTS

4.1 Syntheses of Sodium Sodalites

Three types of sodium sodalite were synthesized using hydrothermal methods. The syntheses were identified by X-ray diffraction pattern matching to existing records in literature. The yields of the syntheses have been evaluated and the dependence of crystallinity on time and crystallization temperature was investigated.

4.1.1 Synthesis of Sodium Chlorosodalite

4.1.1.1 Crystallization

The synthesis of chlorosodalite was the first synthesis performed in this study. The modelling of the general batch composition (see Eqn. 3.1) was done during the synthesis starting from the IZA Verified Synthesis recipe [19]. A temperature

of 75°C was used and it was seen that even at this lower temperature the synthesis results are satisfactory after 12 hours of crystallization.

The synthesis temperature was then fixed at 75°C and the behavior of crystallization with respect to time was investigated by trying synthesis at 2,4,6,12,24 and 48 hours. It was seen that the synthesis was essentially complete after 12 hours and the best results were obtained with 24 hours. A slight decline in crystallinity was observed after 48 hours.

Chlorosodalite crystallization was investigated for yield by a combination of weighting and XRD analysis. The batches are weighed before they are put in the oven for crystallization. After recovery the solid product is dried at about 80°C and weighed. The yield of a particular run is calculated from:

$$Yield = \frac{Weight\ of\ Dry\ Product\ (g)}{Weight\ of\ Batch\ (g)} \cdot 100g \quad (4.1)$$

The yields are thus calculated as grams of product per 100 grams of batch. The maximum possible yield is calculated using the assumption that when one of the framework metals in the batch is depleted, the crystallization will cease. As the batches used contain a Si/Al of unity, the metal used is not important. However, it has been reported [14] that in sodalite synthesis aluminium is usually the limiting reactant. Therefore the maximum yield is calculated as the yield at the point where Al concentration in the solution phase of the batch drops to zero. A sample calculation of the maximum yield is given in Appendix A.2.

The maximum yield calculated for chlorosodalite is 13.8 g/100g. Table 4.1 summarizes the yields obtained at different temperatures. Conversions given in the table are calculated using:

$$Conversion = \frac{Yield}{Maximum\ Yield} \cdot Crystallinity\ Index \quad (4.2)$$

The crystallinity indices used in Table 4.1 are calculated from the XRD scans of the products produced using different crystallization times. These indices are evaluated using the method described in Section 3.3.1.

The increase in crystallinity with respect to time is a good indicator of the rate of both the nucleation and crystallization of the system. Figure 4.1 illustrates the crystallization rate of chlorosodalite with respect to time.

4.1.1.2 Characterization

The most crystalline sample in the sodium chlorosodalite series being the one crystallized for 24 hours at 75°C, the characterization was done on this sample. Firstly, the sample was matched with a 'fingerprint' powder diffraction file (PDF #37-0476) [27]. The match is shown in Figure 4.2. As the match is acceptable, the samples produced were verified as sodium chlorosodalites. The peak listings for the scan is available in Appendix C.5

After identification, the thermal decomposition of the sample has been investigated by scanning samples held in temperatures of 400 to 1000 °C for 2 hours. These scans can be found in Appendix C.2. Sodium chlorosodalite is stable until at least 700°C with conversion to nepheline starting after 900°C.

Thermal gravimetric analysis shows a loss of 14.5 % per weight up to 900°. TGA Scans of chlorosodalite may be seen in Appendix A.3.0.3. This loss is attributed to dehydration in chlorosodalite since the framework is stable up to 900° and water is the only guest that can leave the cages without destroying them.

Analysis by SEM reveals little information as to the morphologies of the crystals. Evidently, the crystal sizes are nanoscopic in the synthesis of chlorosodalite. Figure 4.3 shows the SEM picture of the sample at the highest magnification utilized. The individual crystallites are not distinguishable from the picture. Hence, the morphologies cannot be commented upon and the crystal size can be roughly estimated at around 100 nm.

The chemical $\text{Na}_2\text{O} - \text{Al}_2\text{O}_3 - \text{SiO}_2$ composition of chlorosodalite was found using wet chemical analysis. Appendix A.3 summarizes the findings along with the hydration amount.

Table 4.1: Yield and Conversion Results for Sodium Chlorosodalite

Temperature (°C)	Time (h)	Yield (g/100g)	Maximum Yield (g/100g)	Crystallinity Index	% Conversion
75	2	12.3	13.8	0.23	20.5
75	4	14.0	13.8	0.71	72.0
75	6	13.0	13.8	0.80	75.6
75	12	13.7	13.8	0.98	97.1
75	24	13.9	13.8	1.00	100.8
75	48	13.6	13.8	1.00	94.7
75	96	13.9	13.8	1.00	97.05

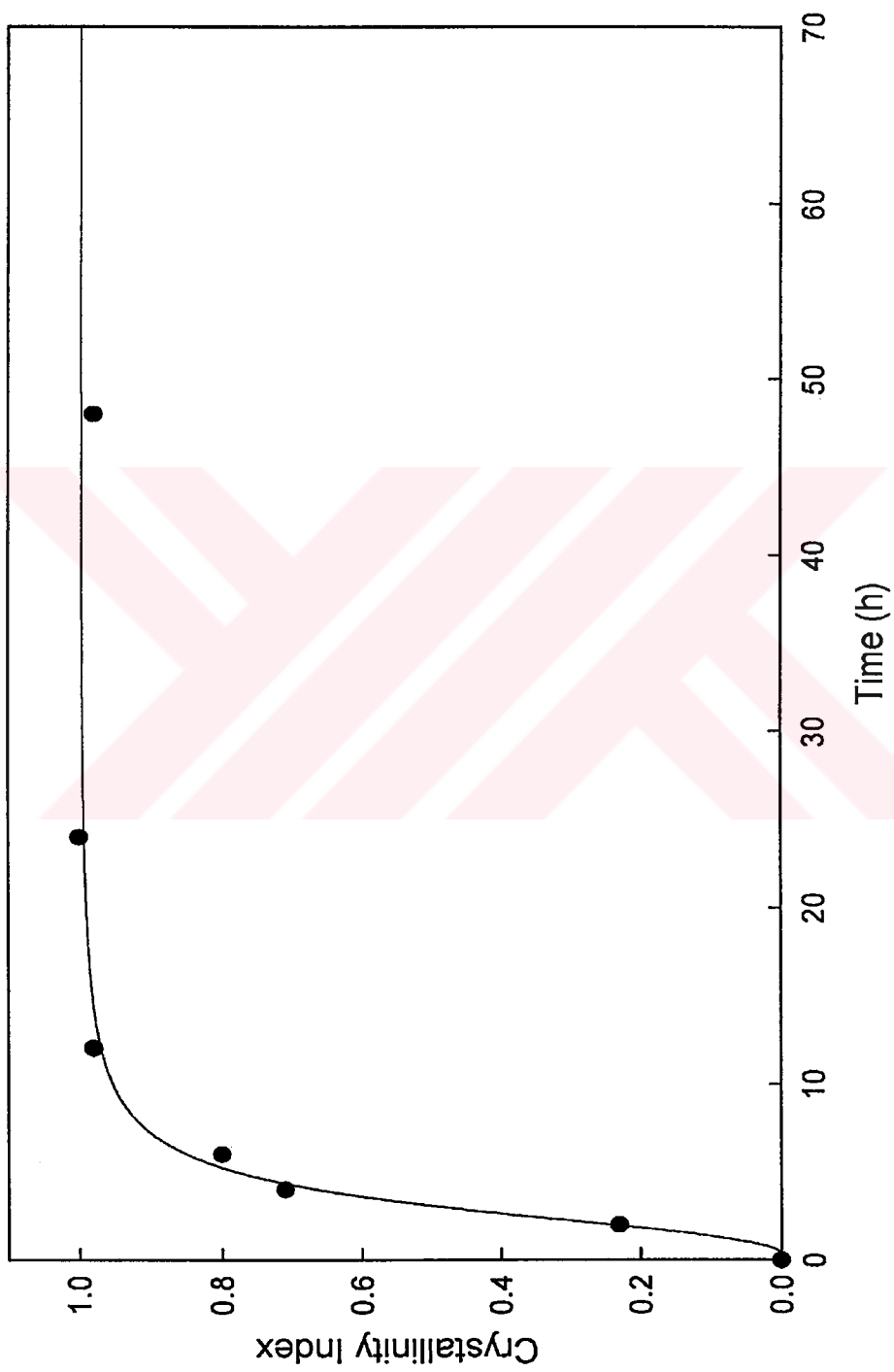
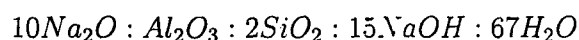


Figure 4.1: Crystallization of Sodium Chlorosodalite over Time

4.1.2 Synthesis of Sodium Basic Sodalite

4.1.2.1 Crystallization

Sodium basic sodalites crystallize without the use of a separate structure directing agent. The sodium hydroxide used for making the sodium aluminosilicate gel is added at a determined excess so that sodium hydroxide will feed the framework with Na_2O and the hydroxides will also act as a template over which the cages will form. Accordingly, a batch composition of



was used in the production of basic sodalite. Although they represent the same raw material the framework Na_2O and the template NaOH are regarded separately in the composition.

The synthesis of basic sodalite was initially essayed at 95° and 130° for 48 hours. The difference between the two syntheses were negligible as shown in Figure 4.4. A temperature of 95° was fixed as the synthesis temperature since increased temperatures did not improve the crystallinity. Going lower than 95° was not opted for since the absolute crystallinity in basic sodalite was significantly inferior to chlorosodalite and hindering the synthesis with lower temperatures was not desired.

The crystallization of basic sodalite is negligible before 6 hours and is only significant after 12 hours of crystallization. Table 4.2 summarizes the yield results obtained as detailed in Section 4.1.1.1. Figure 4.5 shows the crystallization of basic sodalite over time at 95°C and the increased nucleation time is observable from the behavior.

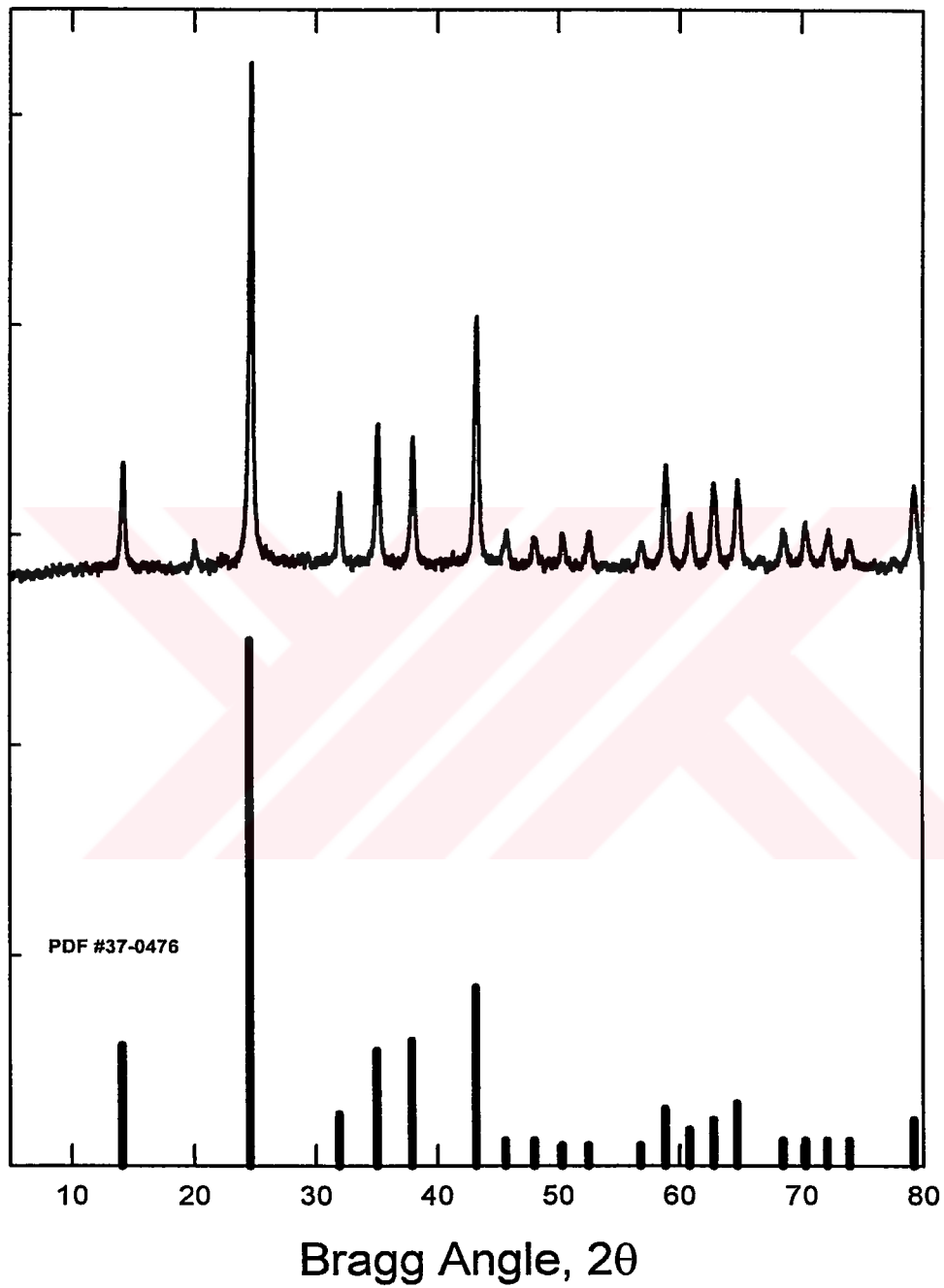


Figure 4.2: Comparison of the Synthesized Sodium Chlorosodalite with Reference Pattern

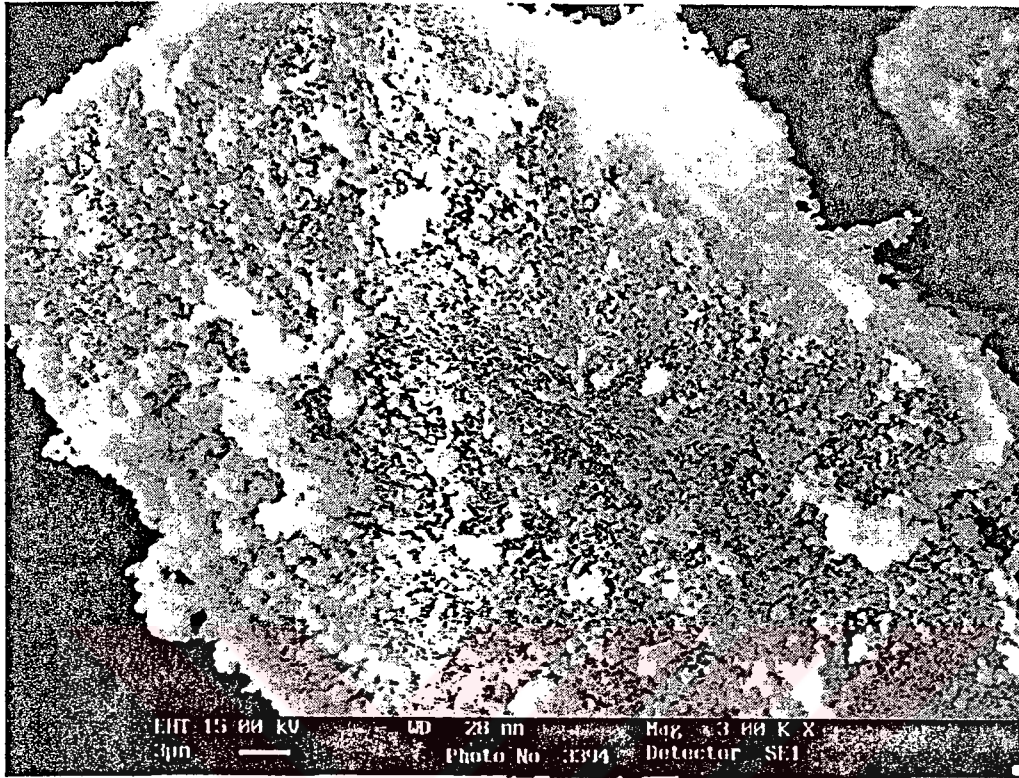


Figure 4.3: SEM Picture of Sodium Chlorosodalite at x6000 Magnification

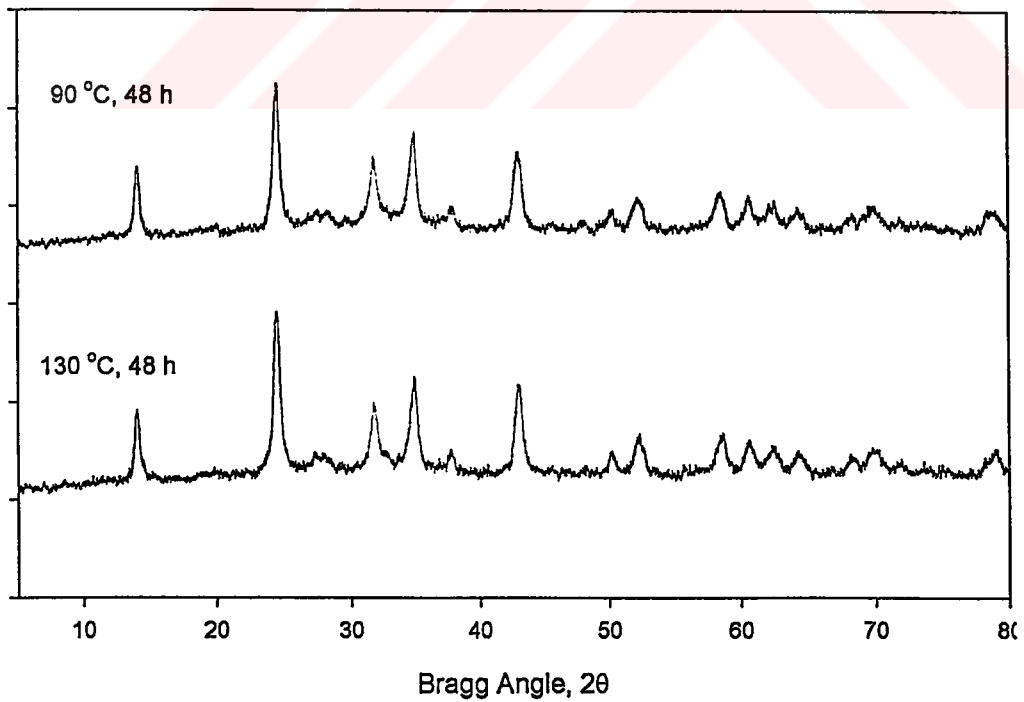


Figure 4.4: Comparison of XRD Scans of Sodium Basic Sodalite at 95 and 130°C 48 hours of crystallization

Table 4.2: Yield and Conversion Results for Sodium Basic Sodalite

Temperature (°C)	Time (h)	Yield (g/100g)	Maximum Yield (g/100g)	Crystallinity Index	% Conversion
95	2	8.6	14.6	0.01	1.0
95	4	7.4	14.6	0.05	4.5
95	6	14.6	14.6	0.36	36.0
95	12	15.3	14.6	0.45	47.2
95	24	13.8	14.6	0.78	73.5
95	36	14.1	14.6	0.96	92.7
95	48	13.4	14.6	1.00	91.6
95	60	13.1	14.6	0.97	87.2

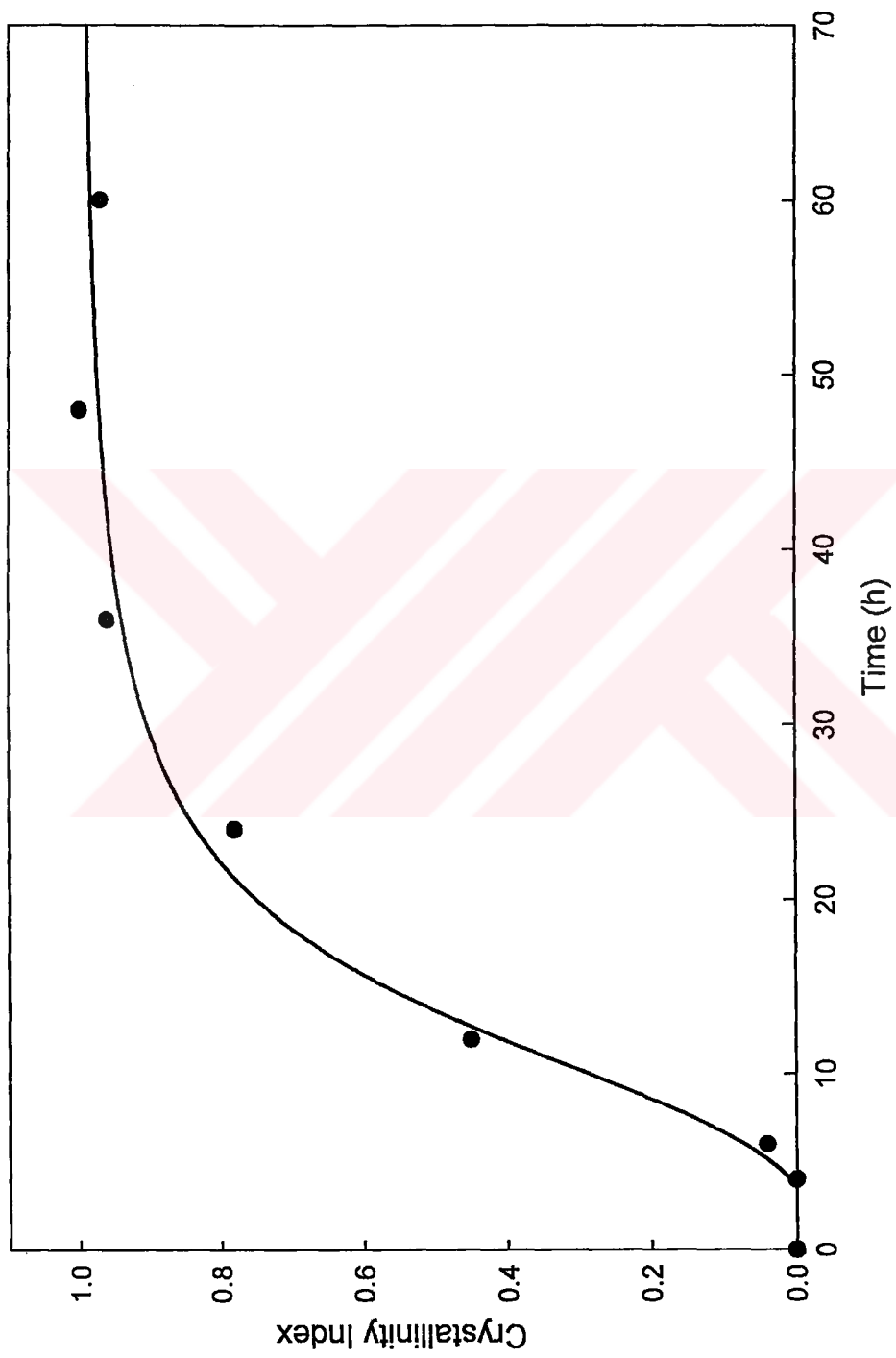


Figure 4.5: Crystallization of Sodium Basic Sodalite over Time

4.1.2.2 Characterization

The most crystalline sample among basic sodalites synthesized was crystallized for 48 hours at 95°C and the characterization was done on this sample. The fingerprint match with the powder diffraction file (PDF #42-0215 [8]) is given in Figure 4.6. The peak listings for the scan can be found in Appendix C.5

SEM pictures of basic sodalites reveal little and are much like chlorosodalites in that the crystals are too small to be observed individually and hence their morphologies cannot be investigated. A sample scanning electron micrograph of sodium basic sodalite is given in Figure 4.7

The thermal decomposition of sodium basic sodalite has been monitored in a manner identical to that of chlorosodalite. The XRD scans of basic sodalites subjected to temperature extremes between 400 and 1000°C can be found in Appendix C.2. Sodium basic sodalite seems to be stable up to at least 900°C with crystallinity degradation and conversion to nepheline starting around 1000°C.

Thermal gravimetric analysis shows a loss of 17.0 % per weight up to 900°C. This loss is thought to be the result of water loss from within the cages, however the profile of the loss is interesting and compares with similar zeolites such as erionite. ([2] pp. 448-449) TGA scans of basic sodalites may be found in Appendix A.3.0.3. The chemical analysis results of basic sodalite can be seen in Appendix A.3

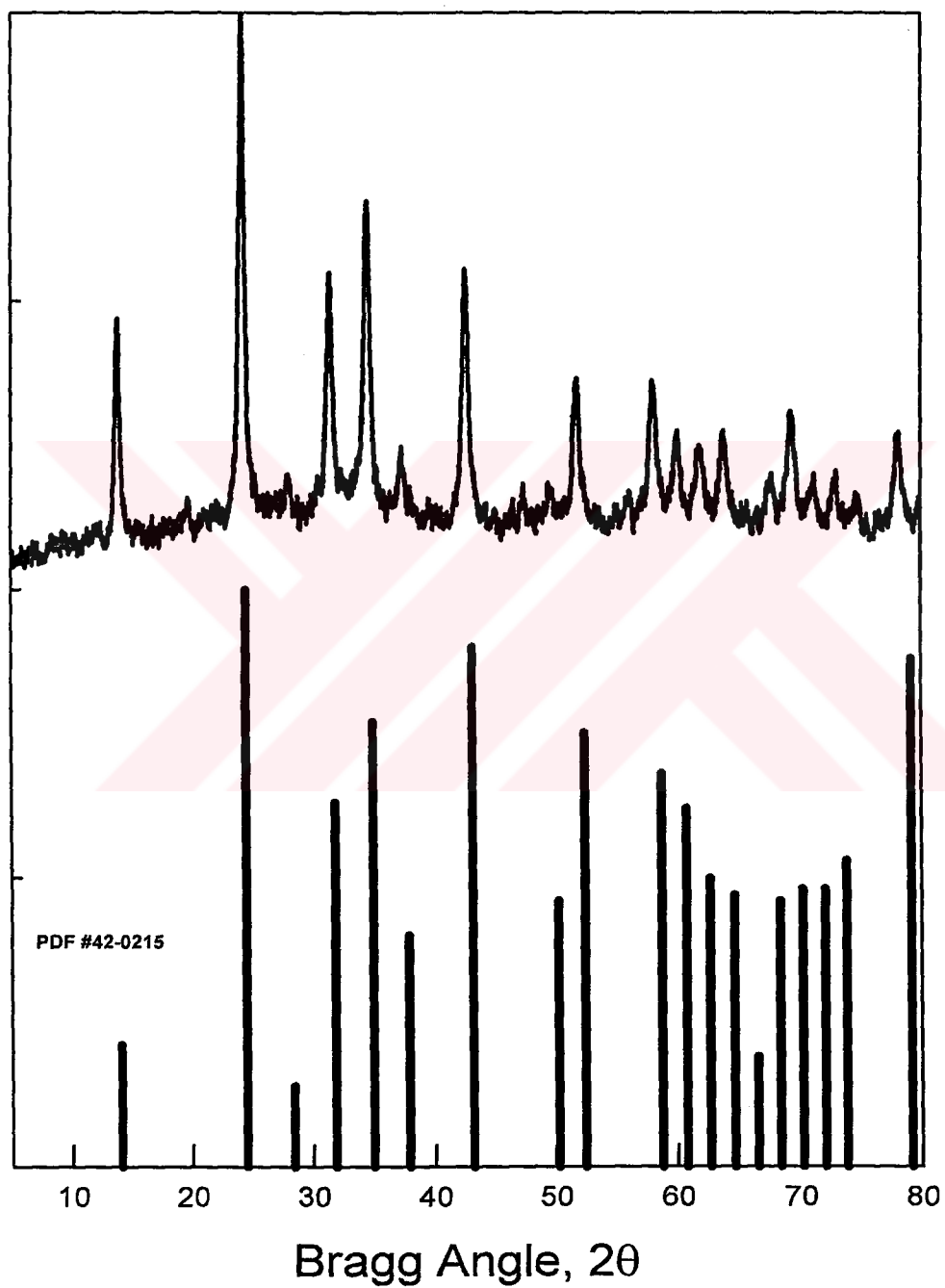


Figure 4.6: Comparison of the Synthesized Sodium Basic Sodalite with Reference Pattern

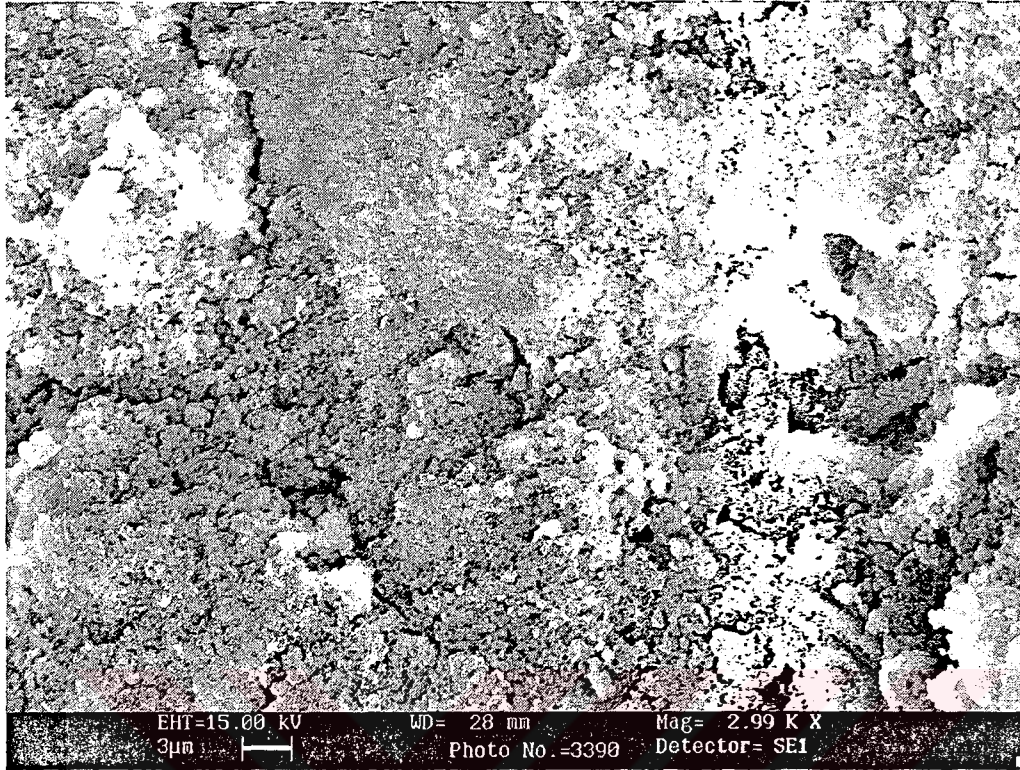
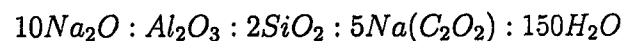


Figure 4.7: SEM Picture of Sodium Basic Sodalite at x6000 Magnification

4.1.3 Synthesis of Sodium Oxalate Sodalite

4.1.3.1 Crystallization

The synthesis of sodium oxalate sodalite presents certain problems not encountered with the other two types. The low solubility of the structure directing agent, sodium oxalate, makes it impossible to use the general batch composition directly. The batch composition used for the synthesis of sodium oxalate sodalite is



The higher water content is necessary in order to dissolve the amount of sodium oxalate used. The result is that the absolute crystallinity of sodium

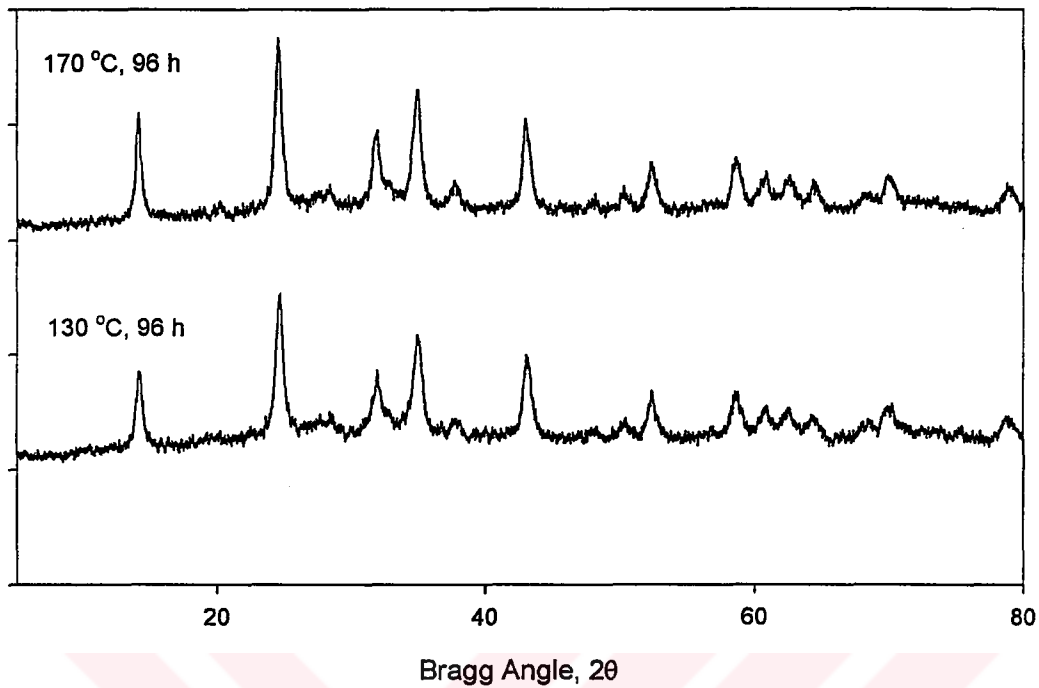


Figure 4.8: Comparison of XRD Scans of Sodium Oxalate Sodalite at 130 and 170°C
96 hours of crystallization

oxalate samples are considerably lower and noise and background levels are much higher than the other types. There are several factors affecting this deficiency and will be discussed in the succeeding sections.

The synthesis of sodium oxalate was initially done at 130°C with 96 hours of crystallization with the above mentioned problems. Hence, the temperature was increased to 170°C, which is deemed the maximum safe temperature since oxalate decomposes at temperatures exceeding 200°C. There is essentially no difference in crystallinity when the samples crystallized for 96 hours at the two temperatures are compared, as can be seen from Figure 4.8

As a result, the time dependence of sodium oxalate sodalites cannot be calculated reliably. The yield treatment was done for the oxalate sodalite samples

with the omission of crystallinity index and hence the conversion. The results are given in Table 4.3

Table 4.3: Yield and Conversion Results for Sodium Oxalate Sodalite

Temperature (°C)	Time (h)	Yield (g/100g)	Maximum Yield (g/100g)
130	96	8.0	8.3
170	96	7.9	8.3

4.1.3.2 Characterization

The SEM results of sodium oxalate sodalites are similar to the other two sodalite types, however there are certain differences. Whereas the other two sodalites tend to conglomerate into larger solid particles (see Figures 4.3 and 4.7), the conglomerations of oxalate sodalite seem to be smaller.

This difference is also evident in the physical feel of the ground powders. The chlorosodalite and basic sodalite powders have an abrasive quality whereas the oxalate powder is softer in the sense that it resembles talcum. Although the crystallite sizes are still too small to make definite observations, these differences hint at a possible difference in the morphology of oxalate sodalite crystallites, which reflects on the large scale qualities of the powder. A representative SEM picture of sodium oxalate sodalite is seen in Figure 4.9.

The TGA analysis of sodium oxalate sodalite shows two successive gradients of weight loss at the lower temperatures (see Appendix A.3.0.3). The first loss is determined to be a loss of water which corresponds to about 5 % wt. The second

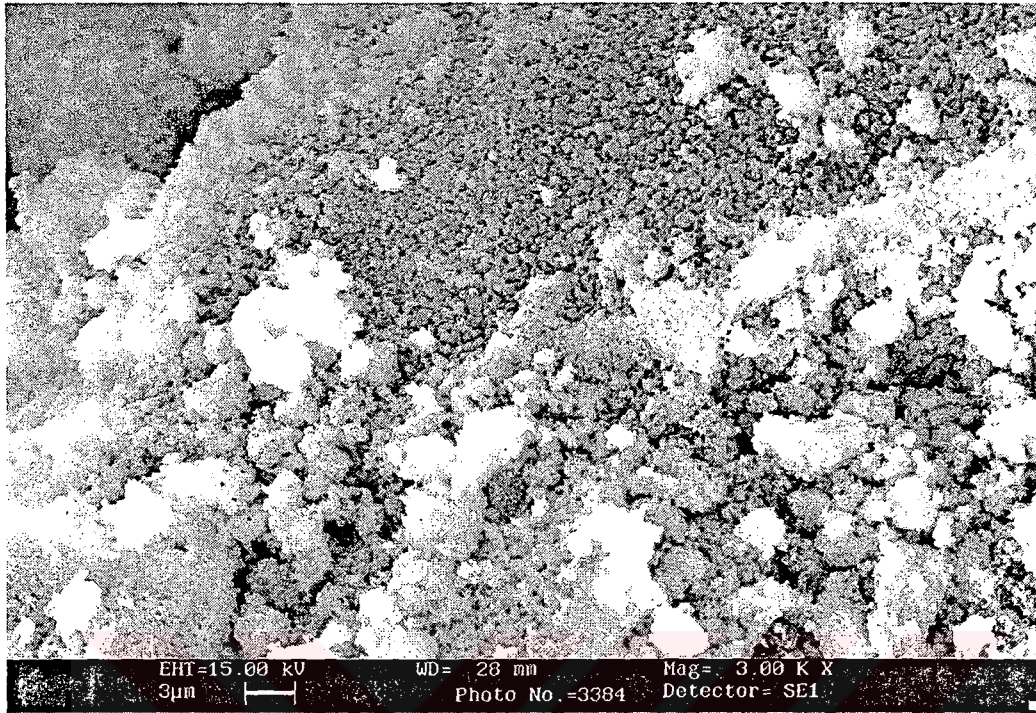


Figure 4.9: SEM Picture of Sodium Oxalate Sodalite at x6000 Magnification
gradient of loss occurs around 250 °C and corresponds to the decomposition of oxalate, which is subsequently released as CO₂.

Temperature decomposition (see Appendix C.2) profiles of sodium oxalate show that although the crystal structure is intact until 900 °C there is change in the framework. The peaks shift slightly between 400 and 700°C indicating that the cages are getting smaller. This effect will be discussed later (see Section 5.1). The chemical makeup of sodium oxalate sodalites as determined by wet chemical analysis in addition to TGA are given in Appendix A.3

4.2 Modification of Sodalites

The modification of sodalites involves loading the sodium forms of the three types of sodalites produced with silver. The loading is done by aqueous ion exchange. Therefore, the word 'loading' is not used in the sense that additional silver is combined with the structure, rather that the sodium cations in the framework are replaced by silver cations. The chemical formulae of the sodalites hence change as postulated by Table 4.4

Table 4.4: Formulae of Sodium and Silver Sodalites

Sodalite Type	Sodium Form	Silver Form
Chlorosodalite	$\text{Na}_8[\text{SiAlO}_4]_6\text{Cl}_2$	$\text{Ag}_8[\text{SiAlO}_4]_6\text{Cl}_2$
Basic Sodalite	$\text{Na}_6[\text{SiAlO}_4]_6$	$\text{Ag}_6[\text{SiAlO}_4]_6$
Oxalate Sodalite	$\text{Na}_5[\text{SiAlO}_4]_6(\text{C}_2\text{O}_2)$	$\text{Ag}_5[\text{SiAlO}_4]_6(\text{C}_2\text{O}_2)$

4.2.1 Ion Exchange Rates

Ion exchange rates for sodalite types were evaluated by monitoring the amount of loading with respect to time. This was done by sampling the reaction at predetermined times and observing the change of the silver concentration in solution. A constant solid-to-liquid ratio of 12 mg/ml was used for the rate experiments. The results of the experiment is summarized in Figure 4.10.

The rates of ion exchange give an idea about the final exchange capacities of the sodalites in question and also provide a time frame as to how long the system might take to reach equilibrium. Using this data it is possible to determine the time for isotherm construction experiments. The cation exchange capacities of the three types of sodalite along with the stoichiometric maximums are given in Table 4.5

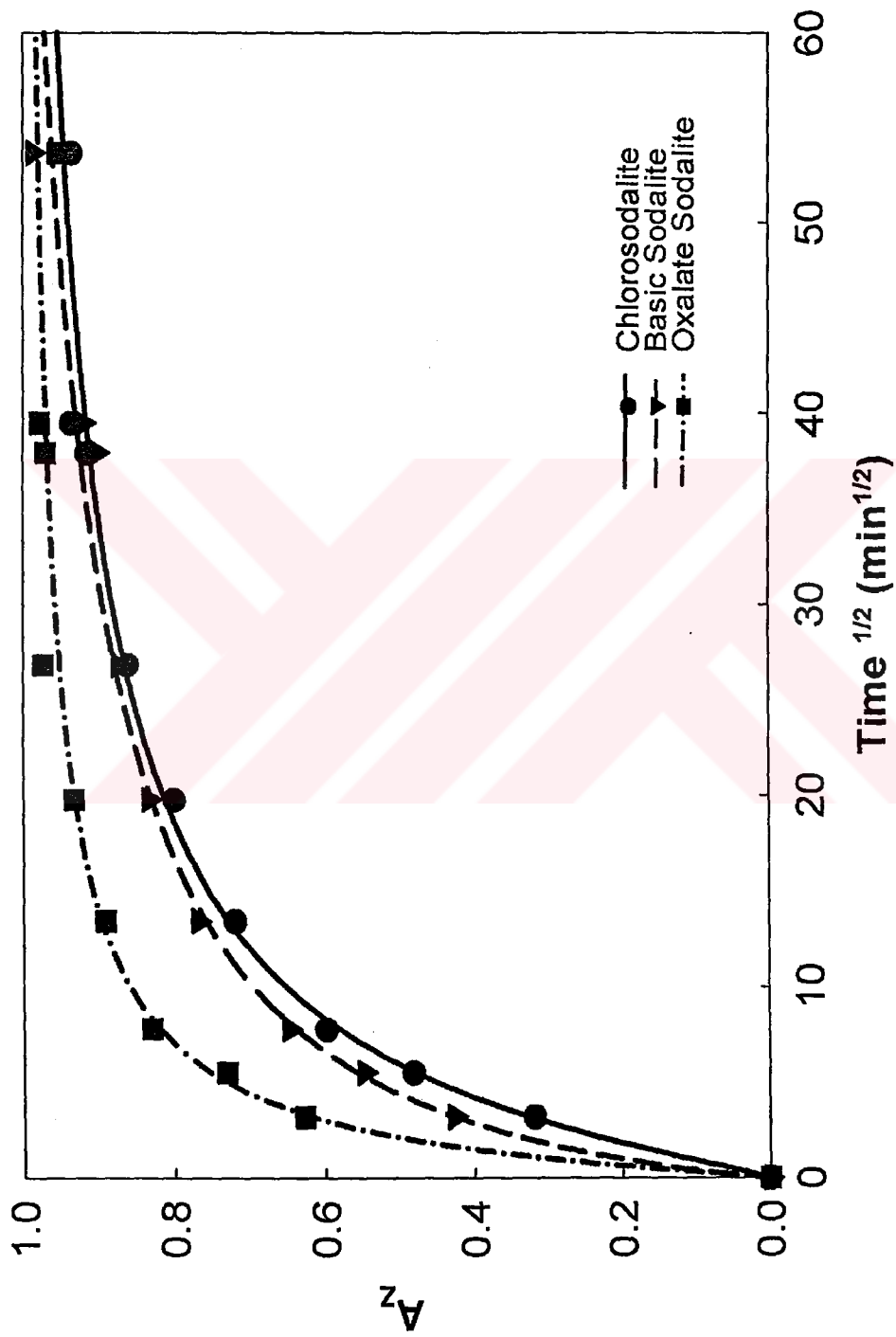


Figure 4.10: Sodium-Silver Ion Exchange Rates of Sodalites at 25°C

Table 4.5: Cation Exchange Capacities of Sodalites

Sodalite Type	Maximum CEC (meq/g)	Observed CEC (meq/g)	% Maximum Achieved
Chlorosodalite	8.25	7.72	93.6
Basic sodalite	7.04	6.88	97.8
Oxalate sodalite	8.38	8.26	98.6

4.2.2 Ion Exchange Equilibria

The ion exchange reactions have been carried out using various solid-to-liquid ratios in order to observe the equilibrium points at different end concentrations, which in turn translates into different points along the isotherm. The ratios are selected such that the stoichiometric point is appropriately at the median of the points. In other words, half of the solid-liquid ratios used for the construction of each isotherm are such that the amount of Ag in solution is less than the exchange capacity of the amount of solid used and for the other half there is an excess of sodium in the solution. The ion exchange is allowed to proceed for 48 hours. This time was determined using the rates of ion exchange. It can be seen from Figure 4.10 that all exchange is essentially complete after 36 hours ($\approx 45 \text{ min}^{1/2}$). As a safety factor, an extra duration of 12 hours have been added to that time.

At the end of the allotted time for equilibrium, the solution is sampled and analyzed for silver by the titration method described in Appendix B.2.

The ion exchange equilibria of sodalites at 25, 50 and 80°C have been constructed from the titration data using the calculations in Appendix B.3.

The isotherms constructed from these data are given in Figures 4.11 4.12 and 4.13. The isotherm data points shown in the figures are fitted with 3 parameter

sigmoidal curves of the form given in Eqn. 4.3. This equation and the curves produced thereof are used as visual aids only and the values of the parameters a, b and c are evidently inconsequential in a physical context. In fact, for the given curves the value of b is at the order of 1×10^{-18} and is hence zero at the limit. The curves therefore are very sensitive to the minute variations in a and c which have mean values of 1.02 and -3.5×10^{-2} respectively. This mathematical model for these curves is hence very unstable and cannot be reasonably attributed a physical meaning.

$$A_Z = \frac{a}{1 + \left(\frac{A_S}{b}\right)^c} \quad (4.3)$$

The isotherm data is then used as per the treatment given in Section 2.2 in order to obtain the Kielland plots for each temperature/type and subsequently the thermodynamic equilibrium constants. The Kielland plots for 25°C are given in Figure 4.14 and plots for the other temperatures may be found in Appendix B.4.

The thermodynamic equilibrium constants and standard free energies of exchange thus calculated may be seen in Table 4.6

Table 4.6: Equilibrium Constants and Standard Free Energies for Sodium-Silver Ion Exchange in Sodalite

	K _a			Δ G° (kJ/mol)		
	at 25 °C	at 50 °C	at 80 °C	at 25 °C	at 50 °C	at 80 °C
Chlorosodalite	62.5	66.6	69.6	-10.25	-10.41	-10.52
Basic sodalite	92.2	111.7	151.9	-11.22	-11.73	-12.49
Oxalate sodalite	34.6	34.7	41.4	-8.78	-8.85	-9.29

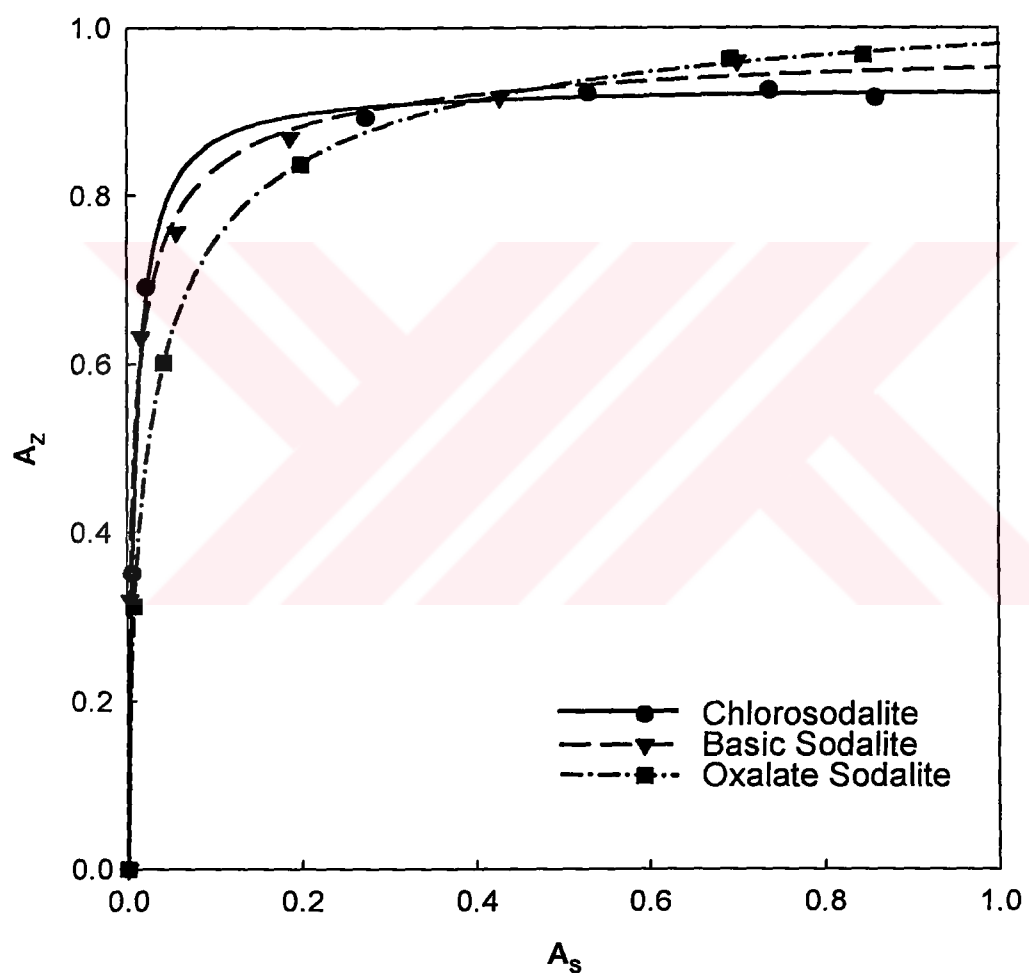


Figure 4.11: Na-Ag Ion Exchange Isotherms for Sodalites at 25°C

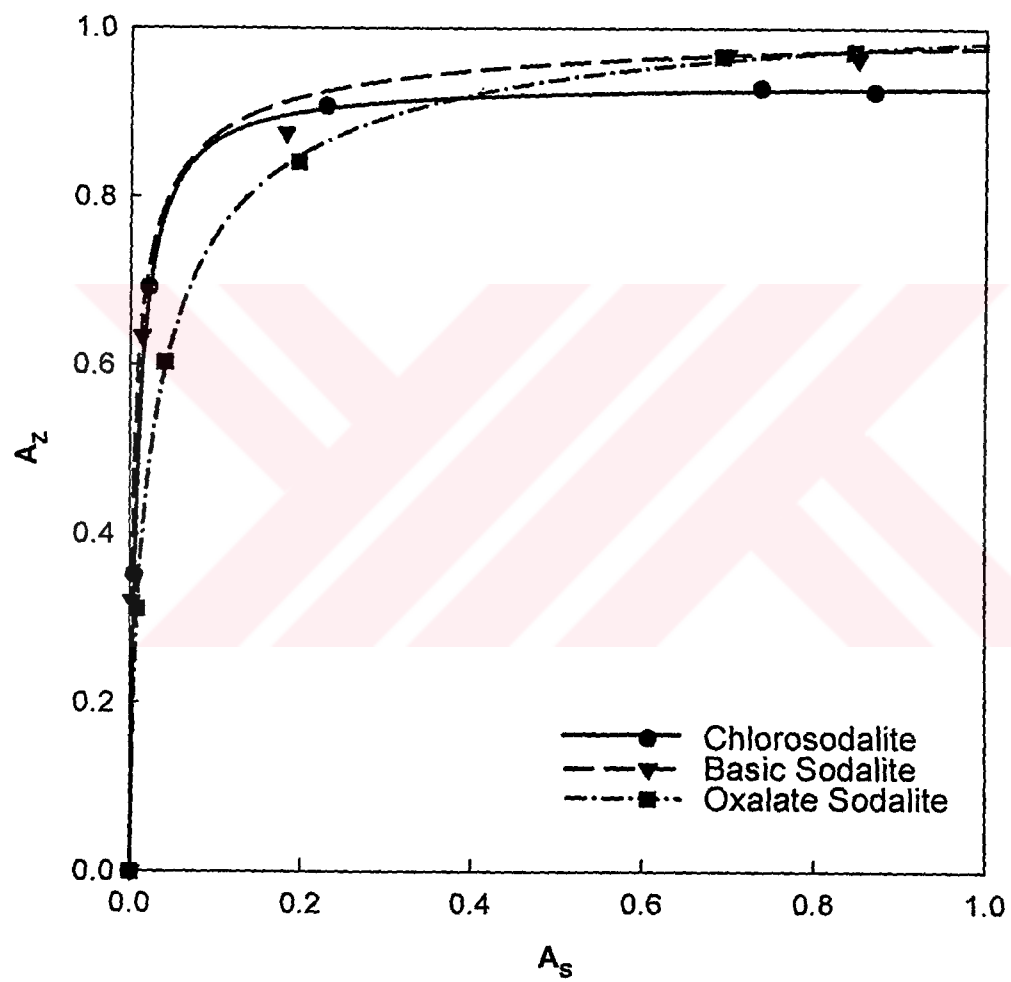


Figure 4.12: Na-Ag Ion Exchange Isotherms for Sodalites at 50°C

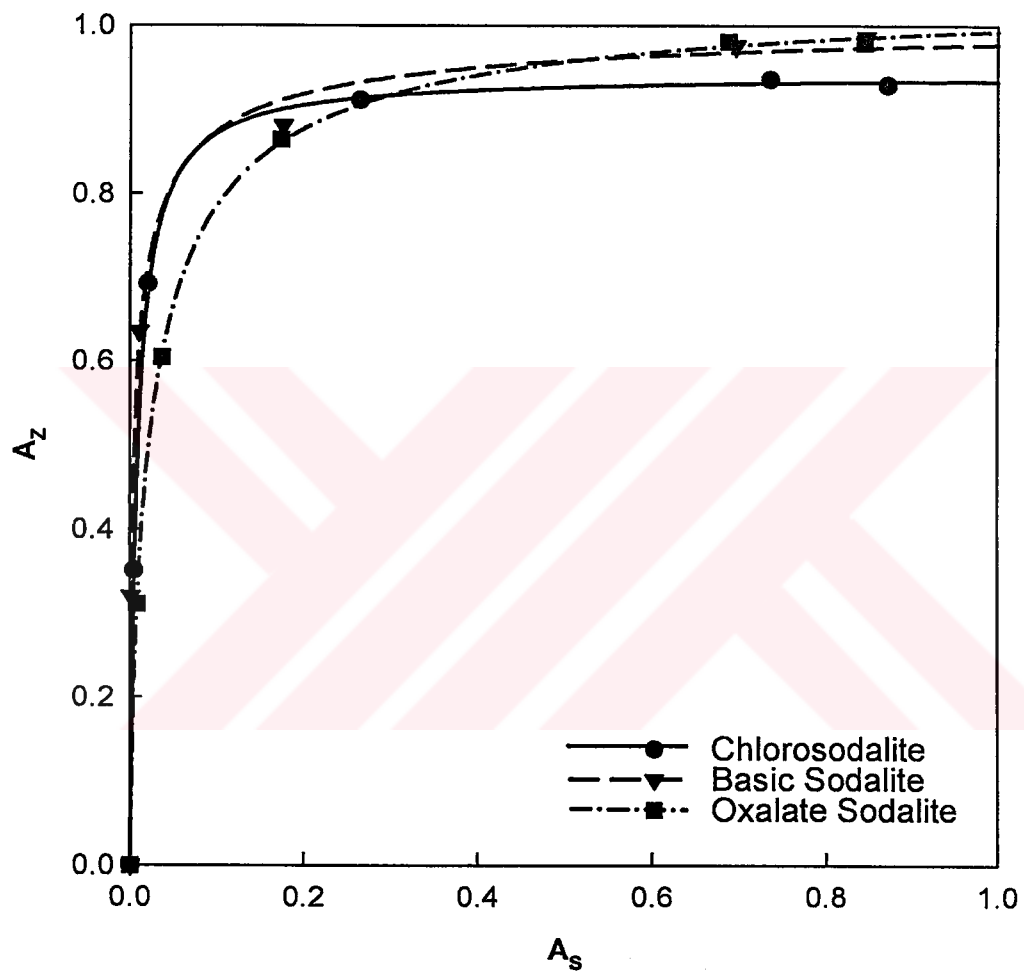


Figure 4.13: Na-Ag Ion Exchange Isotherms for Sodalites at 80°C

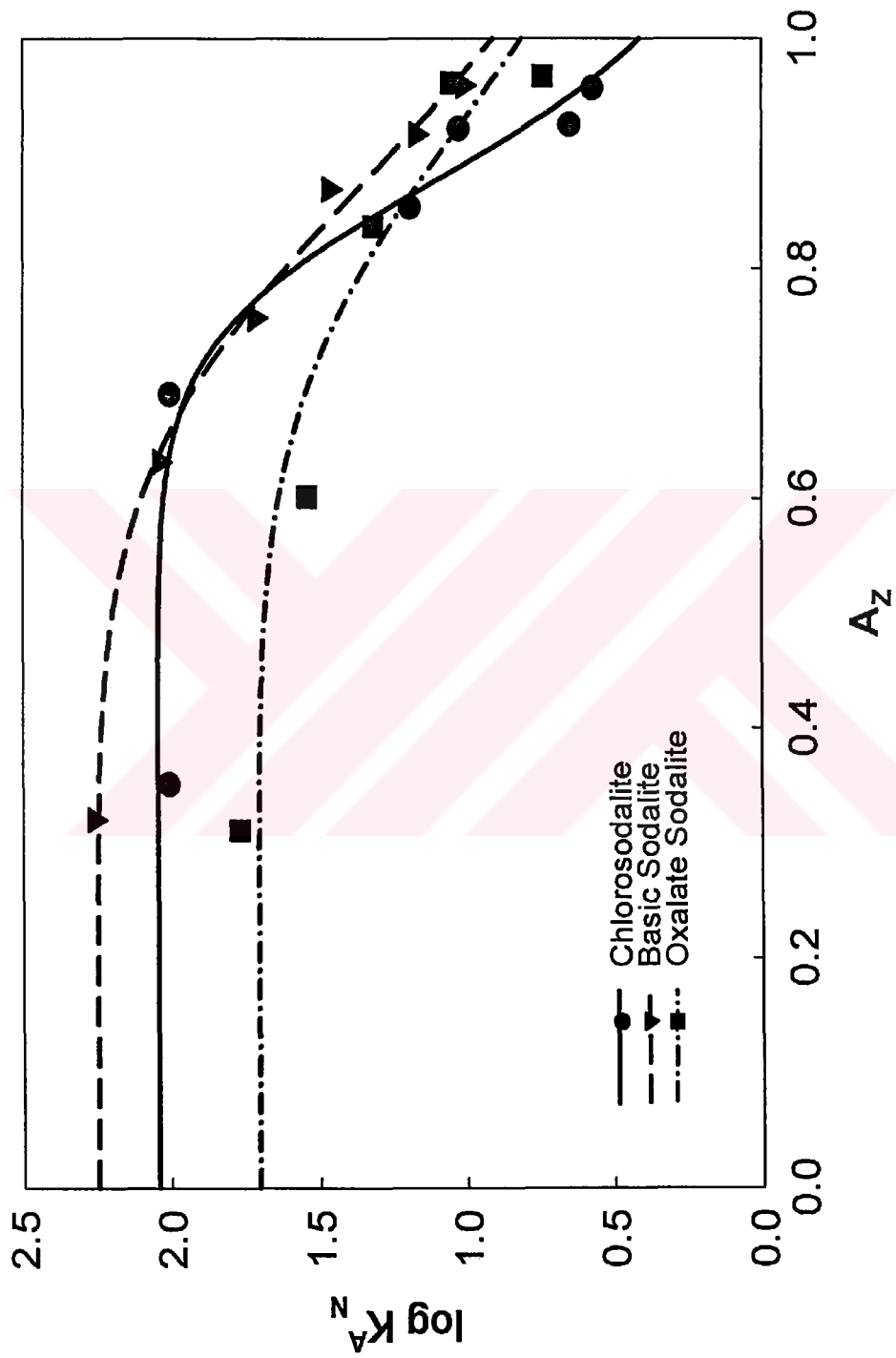


Figure 4.14: Kjelland Plots for Sodalites at 25°C

4.3 Characterization of Solids

4.3.0.1 XRD Structure Determination of Silver Sodalites

There is very little information as to the XRD patterns of silver sodalites in the literature. Barrer and Falconer provide photo based XRD scans of silver basic sodalite [28]. Stein et al. have provided a scan of silver chlorosodalite with a refinement of the pattern along with several select crystallographic parameters in a series of papers dealing with silver halosodalites [6, 7].

Both of these sources, although giving an idea about what to expect, do not constitute satisfactory references due to limited reproduction quality. Hence, the validity of the silver sodalite samples obtained via ion exchange must be ascertained internally. Additionally, the refinement procedure provides valuable crystallographic data about the samples.

The refinement is done as described in Section 3.3.1. There are certain assumptions inherent in the operation that are of consequence.

Initially one must decide on a space group to base the crystal models upon. Several space groups, such as $P\bar{4}3n$, $P\bar{4}3m$, $Im\bar{3}m$ and $I\bar{4}3m$, have been proposed and used, the highest possible symmetry being $I\bar{4}3m$. This is one of the ambiguities inherent; these space groups are all valid and furthermore they are impossible to distinguish between given only powder data [29]. The group most commonly used is $P\bar{4}3n$ (No. 218) however, and this group is used for this study.

The degrees of freedom of the system were decreased dramatically by relating the position of the framework oxygens directly to unit cell edge. Since the framework oxygen in sodalite is attributed a Wyckoff i site, or a general posi-

tion, the fractional coordinate of oxygen will not stay constant as the cell size changes. However, since the framework aluminium and silicon occupy d and c sites respectively, as the cell size increases the distances between the framework metals increase. The oxygens linking the metals will be affected by this change in a controlled manner. The assumption here is that the Al-O and Si-O bond distances do not change [4] and the expansion or shrinkage of the cage is compensated exclusively by tetrahedron rotation, in other words by changes in the oxygen-metal-oxygen bond angles. One other assumption is that the tetrahedra rotate exclusively about directions parallel to the cell edge. Since the distance between framework metal and oxygen is fixed and the distance of adjacent metal atoms is known given a cell size, the calculation of the oxygen position becomes a simple problem of three dimensional geometry. In short, the atomic positional data for the framework constituents can be generated directly given the unit cell size. The method used for finding positional coordinates for the framework atoms, as described by [4] is given in Appendix C.3.

The extra framework atoms, namely the cations and anion, are another matter. The anion provides no problem as it is usually located at the Wyckoff a site, or the center of the cage. The cations, silver or sodium, are assumed to occupy e sites so that all three positional coordinates are equal to the same number, which means there is only one degree of freedom to fix in order to find cation locations.

Note that, for silver oxalate sodalite, only the unit cell size, and therefore the framework dimensions, can be reliably calculated. The reasons are that the oxalate anion can not be satisfactorily modelled due to its multi-atomic nature

and the fact that oxalate sodalites give low quality powder patterns as discussed above.

The dimensions obtained for the silver sodalite crystals can be seen in Table 4.7. The fits obtained for silver chlorosodalite and silver basic sodalite is shown in Figures 4.15 and 4.16 respectively. Crystallographic datasheets of these two silver sodalites can be found in Appendix C.3.

Table 4.7: Framework Data for Silver Sodalites

All lengths are in Å and all angles are in degrees. CoS denotes the center of symmetry for the framework. The aperture sizes have been calculated assuming a diameter of 2.7 Å for oxygen.

	Silver Chlorosodalite	Silver Basic Sodalite	Silver Oxalate Sodalite
Cell Edge	8.872	8.956	9.006
Distances			
Al-O	1.742	1.779	1.618
Si-O	1.619	1.633	1.743
Ag-O	2.424	2.332	-
Ag-CoS	2.554	2.769	-
Angles			
O-Al-O	108.7	109.0	107.8
O-Si-O	108.7	107.8	108.7
O-Ag-O	98.9	104.5	-
Aperture Sizes			
6-Ring	2.472	2.530	2.528
4-Ring	0.917	0.920	1.008

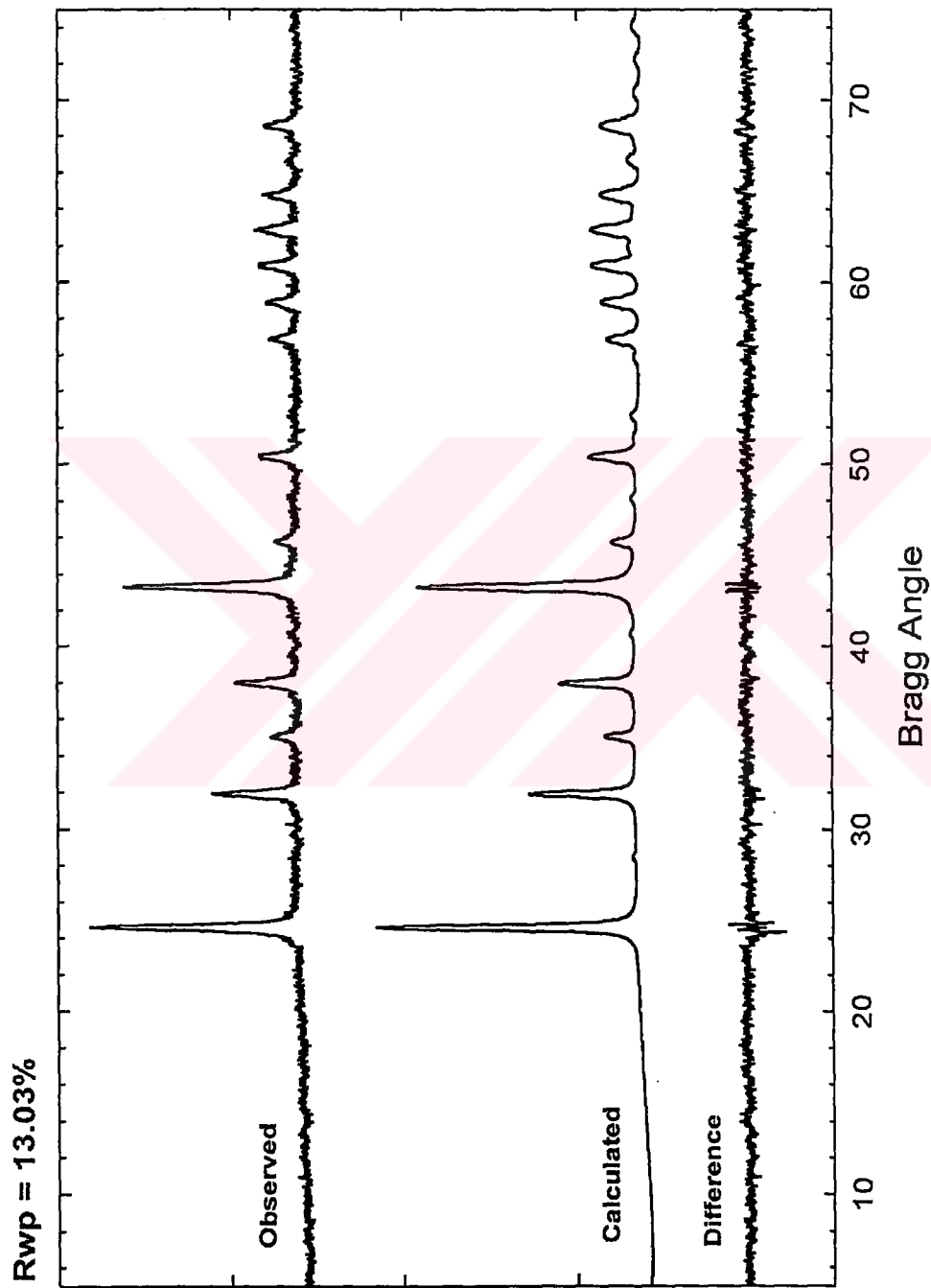


Figure 4.15: Comparison of XRD Scan of Silver Chlorosodalites to Calculated Pattern

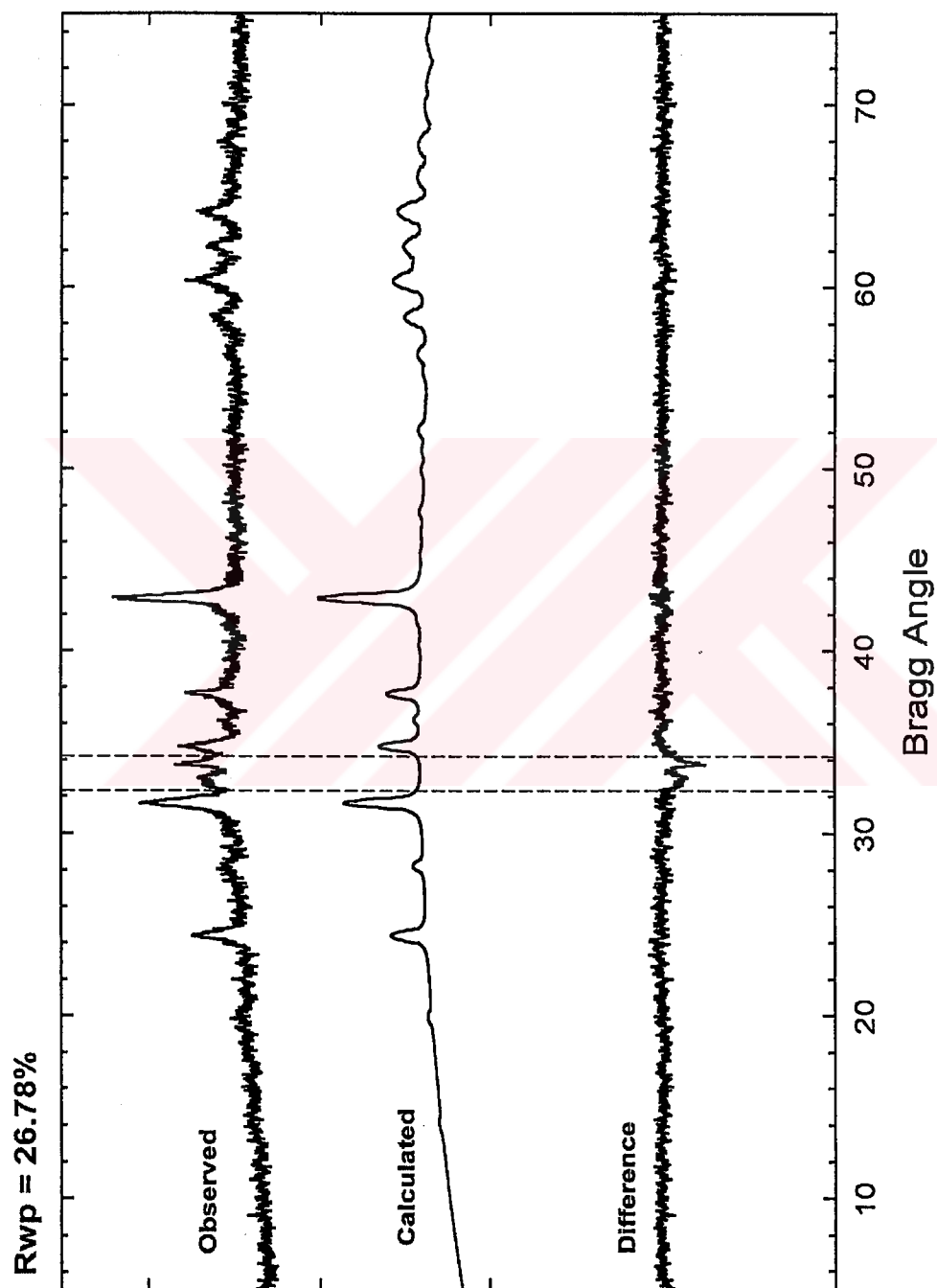


Figure 4.16: Comparison of XRD Scan of Silver Basic Sodalite to Calculated Pattern
The bounded region in (b) indicates peaks that belong to AgO and thus have been excluded from the refinement.

4.3.0.2 Microscopic Analyses

The SEM pictures of silver sodalites show no noticeable difference from their respective sodium forms. The different physical and morphological aspects of sodium oxalate sodalite are also seen in silver oxalate sodalite. Although not much can be derived from these pictures, the resemblance to the respective forms suggest that the changes of the sodalites are indeed internal and no silver compounds are deposited around the crystallites, at least not to the extent that they are visible in SEM picture. Additionally, it is seen that the slight enlargement of the unit cell sizes with silver loading has no apparent effect on the bulk properties of the material.

CHAPTER 5

DISCUSSIONS

5.1 The Effect of Guest Species on Nucleation and Crystallization

The crystallization temperatures of each type is different and depends on the effectiveness of the template anion. It was seen in no uncertain terms that by far the most effective template is chloride used to produce chlorosodalite, followed by hydroxide which was used for basic sodalite. Oxalate does not seem to be an effective directing agent to start with and furthermore cannot be used in sufficient concentration due to limited solubility.

The crystallization temperatures ultimately used¹ were selected such that each form of sodalite can achieve crystallinity index of near unity within 24 hours of crystallization. The exception is oxalate sodalite where a temperature of 170 °C can be used at most since free oxalate decomposes after 200 °C. Even at this

¹ 75°C for sodium chlorosodalite, 95°C for sodium basic sodalite and 170°C for sodium oxalate sodalite.

temperature oxalate sodalite can not achieve its best crystallinity before 48 hours. None of the samples produced show subsequent degradation of the sodalite phase after prolonged crystallization. There are slight decreases ($\sim 96\%$) in the peak intensities of chlorosodalite after 48 hours however, this may be attributed to experimental error.

The XRD patterns of the typical samples for all three sodalites, also show major differences between the pattern qualities, if not the fingerprints. The pattern of chlorosodalite has the best quality in terms of XRD data, with sharp and intense peaks. The peaks of basic sodalite are also sharp with slightly diminished intensity. The pattern of oxalate sodalite shows high background, noise and broadened, low intensity peaks. The reason for this difference lies in the respective structures, or rather the superstructures, of the different types.

The sodalite crystal may be viewed as the superposition of two different repeating structures. One factor in this superposition is the aluminosilicate framework itself. The other factor is the superstructure formed by the cation and anions dispersed in the framework. This superstructure may be viewed as a skewed version of the salt crystal that would result from the anion-cation pairs had they not been entrapped in the sodalite. As is, they still form a regular structure, albeit different from the original salt, interleaved with the framework. When both the framework and the ionic superstructure is repetitive in a regular fashion the result is still a well formed crystal resulting in a sharp and intense pattern. This is the case with chlorosodalite and to some extent, basic sodalite .

The chlorosodalite superstructure is highly regular where in each cage the chloride and four sodium ions are in identical locations so that structure repeats

from cage to cage. In basic sodalite, the existence of residual hydroxide anions recalcitrant to the extraction will disrupt the regularity of the superstructure somewhat but well washed samples provide acceptable and workable XRD patterns.

When one examines the structures of oxalate sodalites, however, the reason for the low quality XRD patterns become apparent. Since oxalate is a -2 charged anion it does not occupy every single cage. Statistically every other cage is occupied by the anion and four cations. In order to preserve the overall charge neutrality the cages devoid of anions still contain the full complement of four cations. This results in a relatively disorganized superstructure since the dispersion of oxalate throughout the cages is not regular. There may be clusters of neighboring cages all holding anions surrounded by envelopes of unoccupied cages, or a one full - one empty cage type of distribution, to give examples of possible arrangements. There may be combinations of different arrangements, the formation of which are relatively random, in different crystallites or within the same crystallite. The fact that the contents of a cage affects the size of the cage makes matters even worse since the irregular arrangement of oxalates within the framework also reflects on the framework, resulting in defects. It follows that, where chlorosodalite may be viewed as an interlacing of two different crystals, oxalate sodalite is in effect the interlaced form of a crystal with a semi-amorphous structure.

This view can be strengthened by investigating the thermal behavior of oxalate sodalite. It is known that free oxalate decomposes into CO_2 at temperatures above 200°C . This decomposition is also seen whilst in the cages of sodalite. TGA results (Table A.4) show a weight loss at $\approx 230^\circ\text{C}$ of proportions comparable to

the theoretical amount of oxalate in the cages. The CO₂ formed would be able to escape the cages given time and energy (i.e. high temperature).

The end result would be that oxalate sodalite at high temperatures would be 'calcined' of its template, oxalate, much like the procedure routinely done for zeolites synthesized with organic templates. The remaining framework structure would be identical to basic sodalite. Furthermore, since the above mentioned strain on the framework would be alleviated, the observed crystallinity should increase.

This is indeed what happens. Figure 5.1 shows XRD patterns of oxalate sodalite, heat treated oxalate sodalite and heat treated basic sodalite with reference lines to compare the peaks. It is seen that the heat treated oxalate peaks shift from their original positions towards basic sodalite peak locations and the overall crystallinity is increased.

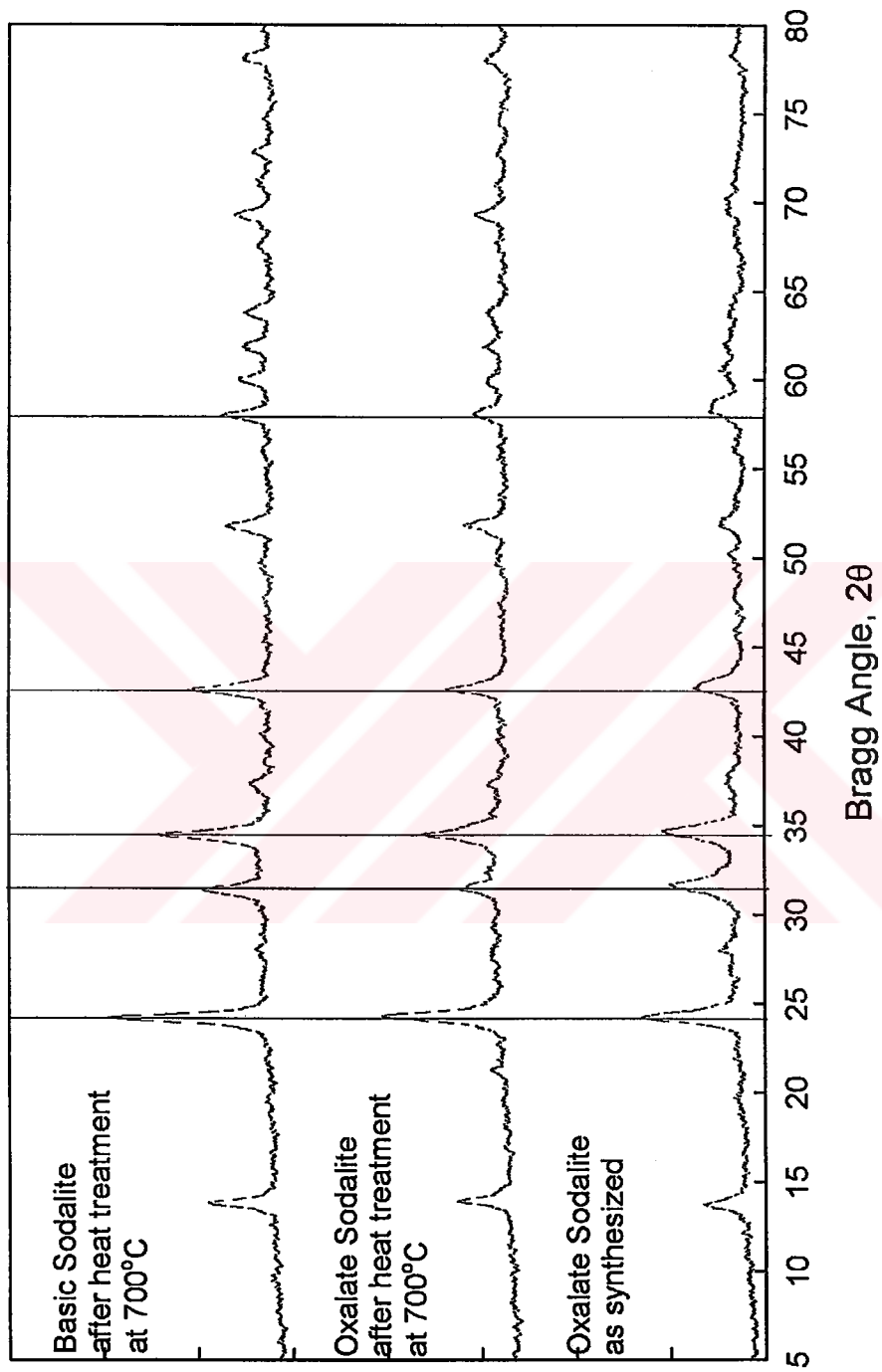


Figure 5.1: High Temperature Conversion of Oxalate Sodalite to Basic Sodalite

5.2 Ion Exchange Behavior of Sodalite with respect to Guest Species

It is clear from Figures 4.11, 4.12, 4.13 and Table 4.6 sodalites, regardless of type, are extremely selective towards silver and although still obeying the mass action law, silver exchange in sodalite should practically be viewed as an irreversible process due to the high equilibrium constants.

The relative differences of selectivity are rather minute and best explained, if need be, by the occlusion of the cages. The selectivity of basic sodalite in relation to sodium - silver ion exchange seems to be marginally higher than chlorosodalite and followed by oxalate sodalite. At this point it is appropriate to consider the extent of occlusion in sodalites:

The extent of occlusion is a qualitative way of expressing the 'fullness' of the cages in sodalite. In other words, since basic sodalite cages contain only the cations and possibly water, the occlusion is least in basic sodalite. Chlorosodalite contains a chloride anion at the center and is thus more occluded. The large oxalate anion in oxalate sodalite all but fills up the cage with little space left for anything else.

It seems that the more occluded the cages of a sodalite, the less selective it becomes to the larger Ag^+ cation, although it apparently prefers it over Na^+ chemically. It has been argued by Stein et al. [6, 7], in their study of sodium silver halosodalites, that halides within the cage do indeed hinder ion exchange.

One other point discussed in their study is the inability of ion exchange to follow to completion, when done in aqueous media. This point is mirrored by the

results obtained in this study as shown in Table 4.5. Stein et al. suggest the use of melt exchange to overcome the problem, however this kind of exchange is not the emphasis of the present study.

The ion exchange rates of sodalites produce a different picture (see Figure 4.10). Oxalate sodalite shows a relatively rapid exchange, whereas chlorosodalite and basic sodalite are slower with almost identical rate behavior. The reason is found in the cage sizes of sodalites. The cage size of oxalate sodalite, along with the aperture sizes for the 6 and 4 rings of the cage, is larger compared to the other two types. Hence, it is evident that the rate of exchange is dependent on the intra-framework diffusion of cations within sodalite.

The ion exchange equilibria of the sodalites studied have a relatively low dependence on temperature, with the equilibrium of basic sodalite affected most by the temperature change. Figure 5.2 shows the variation of $\ln K_a$ with absolute temperature. The extent of dependencies on temperature for the region studied are apparent. The plots have been fitted with linear regression in order to illustrate accordance with the *Van't Hoff* equation [21].

5.3 Optical Properties Observed in Silver Sodalites

During the different experiments several interesting optical properties of silver sodalites have been observed. All the silver sodalite darken in time with exposure to daylight. Trials with artificial sources of light have shown that the darkening occurs with short wave UV light (254 nm) and darkening does not occur under long wave UV (370 nm). Apart from this silver basic sodalites and silver oxalate sodalites have been seen to darken under pressure whilst preparing pellets. These

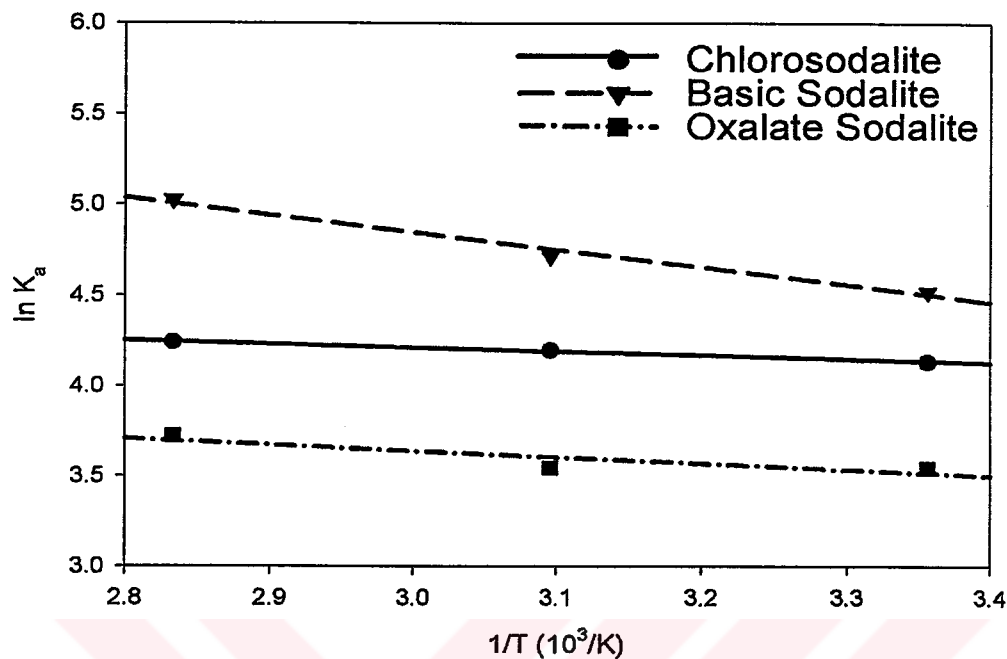


Figure 5.2: Variation of Sodalite Na-Ag Exchange Equilibrium Constants with Temperature

two sodalites are also sensitive to X-rays and show tenebrescence. After exposure to X-rays silver oxalate sodalite will temporarily become yellowish orange and silver basic sodalite takes a violet color, both of which wear off in a matter of minutes.

Possibly the most interesting of all is the fluorescent behavior of silver oxalate sodalites which begin to fluoresce under long wave UV when first exposed short wave UV light. The most probable explanation to this is the decomposition of oxalate within the cages due to the UV radiation, which in turn results in AgO and metallic Ag clusters in the cages. These clusters are thought to fluoresce under long wave UV light [30].

This activation of fluorescence seems to be permanent and could be useful for a range of applications involving data recording. And the fact that the recording

and retrieval is done through the emission of the material instead of reflection or absorbance, as is the case in today's optical media, makes it possible to implement three dimensional data storage.

In this case a combination of light sources, most possibly lasers, in the lower and upper UV range would be used to read and write data. During writing the low frequency UV laser can be used to select the plane on which the recording is to be done, while the high power laser is used to record the bit pattern. When reading, only the low frequency laser is enough as when the same plane is illuminated by low frequency, the previously written bit pattern will become apparent by fluorescing.

CHAPTER 6

CONCLUSION

Three sodalite variants of the sodium form have been produced using hydrothermal synthesis at relatively low temperatures and autogenous pressure. The yield and ultimate crystallinity obtained is strongly dependent on the structure directing anion which also determines the variant produced. Chloride anions facilitate the synthesis, making it possible to produce a highly crystalline product with high yield very rapidly at low temperature. Hydroxide is less effective in this manner and oxalate is least effective, in that synthesis with oxalate requires higher temperatures and more time and ultimately has lower yield. An advantage in sodalite synthesis is that regardless of the anion employed the system can be 'forced' by large excesses of sodium to exclusively produce sodalite. Accordingly, in all of the syntheses performed the only crystalline phase was sodalite.

The sodium forms of these sodalites have been loaded with silver by ion exchange. In the sodium - silver system, all three types of sodalite are extremely selective towards silver. The temperature dependence of thermodynamic equi-

librium constants for chlorosodalites and oxalate sodalites are low whereas basic sodalite show significantly higher temperature dependence in ion exchange. Several interesting optical properties have been observed in silver sodalites which might be useful in optical data recording.

The produced sodalites have crystal sizes of about 100 nm. Through powder diffraction analyses it was possible to determine the basic crystallographic properties of the silver sodalites produced and important framework structure details such as aperture and cage sizes have been derived.



REFERENCES

- [1] N. Gobeltz A. Demortier J. P. Lelieur and C. Duhayon. Encapsulation of the Chromophores into the Sodalite Structure during the Synthesis of the Blue Ultramarine Pigment. *J. Chem. Soc., Faraday Trans.*, 15:2257 – 2260, 1998.
- [2] D.W. Breck. *Zeolite Molecular Sieves*. John Wiley & Sons, New York, 1974.
- [3] D.J. Vaughan and R.A.D Patrick; Eds. *Mineral Surfaces*. Chapman and Hall, London, 1995.
- [4] I. Hassan and H.D. Grundy. The Crystal Structures of Sodalite-Group Minerals. *Acta Cryst.*, B40:6–13, 1984.
- [5] R.M. Barrer. *The Hydrothermal Chemistry of Zeolites*. Academic Press, London, 1982.
- [6] A. Stein G.A. Ozin P.M. MacDonald G.D. Stucky and R. Jelinek. Silver, Sodium Halosodalites: Class A Sodalites". *J. Am. Chem. Soc.*, 112(13):3171–3180, 1992.
- [7] A. Stein G.A. Ozin and G.D. Stucky. Class B Sodalites: Nonstoichiometric Silver,Sodium Halosodalites. *J. Am. Chem. Soc.*, 114(21):8119–8129, 1992.
- [8] G. Engelhardt J. Felsche and P. Seiger. The Hydroxysodalite System. *J. Am. Chem. Soc.*, 114(4):1173–1182, 1992.
- [9] Volynets et al. Photochromic and/or Cathodochromic Sodalite Material... U.S. Patent 4490286, 1984.
- [10] Vakhidov et al. Method of Producing Photochromic Sodalite Crystals. U.S. Patent 3964984, 1976.
- [11] T. Koyama. Method to Crystallize Dense Sodalite... U.S. Patent 5340506, 1994.
- [12] M. A. Lewis and I. Pereira. Method of preparing sodalite from chloride salt occluded zeolite. U.S. Patent 5613240, 1995.
- [13] R.M. Barrer and J.F. Cole. Salt Entrainment by Sodalite and Cancrinite during Their Synthesis. *J. Chem. Soc. (A)*, page 1523, 1970.

- [14] B. Herreros and J. Klinowski. *J. Chem. Soc. Faraday Trans.*, 97(7):1147–1154, 1995.
- [15] D.M. Bibby and M.P. Dale. *Nature*, (317):157–158, 1985.
- [16] B.J. Schoeman J. Sterte and J.E. Otterstedt. The synthesis of colloidal zeolite hydroxysodalite sols by homogenous nucleation. *Zeolites*, 14:208–216, 1994.
- [17] S. Tsuyoshi T. Wakihara M. Sadakata M. Yoshimura and T. Okubo. Millimeter-sized sodalite single crystals grown under high-temperature, high-pressure hydrothermal conditions. *Micropor. Mesopor. Mater.*, 42:229, 2001.
- [18] J.C. Buhl and J. Löns. Synthesis and crystal structure of nitrite encalhydrated sodalite. *J. Alloy. Comp.*, 235:41–47. 1996.
- [19] A. Stein. Verified syntheses of zeolitic materials. *Micropor. Mesopor. Mater.*, 22(46), 1998.
- [20] A. Dyer H. Enamy and R.P. Townsend. The Plotting and Interpretation of Ion Exchange Isotherms in Zeolite Systems. *Sep. Sci. Tech.*, 16(2):173–183, 1981.
- [21] S.I. Sandler. *Chemical and Engineering Thermodynamics*. John Wiley & Sons, New York, 2nd edition, 1989.
- [22] D.A. Skoog D.M. West and F.J. Holler. *Fundamentals of analytical chemistry*. Saunders College Pub., Fort Worth, 7th edition, 1996.
- [23] [<http://www.ccp14.ac.uk/>].
- [24] J. Laugier and B.Bochu. LMGP Suite of Programs for the interpretation of X-ray Experiments, 2000. [<http://www.ccp14.ac.uk/ccp/web-mirrors/lmgp-laugier-bochu/>].
- [25] W.KrausandG.NolzePowderCell, 2000. [http://www.ccp14.ac.uk/ccp/web-mirrors/powdcell/a_v/v_1/powder/e_cell.html].
- [26] Ch. Baerlocher. Zeolite Structure Refinements using Powder Data. *Zeolites*, 6:325, September 1986.
- [27] Keller L; Rask J; Buseck P;. PDF No.42-0215, Arizona State University, Tempe, Arizona, 1986.
- [28] R.M. Barrer and J.D. Falconer. *Ion exchange in feldspathoids as a solid-state reaction*, volume 236 of *Proceedings of the Royal Society of London*, pages 227–249. Mathematical and Physical Sciences, 1956.
- [29] J. Godber and G.A. Ozin. Cation Dynamics in Sodalite. *J. Phys. Chem.*, 92:2841–2849, 1988.

- [30] Ozin G.A; Stein A; Stucky G.D; Godber J.P;. *Inclusion Phenomena and Molecular Recognition*, J.Atwood, ed., pages 379–393. Plenum Press, New York, 1990.
- [31] R.D. Shannon. Revised effective ionic radii and systematic studies of distances in halides and chalcogenides. *Acta. Cryst.*, A32:751, 1976.



APPENDIX A

Synthesis Calculations

A.1 Synthesis Details

Table A.1: List of Samples Produced

Sample	Batch Weight (g)	Sample Weight (g)	Temp	Time
CLSOD-1	62.65	8.17	75	6
CLSOD-2	47.75	6.53	75	12
CLSOD-3	55.8	7.76	75	24
CLSOD-4	64.66	9.02	75	96
CLSOD-5	59.63	8.35	75	4
CLSOD-6	63.55	7.82	75	2
CLSOD-7	115.23	15.69	75	48
CLSOD-8	108.45	14.89	75	48
BSSOD-1	46.81	6.22	130	48
BSSOD-2	54.05	7.23	95	48
BSSOD-3	61.94	9.48	95	12
BSSOD-4	50.02	6.88	95	24
BSSOD-5	51.98	7.47	95	48
BSSOD-6	57.07	7.92	95	12
BSSOD-7	59.91	7.86	95	60
BSSOD-8	46.59	6.57	95	36
BSSOD-9	63.25	8.47	95	12
BSSOD-10	63.43	9.27	95	6
BSSOD-11	53.54	4.59	95	2
BSSOD-12	52.13	3.88	95	4
OXSOD-1	61.87	4.97	130	96
OXSOD-2	59.86	4.74	170	96

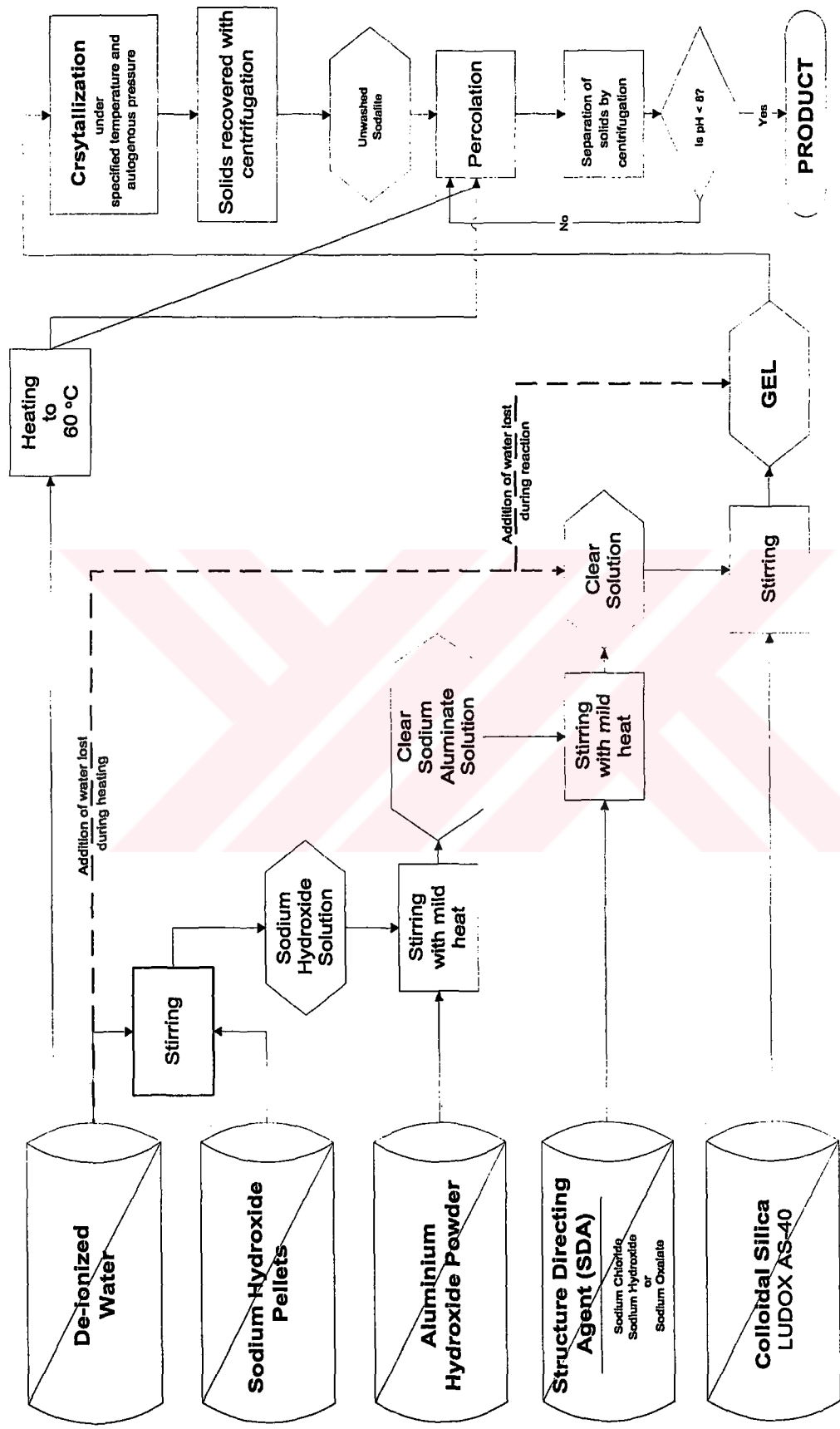
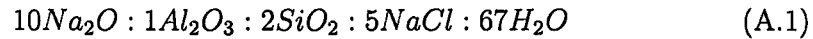


Figure A.1: Flowchart of Synthesis Procedure

A.2 Yield Calculations

Batch composition used for sodium chlorosodalite synthesis:



Molecular Weights of Components (g/gmole):

$$Na_2O \quad 61.98$$

$$Al_2O_3 \quad 101.96$$

$$SiO_2 \quad 60.08$$

$$NaCl \quad 58.44$$

$$H_2O \quad 18.01$$

Weight of Batch for 1 mole of Al_2O_3 :

$$61.98 \times 10 + 101.96 \times 1 + 60.08 \times 2 + 58.44 \times 5 + 18.01 \times 67 = 2340.8 \text{ g} \quad (A.2)$$

\Rightarrow Weight of Batch for 1 mole of Al:

$$\frac{2340.8}{2} = 1170.4 \text{ g} \quad (A.3)$$

Formula of Sodium Chlorosodalite: $Na_8[SiAlO_4]_6Cl_2$ (MW = 969.21 g/gmole)

6 Al atoms in structure

$$\Rightarrow 1 \text{ mole of Al} \equiv \frac{969.21}{6} = 161.53 \text{ g sodalite} \quad (A.4)$$

Using Eqn. 4.1 the maximum yield of chlorosodalite for batch composition given in A.1 can be found:

$$Yield = \frac{161.53 \text{ g}}{1170.4 \text{ g}} = 13.8 \text{ g}/100\text{g} \quad (A.5)$$

A.3 Miscellaneous Analysis Results for Sodium Sodalites

Table A.2: Chemical Composition of Sodium Chlorosodalite

Na	4.75 % wt
Na ₂ O	19.20 %wt
Al ₂ O ₃	20.39 %wt
SiO ₂	31.42 %wt
H ₂ O	14.25 %wt
Si/Al	1.31

Table A.3: Chemical Composition of Sodium Basic Sodalite

Na ₂ O	23.72 %wt
Al ₂ O ₃	28.34 %wt
SiO ₂	33.02 %wt
H ₂ O	17.25 %wt
Si/Al	0.989

Table A.4: Chemical Composition of Sodium Oxalate Sodalite

Na	5.50 % wt
Na ₂ O	22.23 %wt
Al ₂ O ₃	26.06 %wt
SiO ₂	30.51 %wt
H ₂ O	0.05 %wt
Si/Al	0.993

A.3.0.3 Thermal Gravimetric Analysis

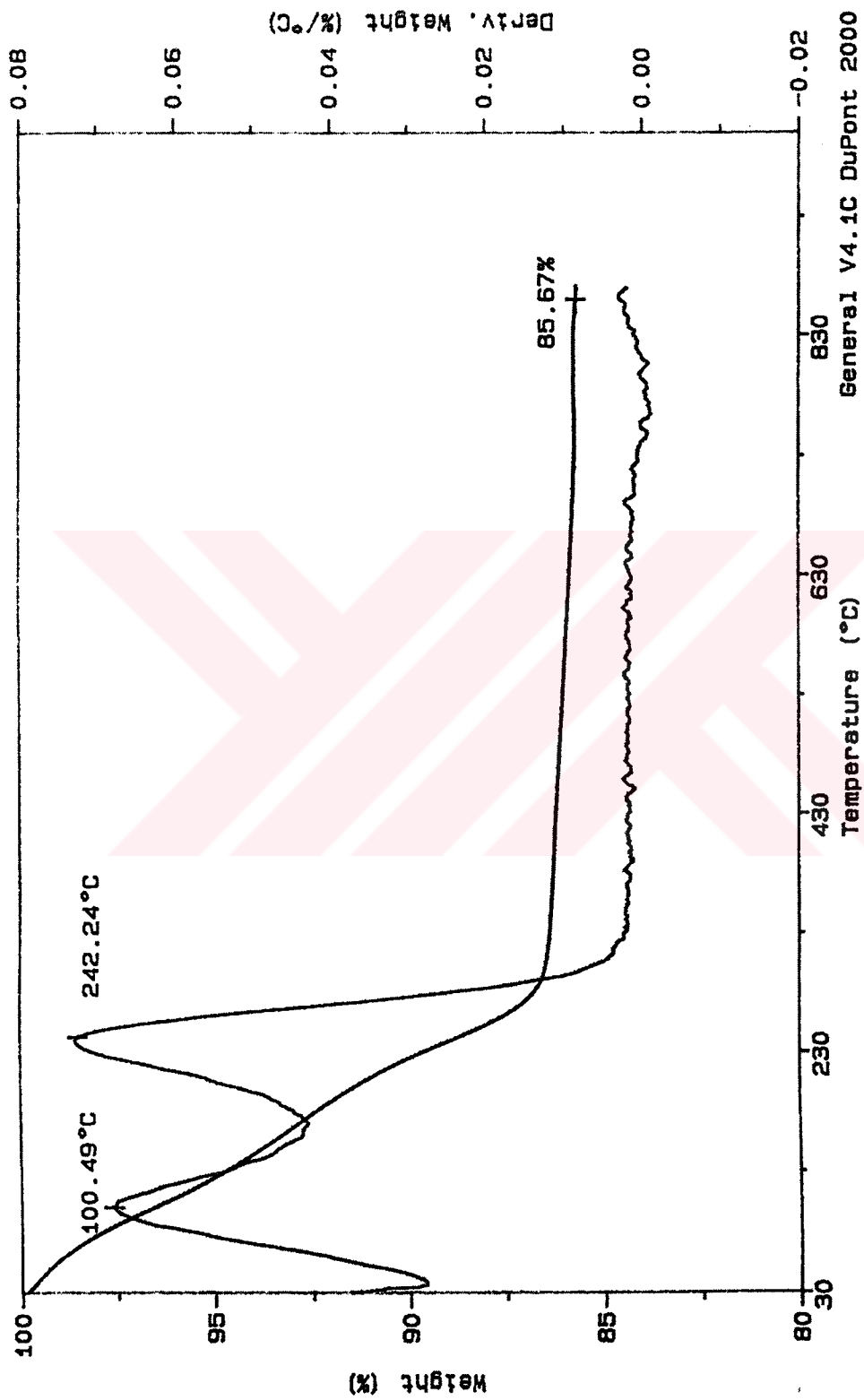


Figure A.2: TGA Scan of Sodium Chlorosodalite

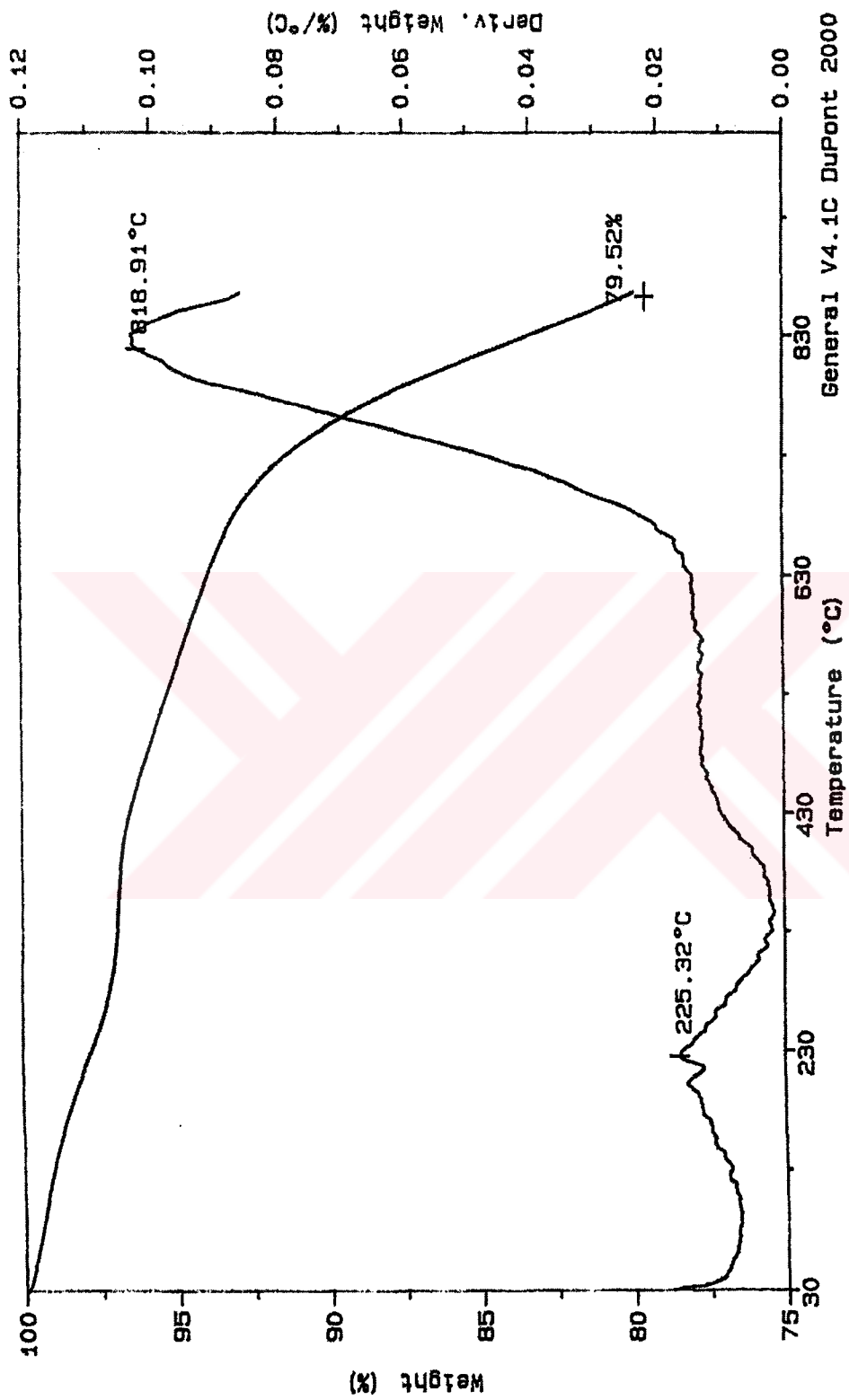


Figure A.3: TGA Scan of Sodium Basic Sodalite

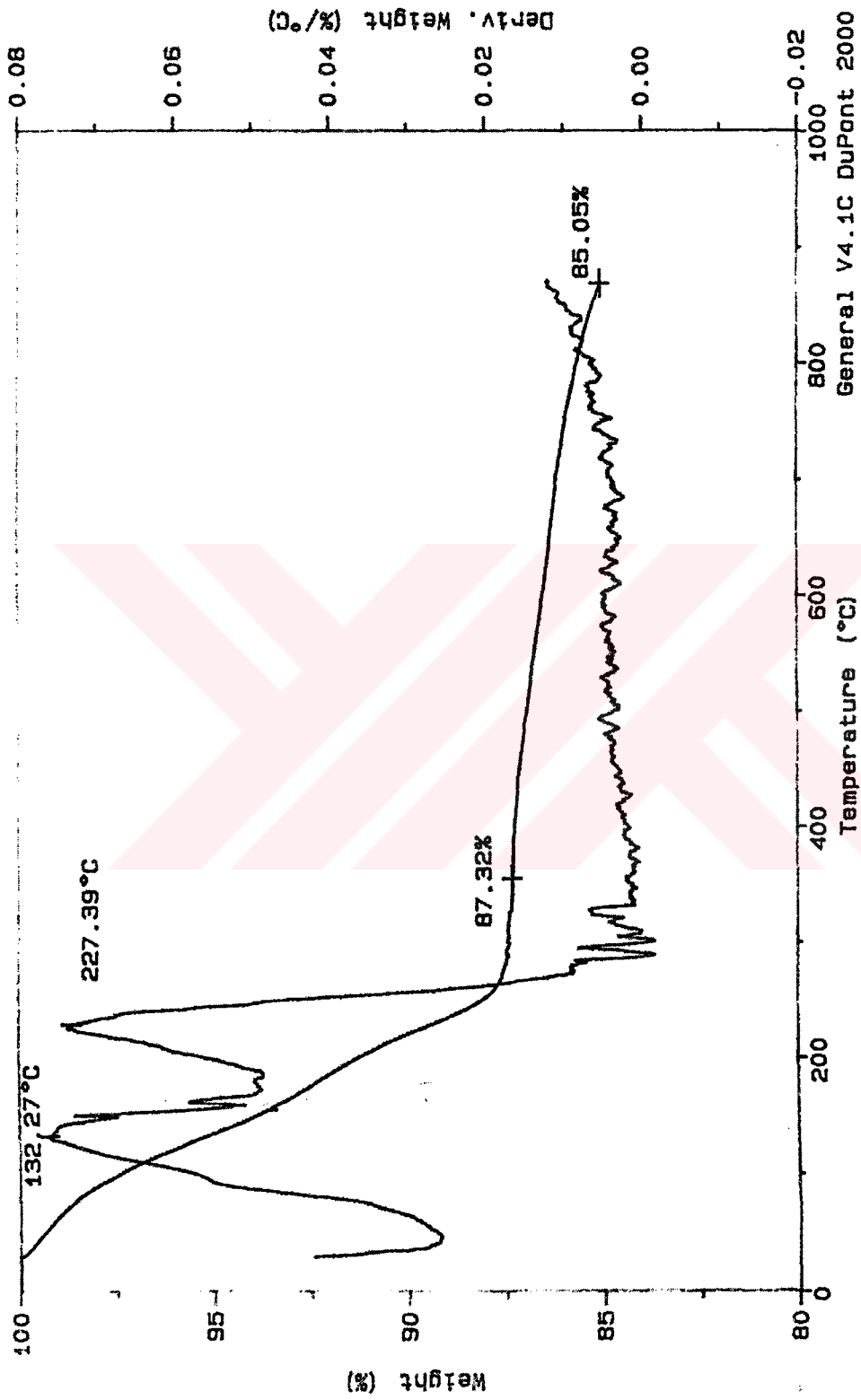


Figure A.4: TGA Scan of Sodium Oxalate Sodalite

A.3.0.4 Scanning Electron Micrographs

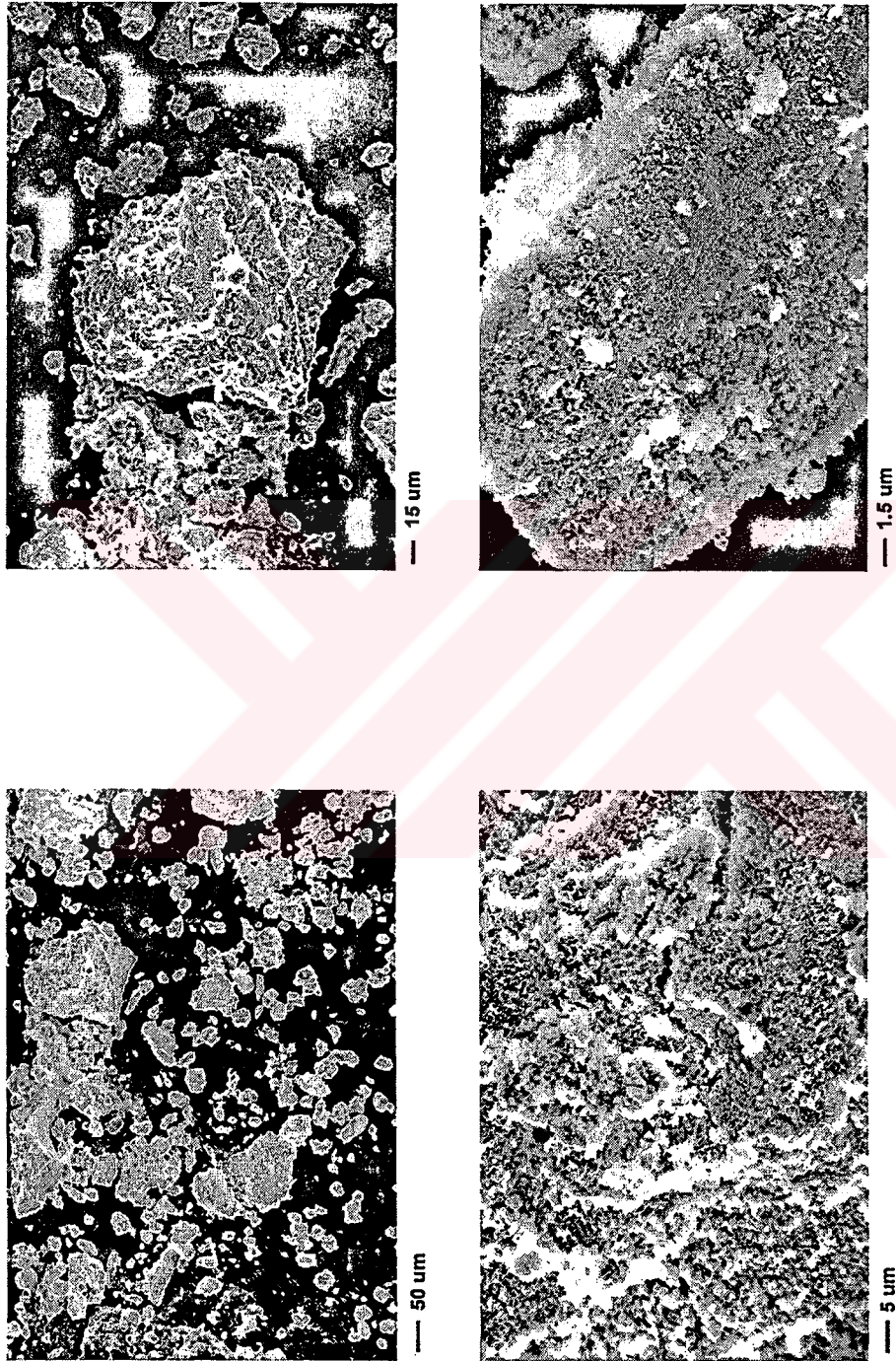
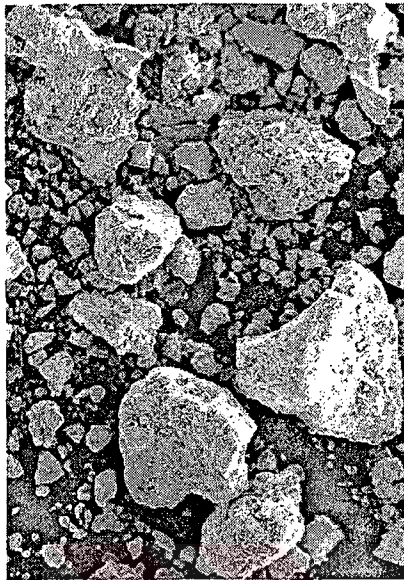
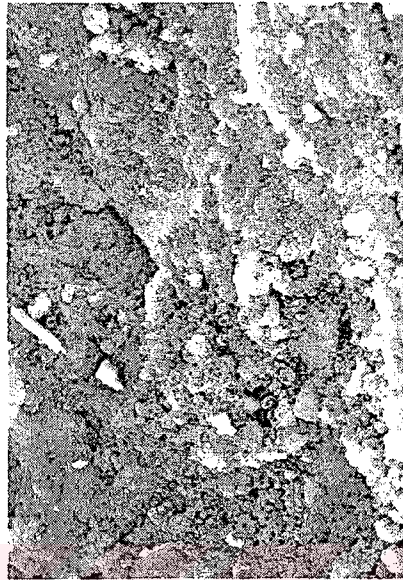


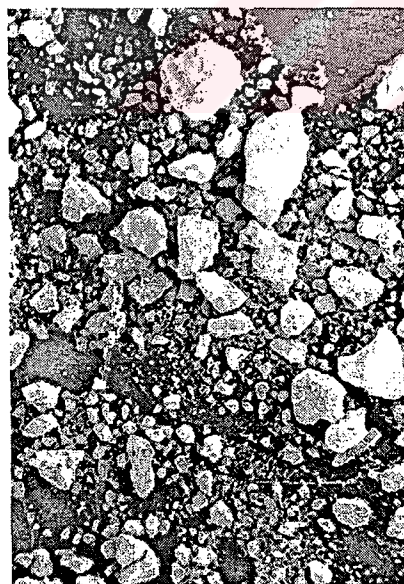
Figure A.5: SEM Images of Sodium Chlorosodalite
Magnifications (Clockwise from top left): 200, 500, 2000 and 6000 X.



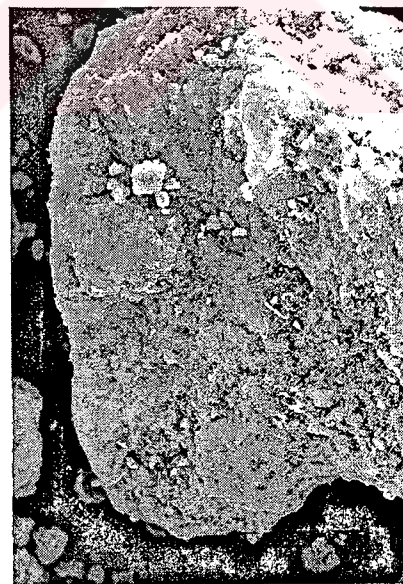
— 15 μm



— 1.5 μm

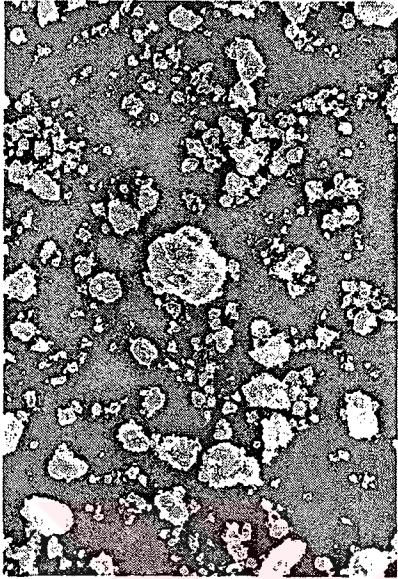


— 50 μm

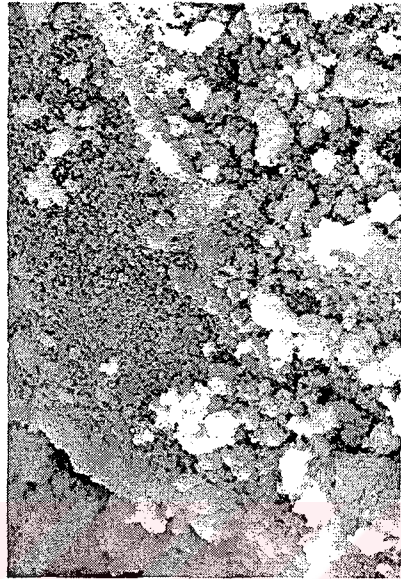


— 5 μm

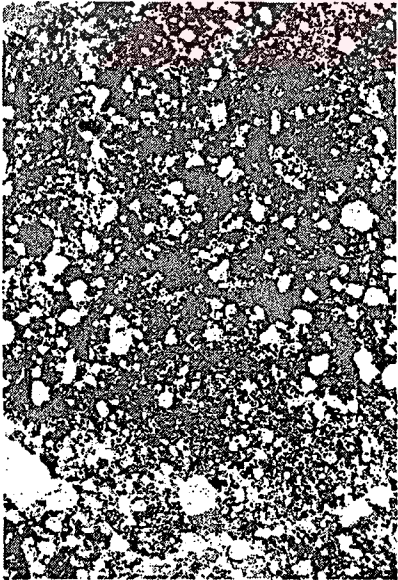
Figure A.6: SEM Images of Sodium Basic Sodalite
Magnifications (Clockwise from top left): 200, 500, 2000 and 6000 X.



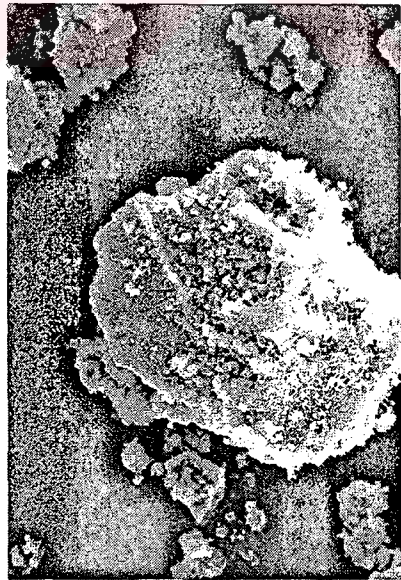
— 15 μm



— 1.5 μm



— 50 μm



— 5 μm

Figure A.7: SEM Images of Sodium Oxalate Sodalite
Magnifications (Clockwise from top left): 200, 500, 2000 and 6000 X.

APPENDIX B

Ion Exchange Calculations

B.1 Estimation of Mean Ionic Activities

The modified Debye-Hückel relation:

$$\ln \gamma_{\pm} = \frac{\alpha |z_+ z_-| \sqrt{\mu}}{1 + \beta a \sqrt{\mu}} \quad (\text{B.1})$$

where a is the ionic radius and μ is the ionic strength defined by:

$$\mu = 0.5 \sum_i z_i^2 M_i \quad (\text{B.2})$$

and is equal to 0.05 since the z_i are all unity and $\sum_i M_i$ is always constant at 0.1N

Table B.1: Values of Debye-Hückel Parameters at Relevant Temperatures

T (°C)	$\alpha (\sqrt{\text{mol/l}})$	$\beta [\sqrt{\text{mol/l}\text{\AA}}]^{-1}$
25	1.178	0.3291
50	1.237	0.3346
80	1.328	0.3426

Mean ionic radii[31] for $\text{Ag}^+ = 1.18 \text{\AA}$ and $\text{Na}^+ = 1.08 \text{\AA}$

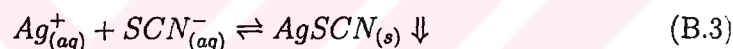
Table B.2: Calculated Mean Ionic Activity Coefficients

T (°C)	$\gamma_{\pm AgX}$	$\gamma_{\pm NaX}$	$\left(\frac{\gamma_{\pm NaX}}{\gamma_{\pm AgX}}\right)^2$
25	1.274(2)	1.276(3)	1.003(3)
50	1.289(3)	1.291(6)	1.003(5)
80	1.313(0)	1.315(5)	1.003(8)

B.2 Silver Determination in Solution

A variation of the Volhard Method [22] is used for silver determination. In this method the titrant is a 0.05 M KSCN solution and the indicator is a solution of $Fe(NO_3)_3$

The interaction of the titrant with Ag^+ is as follows:



The Fe^{3+} , which normally gives a yellowish hue, forms a complex with excess SCN^- turning the solution brick red:



The K_{sp} for reaction B.3 is $1.1e-12$ and the K_f of $Fe(SCN)^{2+}$ is $1.05e-12$ [22]. Hence, there is no $Fe(SCN)^{2+}$ formation until Ag^+ is depleted. The red color of $Fe(SCN)^{2+}$ is detectable when its concentration is $6.4e-6$ M. Hence the equivalence point is:

$$[Ag^+] = [SCN^-] + 6.4e - 6M \quad (B.5)$$

Thus for 0.01 M KSCN solution, 1 ml of titrant will be equivalent to 1.0787 mg Ag.

B.3 Experimental Data and Intermediate Calculations

A_Z and A_S values are calculated using titration data. At the end of equilibration, samples of 1 - 3 ml are taken from the reaction vessels and added to 20 ml of ~0.1M Iron(III)Nitrate solution. The sample size used is the same throughout each experiment and initially the standard 0.1N silver nitrate solution of the same sample size is titrated to obtain the blank titration. The subsequent results are treated as a ratio of the blank titration which is taken as the reference of 0.1N Ag^+ .

A sample calculation would be:
Ion exchange experiment at 25°C for chlorosodalite.

Weight of Sodalite used: 0.1 g

Molecular Weight of Sodium Chlorosodalite: 969.21 g/gmole

Moisture in chlorosodalite: 14.25% wt

Ag solution volume: 25 ml

Ag solution concentration: 0.1 mol/L

Blank titration: 39.37 ml

Titrant used: 29.05 ml

The capacity of the sodalite is:

$$Capacity(mol) = \frac{Weight\ used\ (g)}{M.Weight} \cdot \frac{100 - Moisture}{100} \cdot 8 \quad (B.6)$$

since there are 8 cations per formula unit. Hence:

$$Capacity(mol) = \frac{0.1\ g}{969.21\ g/mol} \cdot \frac{100 - 14.25}{100} \cdot 8 = 7.078 \times 10^{-4}\ mol \quad (B.7)$$

The final silver concentration in solution is given by:

$$[Ag^+]_{final} = 0.1M \cdot \frac{\text{Titrant used (ml)}}{\text{Blank titration (ml)}} \quad (\text{B.8})$$

therefore:

$$[Ag^+]_{final} = 0.1M \cdot \frac{29.05 \text{ ml}}{39.37 \text{ ml}} = 7.379 \times 10^{-2} M \quad (\text{B.9})$$

The vessel contains 25 ml of solution.

$$\Rightarrow Ag^+_{final} = 7.379 \times 10^{-2} \cdot 2.5 \times 10^{-2} L = 1.845 \times 10^{-3} mol \quad (\text{B.10})$$

Since the initial amount of Ag in solution was 0.0025 mol, $0.0025 - 1.845 \times 10^{-3} = 6.553 \times 10^{-4}$ moles of Ag were exchanged:

$$\frac{\text{Moles exchanged}}{\text{Capacity}} = \frac{6.553 \times 10^{-4} \text{ mol}}{7.078 \times 10^{-4} \text{ mol}} = 0.926 \quad (\text{B.11})$$

gives the ratio of sites occupied by Ag and also happens to be A_z by definition. $\Rightarrow A_z = 0.926$

Since for every Ag cation exchanged a Na cation is released, the total concentration of the solution is constant at 0.1M. Then by Eqn. 2.2,

$$A_s = \frac{[Ag^+]_{final}}{0.1 M} = \frac{7.379 \times 10^{-2} M}{0.1 M} = 0.738 \quad (\text{B.12})$$

The following tables summarize the above calculations for all experiments.

Table B.3: Experimental Data and Intermediate Calculations for Chlorosodalite Isotherm at 25°C

Sample Weight (g)	Blank Titration (ml)	Titrant Used (ml)	Capacity of sodalite (mol)	Initial Ag in Solution (mol)	Ag Exchanged (mol)	Final Ag in Solution (mol)	Final Ag Occupancy (mol)	As	Az	K_N^A	$\text{Log } K_N^A$
0.05	39.37	33.82	3.843E-04	0.0025	3.524E-04	2.148E-03	3.524E-04	0.859	0.917	1.81	0.26
0.1	39.37	29.05	7.078E-04	0.0025	6.553E-04	1.845E-03	6.553E-04	0.738	0.926	4.44	0.65
0.2	39.37	20.86	1.274E-03	0.0025	1.175E-03	1.325E-03	1.175E-03	0.530	0.923	10.57	1.02
0.3	39.37	10.8	2.031E-03	0.0025	1.814E-03	6.858E-04	1.814E-03	0.274	0.893	22.10	1.34
0.5	39.37	0.86	3.539E-03	0.0025	2.445E-03	5.461E-05	2.445E-03	0.022	0.691	100.13	2.00
1.0	39.37	0.21	7.078E-03	0.0025	2.487E-03	1.334E-05	2.487E-03	0.005	0.351	101.00	2.00

Table B.4: Experimental Data and Intermediate Calculations for Chlorosodalite Isotherm at 50°C

Sample Weight (g)	Blank Titration (ml)	Titrant Used (ml)	Capacity of sodalite (mol)	Initial Ag in Solution (mol)	Ag Exchanged (mol)	Final Ag in Solution (mol)	Final Ag Occupancy (mol)	As	Az	K_N^A	$\text{Log } K_N^A$
0.05	40.02	34.78	3.539E-04	0.0025	3.273E-04	2.173E-03	3.273E-04	0.869	0.925	1.86	0.27
0.1	40.02	29.49	7.078E-04	0.0025	6.578E-04	1.842E-03	6.578E-04	0.737	0.929	4.70	0.67
0.3	40.02	9.16	2.123E-03	0.0025	1.928E-03	5.722E-04	1.928E-03	0.229	0.908	33.21	1.52
0.5	40.02	0.84	3.539E-03	0.0025	2.448E-03	5.247E-05	2.448E-03	0.021	0.692	104.60	2.02
1.0	40.02	0.195	7.078E-03	0.0025	2.488E-03	1.218E-05	2.488E-03	0.005	0.351	110.69	2.04

Table B.5: Experimental Data and Intermediate Calculations for Chlorosodalite Isotherm at 80°C

Sample Weight (g)	Blank Titration (ml)	Titrant Used (ml)	Capacity of sodalite (mol)	Initial Ag in Solution (mol)	Ag Exchanged (mol)	Final Ag in Solution (mol)	Final Ag Occupancy (mol)	As	Az	K_N^A	Log K_N^A
0.05	58.52	50.98	3.468E-04	0.0025	3.221E-04	2.178E-03	3.221E-04	0.871	0.929	1.93	0.29
0.1	58.52	43.02	7.078E-04	0.0025	6.622E-04	1.838E-03	6.622E-04	0.735	0.936	5.23	0.72
0.3	58.52	15.5	2.017E-03	0.0025	1.838E-03	6.622E-04	1.838E-03	0.265	0.911	28.44	1.45
0.5	58.52	1.2	3.539E-03	0.0025	2.449E-03	5.126E-05	2.449E-03	0.021	0.692	107.29	2.03
1.0	58.52	0.28	7.078E-03	0.0025	2.488E-03	1.196E-05	2.488E-03	0.005	0.352	112.75	2.05

Table B.6: Experimental Data and Intermediate Calculations for Basic Sodalite Isotherm at 25°C

Sample Weight (g)	Blank Titration (ml)	Titrant Used (ml)	Capacity of sodalite (mol)	Initial Ag in Solution (mol)	Ag Exchanged (mol)	Final Ag in Solution (mol)	Final Ag Occupancy (mol)	As	Az	K_N^A	Log K_N^A
0.1	19.26	13.50	7.790E-04	0.0025	7.477E-04	1.752E-03	7.477E-04	0.701	0.960	10.16	1.01
0.2	19.26	8.25	1.558E-03	0.0025	1.429E-03	1.071E-03	1.429E-03	0.428	0.917	14.79	1.17
0.3	19.26	3.60	2.337E-03	0.0025	2.033E-03	4.673E-04	2.033E-03	0.187	0.870	29.05	1.46
0.4	19.26	1.09	3.116E-03	0.0025	2.359E-03	1.415E-04	2.359E-03	0.057	0.757	51.89	1.72
0.5	19.26	0.30	3.895E-03	0.0025	2.461E-03	3.894E-05	2.461E-03	0.016	0.632	108.45	2.04
1	19.26	0.05	7.790E-03	0.0025	2.494E-03	6.490E-06	2.494E-03	0.003	0.320	180.86	2.26

Table B.7: Experimental Data and Intermediate Calculations for Basic Sodalite Isotherm at 50°C

Sample Weight (g)	Blank Titration (ml)	Titrant Used (ml)	Capacity of sodalite (mol)	Initial Ag in Solution (mol)	Ag Exchanged (mol)	Final Ag in Solution (mol)	Final Ag Occupancy (mol)	As	Az	K_N^A	Log K_N^A
0.05	39.37	33.32	3.895E-04	0.0025	3.842E-04	2.116E-03	3.842E-04	0.846	0.986	13.04	1.12
0.1	39.37	27.4	7.790E-04	0.0025	7.601E-04	1.740E-03	7.601E-04	0.696	0.976	17.52	1.24
0.3	39.37	6.95	2.337E-03	0.0025	2.059E-03	4.413E-04	2.059E-03	0.177	0.881	34.49	1.54
0.5	39.37	0.41	3.895E-03	0.0025	2.474E-03	2.604E-05	2.474E-03	0.010	0.635	165.41	2.22
1	39.37	0.06	7.790E-03	0.0025	2.496E-03	3.810E-06	2.496E-03	0.002	0.320	308.90	2.49

Table B.8: Experimental Data and Intermediate Calculations for Basic Sodalite Isotherm at 80°C

Sample Weight (g)	Blank Titration (ml)	Titrant Used (ml)	Capacity of sodalite (mol)	Initial Ag in Solution (mol)	Ag Exchanged (mol)	Final Ag in Solution (mol)	Final Ag Occupancy (mol)	As	Az	K_N^A	Log K_N^A
0.05	39.86	33.87	3.895E-04	0.0025	3.757E-04	2.124E-03	3.757E-04	0.850	0.964	4.80	0.68
0.1	39.86	27.83	7.790E-04	0.0025	7.545E-04	1.745E-03	7.545E-04	0.698	0.969	13.30	1.12
0.3	39.86	7.23	2.337E-03	0.0025	2.047E-03	4.535E-04	2.047E-03	0.181	0.876	31.78	1.50
0.5	39.86	0.52	3.895E-03	0.0025	2.467E-03	3.261E-05	2.467E-03	0.013	0.633	130.73	2.12
1	39.86	0.08	7.790E-03	0.0025	2.495E-03	5.018E-06	2.495E-03	0.002	0.320	234.28	2.37

Table B.9: Experimental Data and Intermediate Calculations for Oxalate Sodalite Isotherm at 25°C

Sample Weight (g)	Blank Titration (ml)	Titrant Used (ml)	Capacity of sodalite (mol)	Initial Ag in Solution (mol)	Ag Exchanged (mol)	Final Ag in Solution (mol)	Final Ag Occupancy (mol)	As	Az	K_N^A	$\text{Log } K_N^A$
0.1	39.25	33.2	3.982E-04	0.0025	3.854E-04	2.115E-03	3.854E-04	0.846	0.968	5.47	0.74
0.1	39.25	27.22	7.964E-04	0.0025	7.662E-04	1.734E-03	7.662E-04	0.694	0.962	11.24	1.05
0.3	39.25	7.84	2.389E-03	0.0025	2.001E-03	4.994E-04	2.001E-03	0.200	0.837	20.63	1.31
0.5	39.25	1.64	3.982E-03	0.0025	2.396E-03	1.045E-04	2.396E-03	0.042	0.602	34.63	1.54
1.0	39.25	0.3	7.964E-03	0.0025	2.481E-03	1.911E-05	2.481E-03	0.008	0.312	58.75	1.77

Table B.10: Experimental Data and Intermediate Calculations for Oxalate Sodalite Isotherm at 50°C

Sample Weight (g)	Blank Titration (ml)	Titrant Used (ml)	Capacity of sodalite (mol)	Initial Ag in Solution (mol)	Ag Exchanged (mol)	Final Ag in Solution (mol)	Final Ag Occupancy (mol)	As	Az	K_N^A	$\text{Log } K_N^A$
0.1	41.08	34.72	3.982E-04	0.0025	3.870E-04	2.113E-03	3.870E-04	0.845	0.972	6.37	0.80
0.1	41.08	28.43	7.964E-04	0.0025	7.698E-04	1.730E-03	7.698E-04	0.692	0.967	12.91	1.11
0.3	41.08	8.06	2.389E-03	0.0025	2.009E-03	4.905E-04	2.009E-03	0.196	0.841	21.69	1.34
0.5	41.08	1.65	3.982E-03	0.0025	2.400E-03	1.004E-04	2.400E-03	0.040	0.603	36.24	1.56
1.0	41.08	0.345	7.964E-03	0.0025	2.479E-03	2.100E-05	2.479E-03	0.008	0.311	53.37	1.73

Table B.11: Experimental Data and Intermediate Calculations for Oxalate Sodalite Isotherm at 80°C

Sample Weight (g)	Blank Titration (ml)	Titrant Used (ml)	Capacity of sodalite (mol)	Initial Ag in Solution (mol)	Ag Exchanged (mol)	Final Ag in Solution (mol)	Final Ag Occupancy (mol)	As	Az	K_N^A	$\text{Log } K_N^A$
0.1	39.64	33.46	3.982E-04	0.0025	3.898E-04	2.110E-03	3.898E-04	0.844	0.979	8.54	0.93
0.1	39.64	27.26	7.964E-04	0.0025	7.808E-04	1.719E-03	7.808E-04	0.688	0.980	22.73	1.36
0.3	39.64	6.9	2.389E-03	0.0025	2.065E-03	4.352E-04	2.065E-03	0.174	0.864	30.21	1.48
0.5	39.64	1.46	3.982E-03	0.0025	2.408E-03	9.208E-05	2.408E-03	0.037	0.605	40.01	1.60
1.0	39.64	0.31	7.964E-03	0.0025	2.480E-03	1.955E-05	2.480E-03	0.008	0.311	57.39	1.76

B.4 Kielland Plots for Sodalite

Table B.12: Integration Results for Kielland Plots

	$\int_0^1 \log K_N^A dA_Z$		
	25°C	50°C	80°C
Chlorosodalite	1.796	1.823	1.842
Basic Sodalite	1.965	2.048	2.181
Oxalate Sodalite	1.539	1.54	1.617

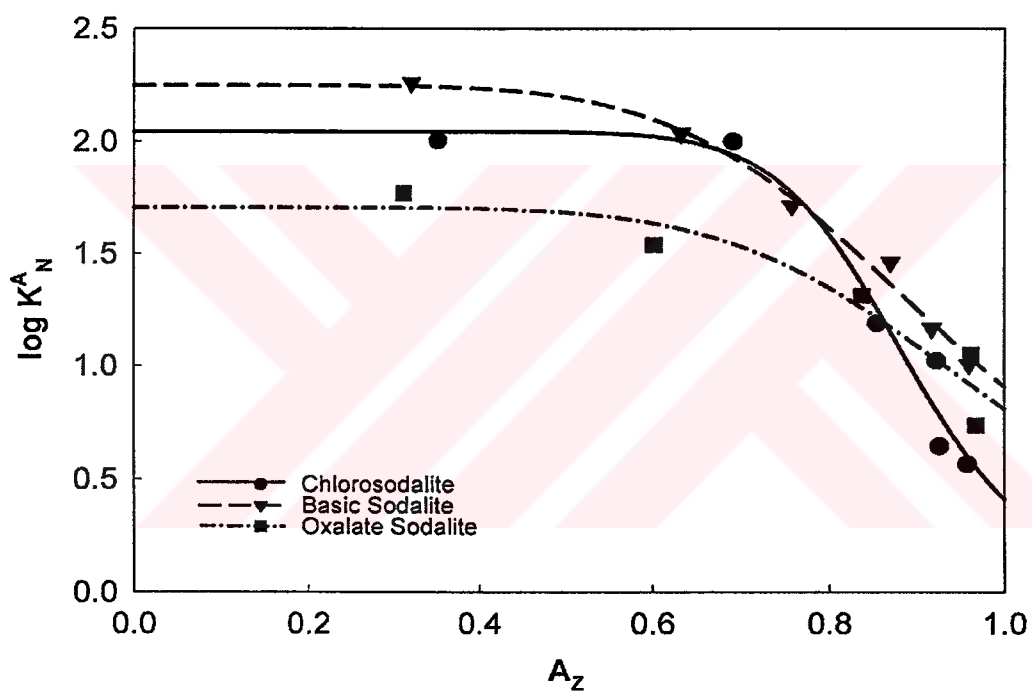


Figure B.1: Kielland Plots for Sodalites at 25°C

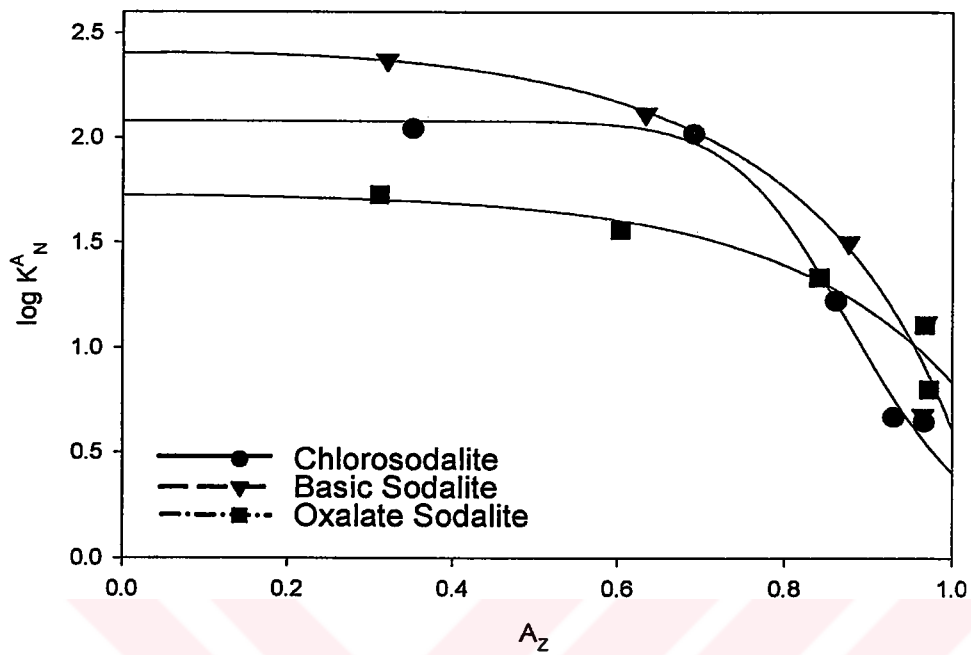


Figure B.2: Kielland Plots for Sodalites at 50°C

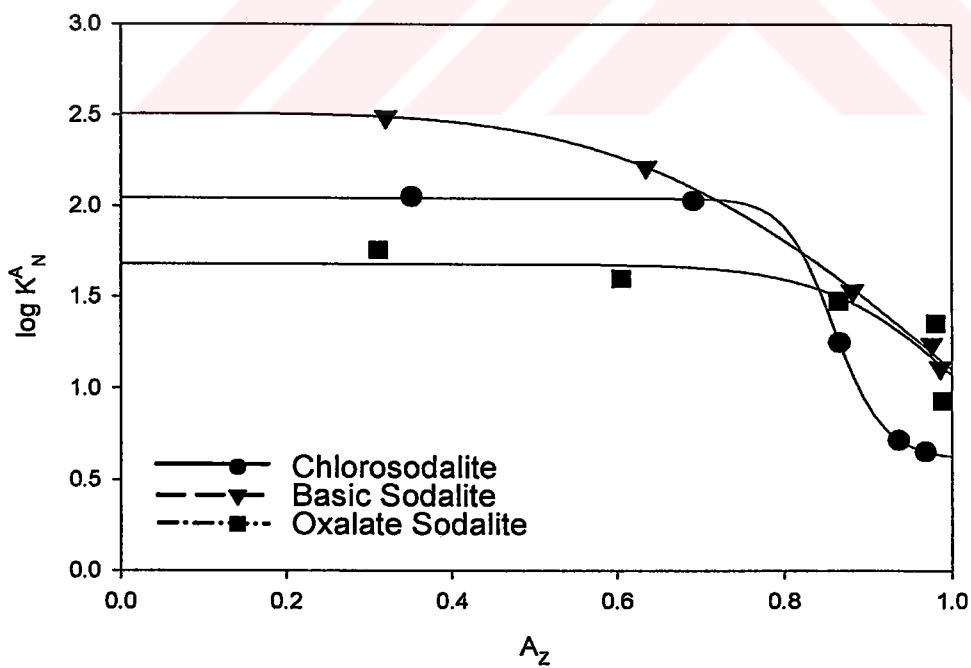


Figure B.3: Kielland Plots for Sodalites at 80°C

B.5 Miscellaneous Analysis Results for Silver Sodalites

B.5.0.5 Thermal Gravimetric Analysis

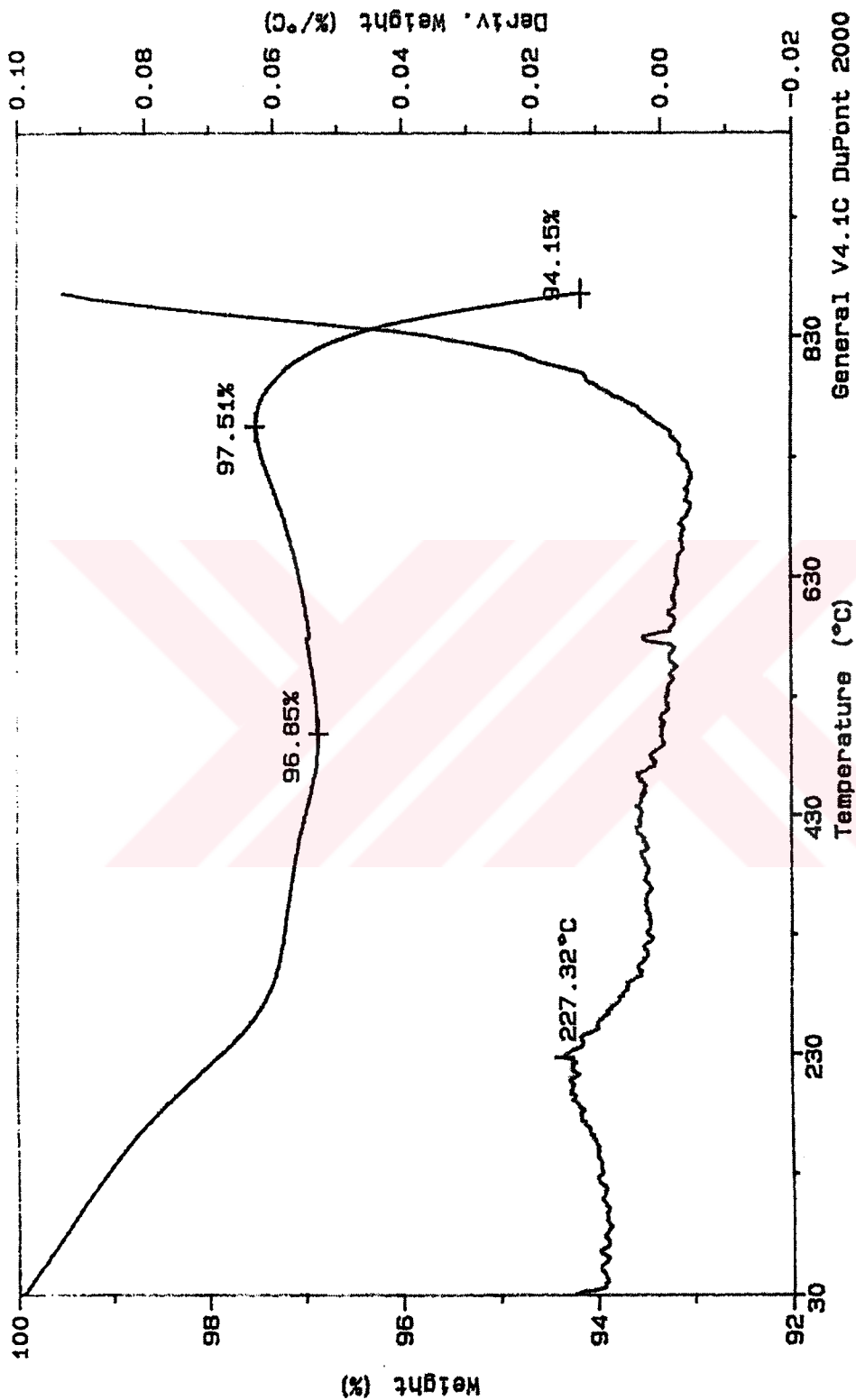


Figure B.4: TGA Scan of Silver Chlorosodalite

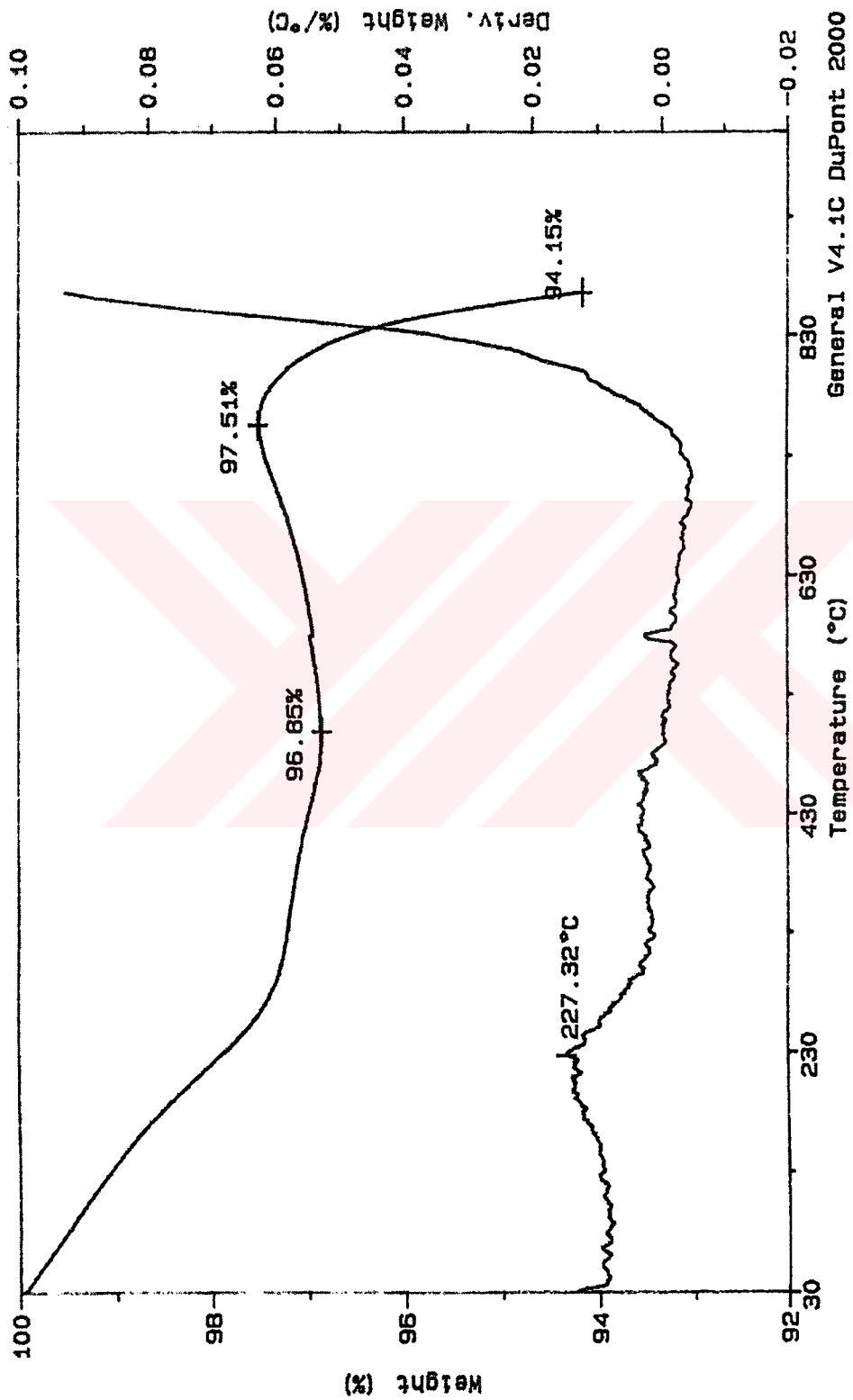


Figure B.4: TGA Scan of Silver Chlorosodalite

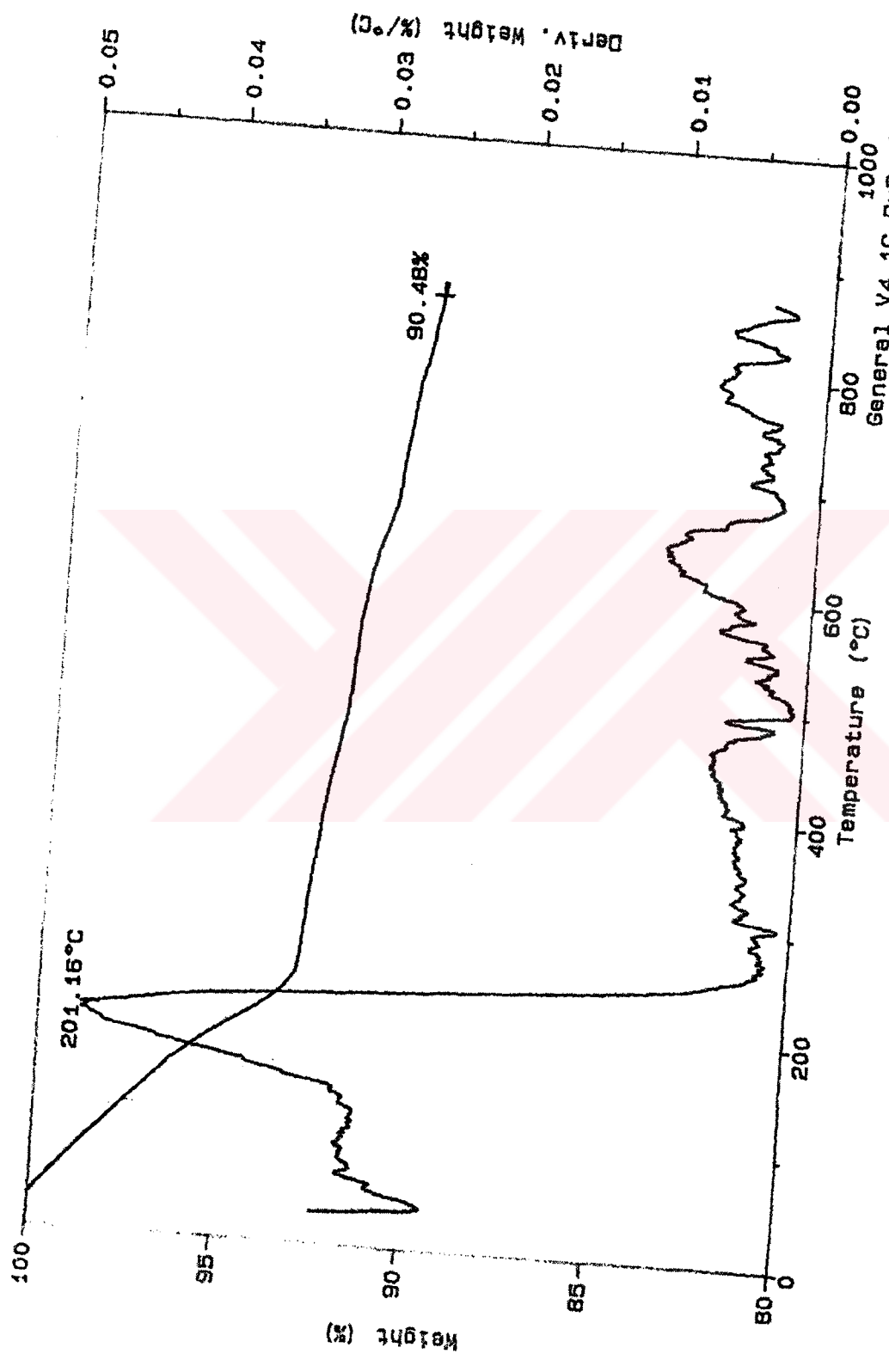


Figure B.5: TGA Scan of Silver Basic Sodalite

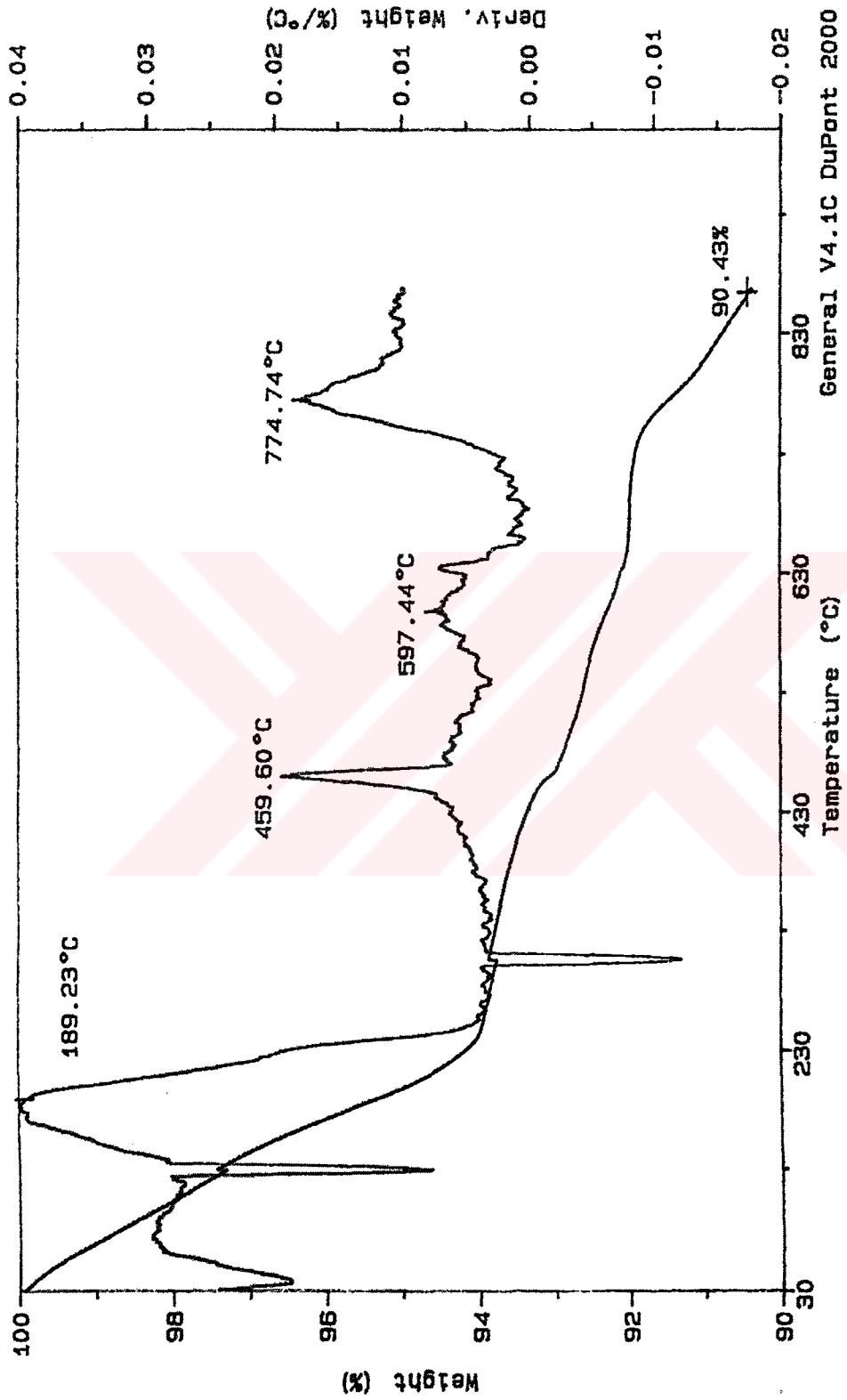


Figure B.6: TGA Scan of Silver Oxalate Sodalite

B.5.0.6 Scanning Electron Micrographs

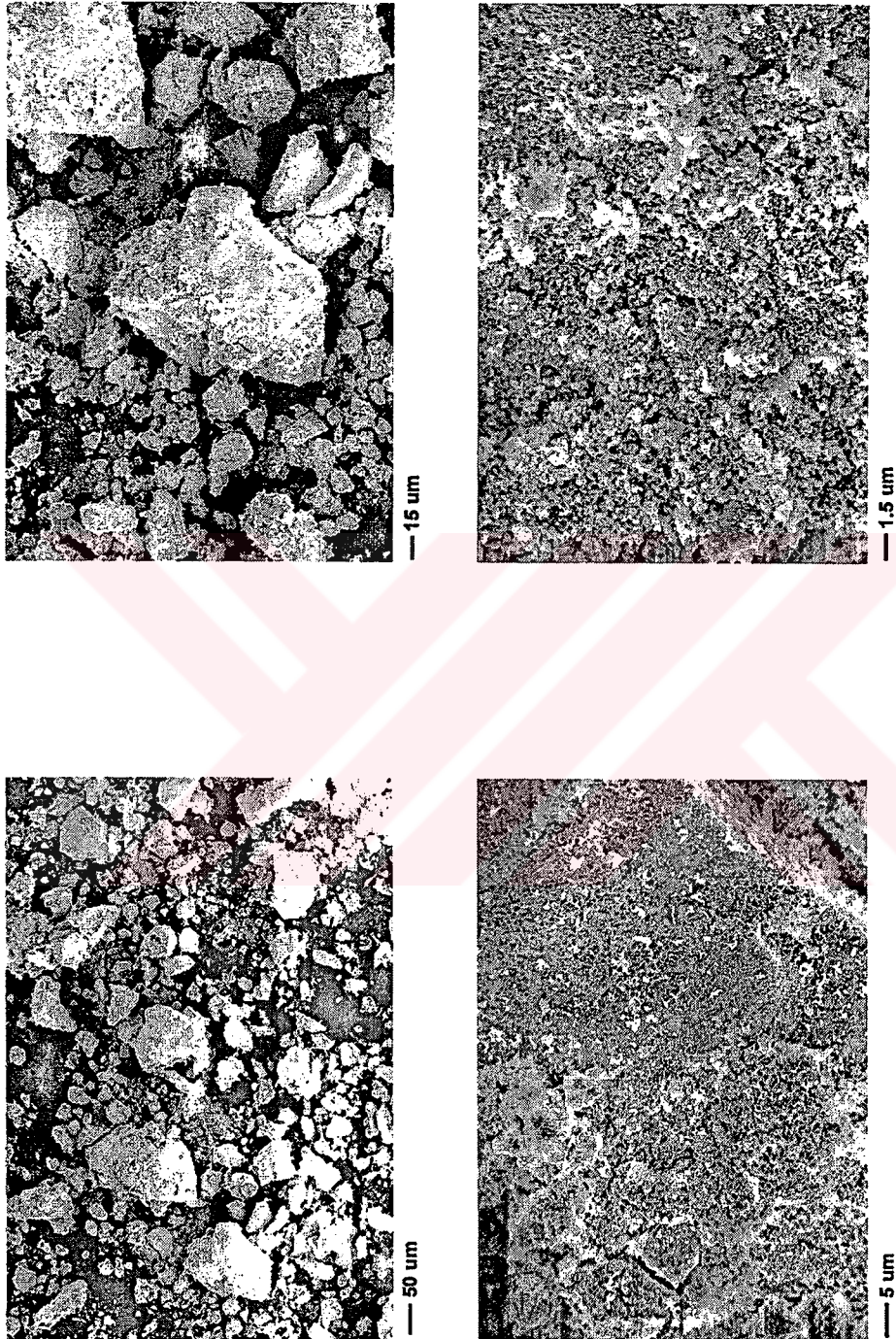
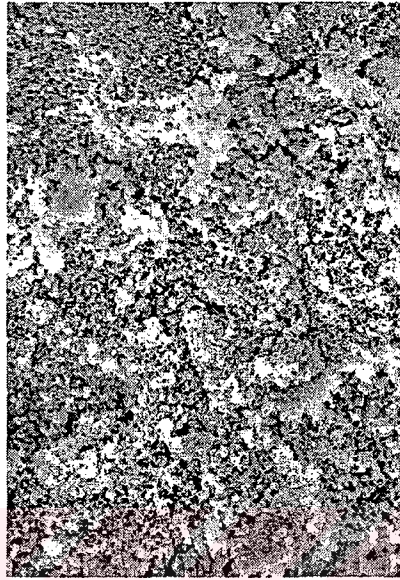


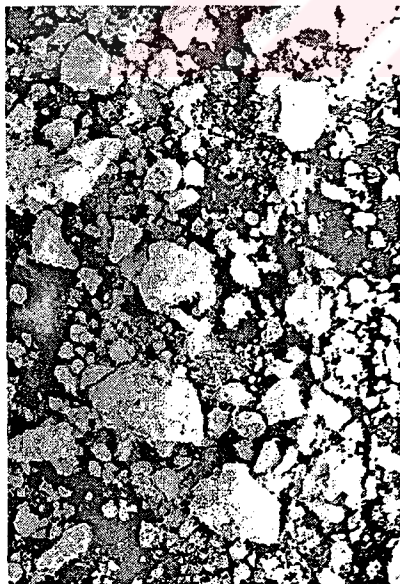
Figure B.7: SEM Images of Silver Chlorosodalite
Magnifications (Clockwise from top left): 200, 500, 2000 and 6000 X.



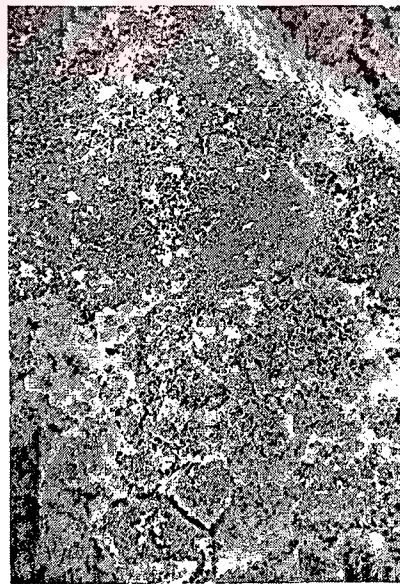
— 15 μm



— 1.5 μm



— 50 μm



— 5 μm

Figure B.7: SEM Images of Silver Chlorosodalite
Magnifications (Clockwise from top left): 200, 500, 2000 and 6000 X.

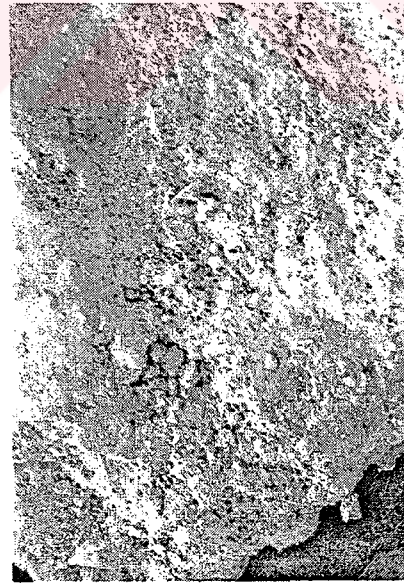
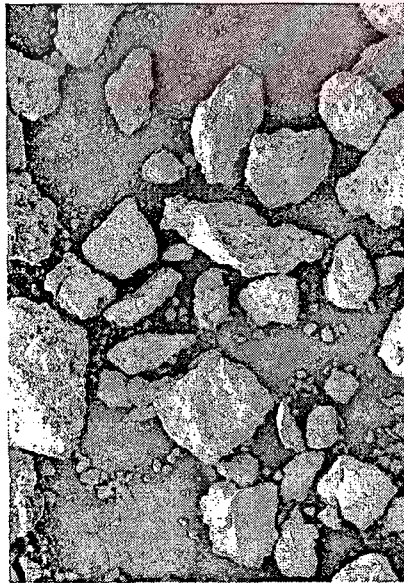
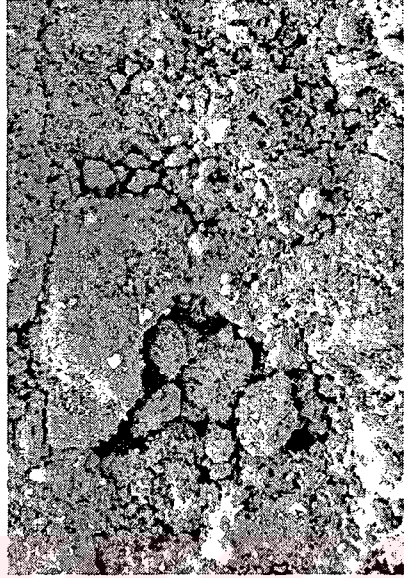
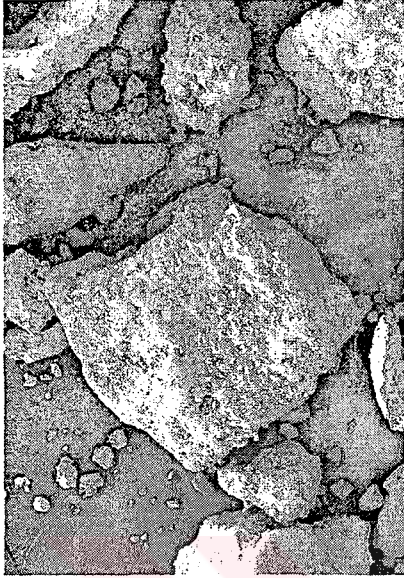


Figure B.8: SEM Images of Silver Basic Sodalite
Magnifications (Clockwise from top left): 200, 500, 2000 and 6000 X.

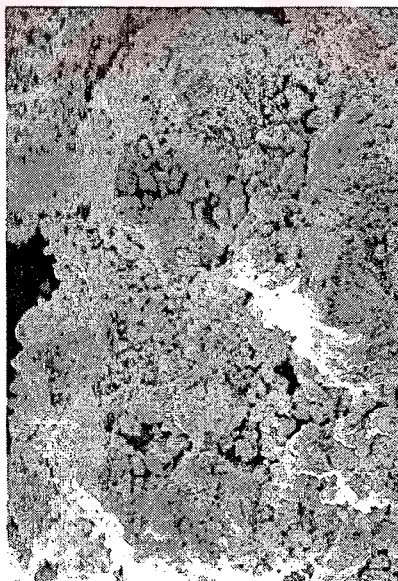
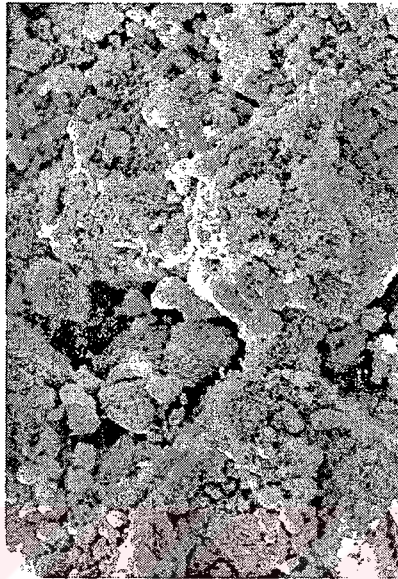
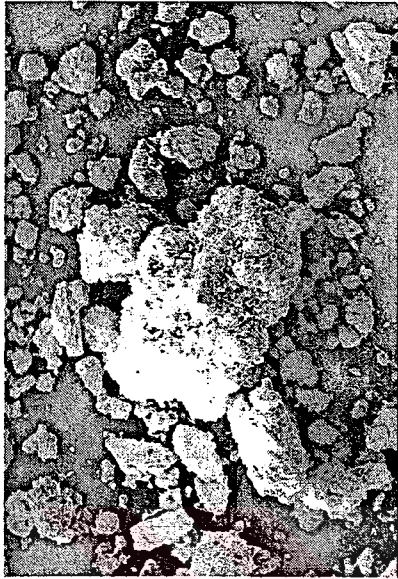


Figure B.9: SEM Images of Silver Oxalate Sodalite
Magnifications (Clockwise from top left): 200, 500, 2000 and 6000 X.

APPENDIX C

X-Ray Diffraction and Structure Determination

Calculations

C.1 Crystallinity Measurements

Crystallinity measurement is done by preparing standards of known relative crystallinity. These standards are obtained by mixing 20, 40, 60, 80 % wt powder mixtures of the most crystalline sample with an amorphous aluminosilicate material used for zeolite synthesis (Zeolex).

The XRD patterns in Figures C.1 and C.3 give the change in observed peak intensities and shapes with different amounts of amorphous material. Figures C.2 and C.4 give the calibration graphs obtained from these patterns by plotting the sum of peak intensities against crystallinity.

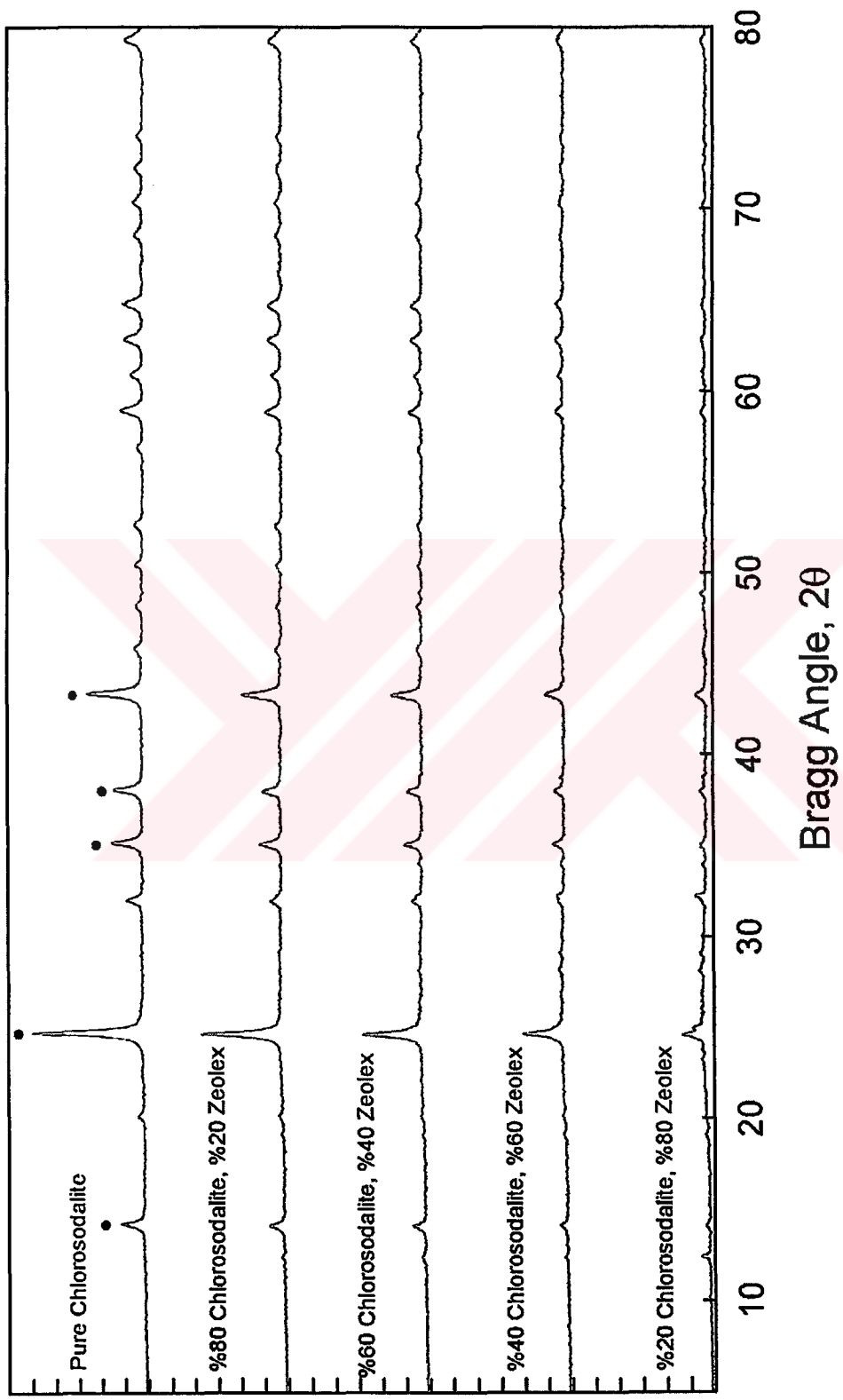


Figure C.1: XRD Patterns of Crystallinity References for Chlorosodalite

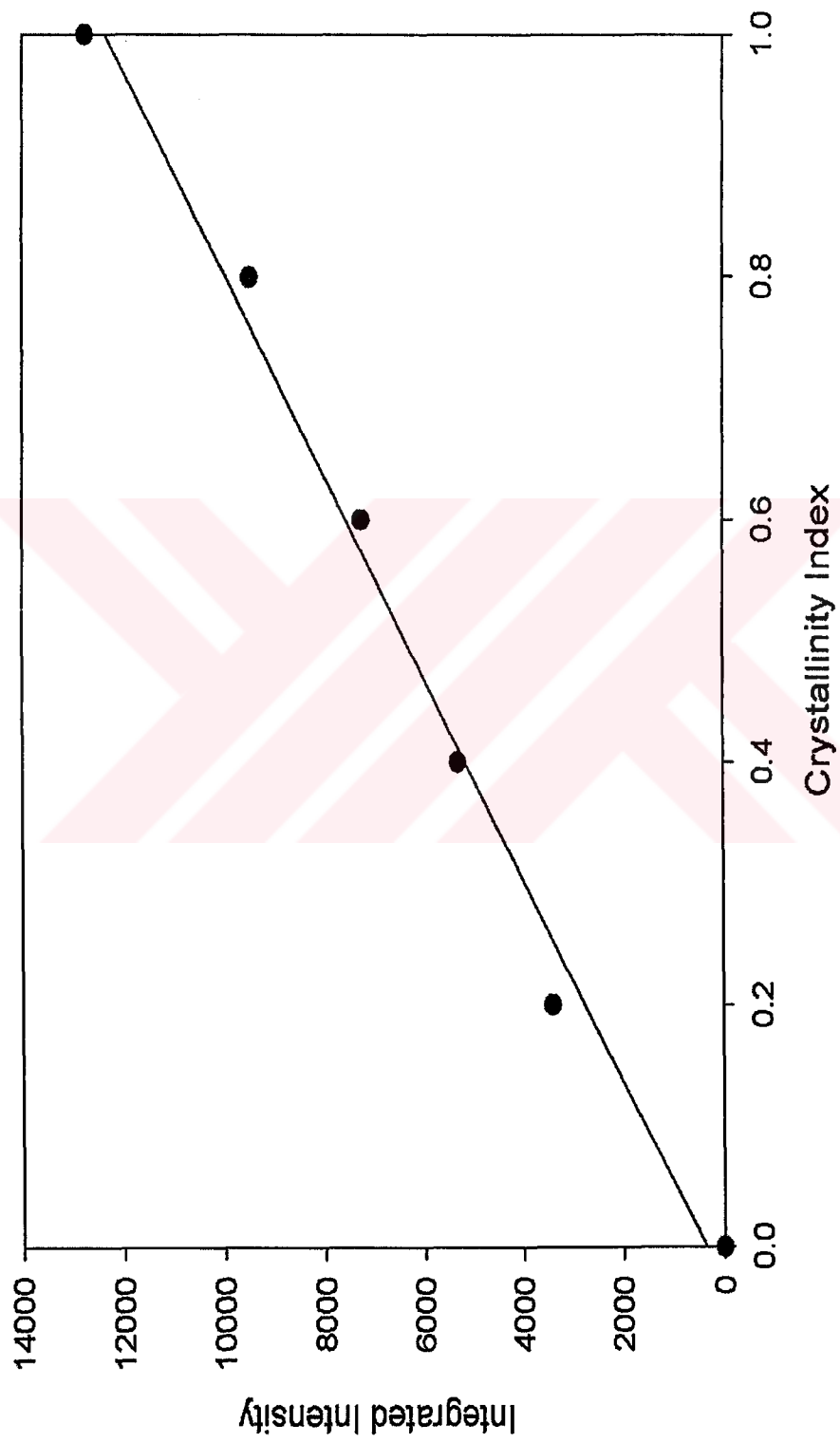


Figure C.2: Crystallinity Index versus Integrated Peak Intensities for Chlorosodalite

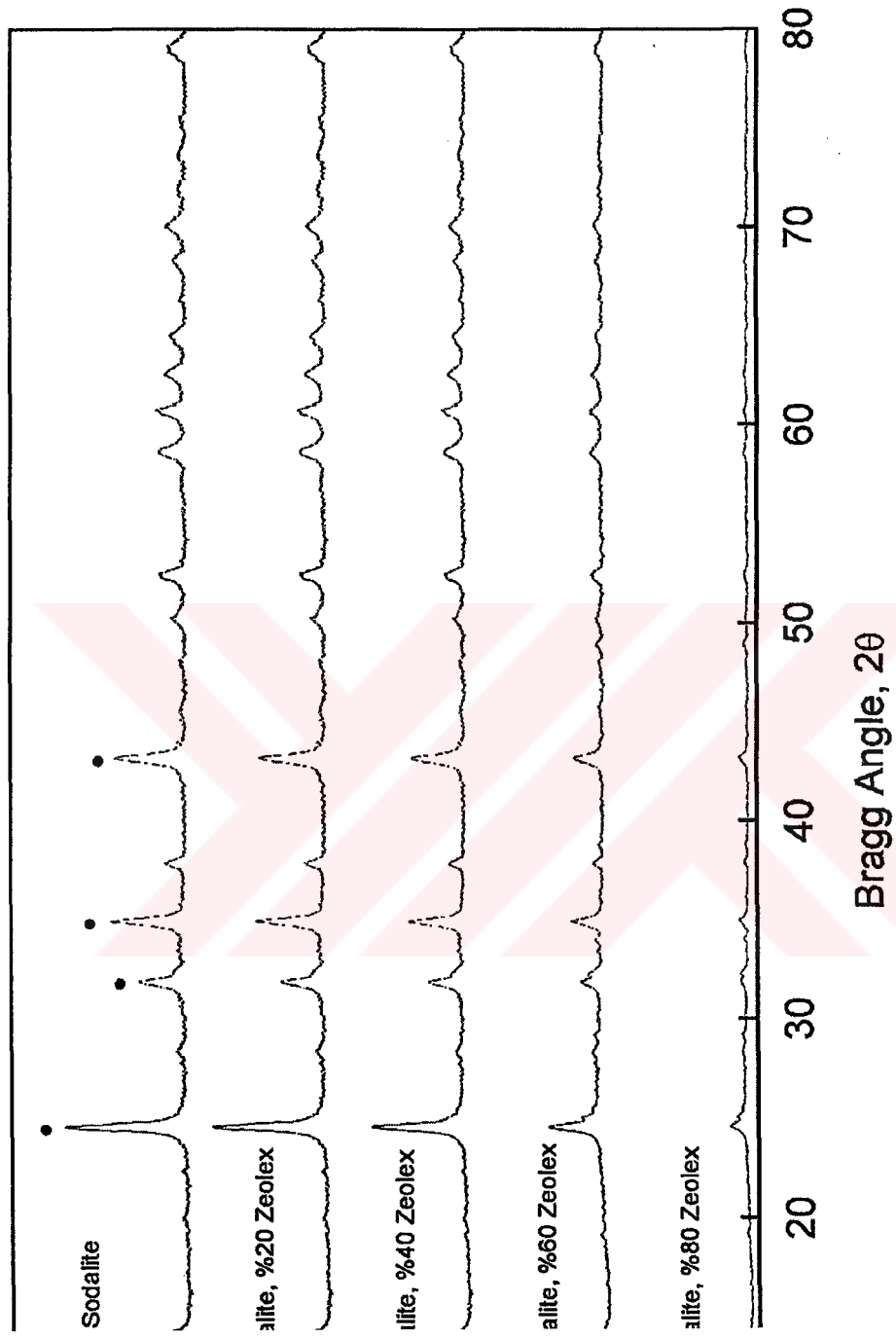


Figure C.3: XRD Patterns of Crystallinity References for Basic Sodalite
 The peaks used for integrated intensities are marked with •'s.

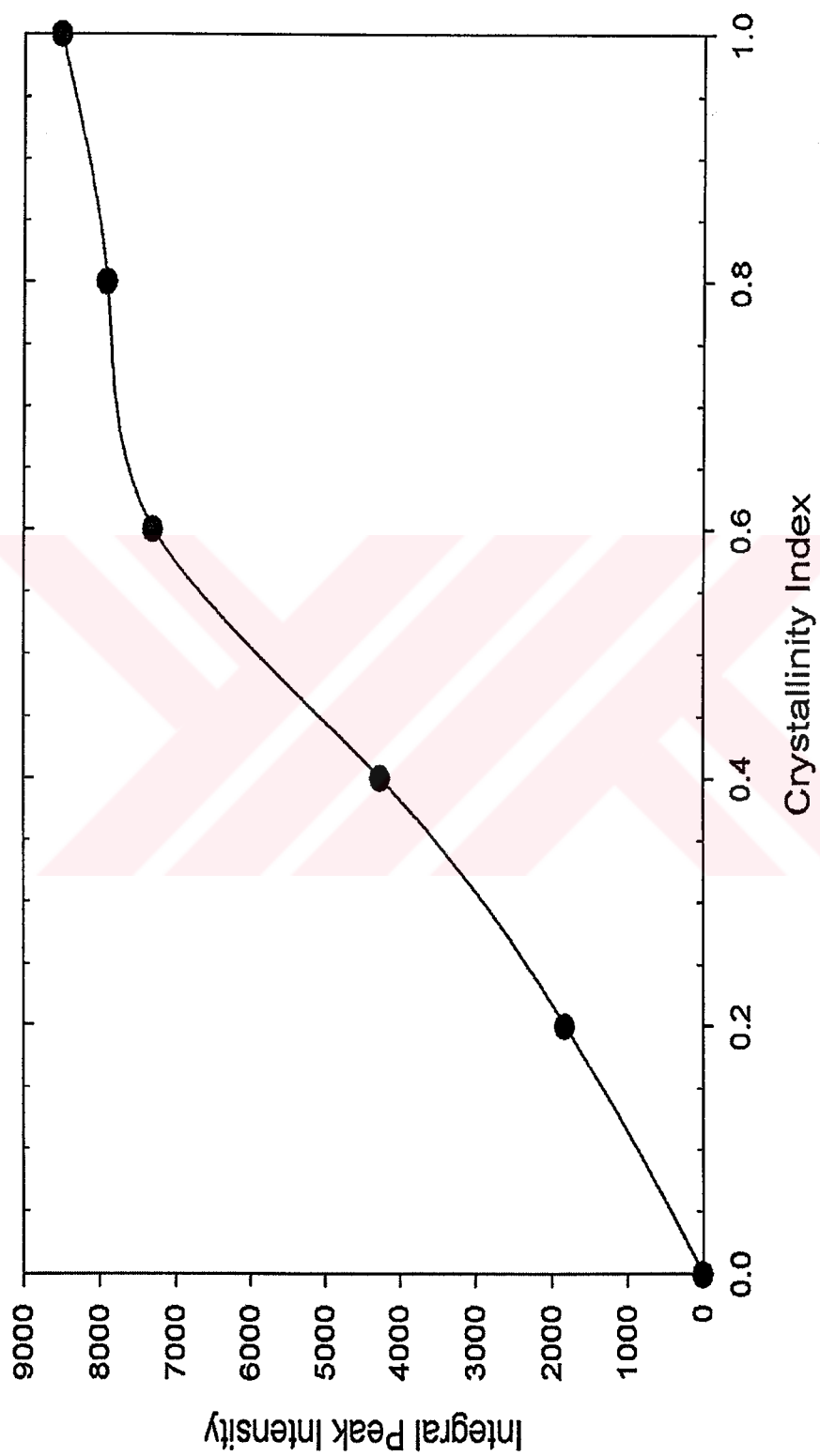


Figure C.4: Crystallinity Index versus Integrated Peak Intensities for Basic Sodalite
The peaks used for integrated intensities are marked with ●'s.

C.2 High Temperature Decomposition of Sodalites

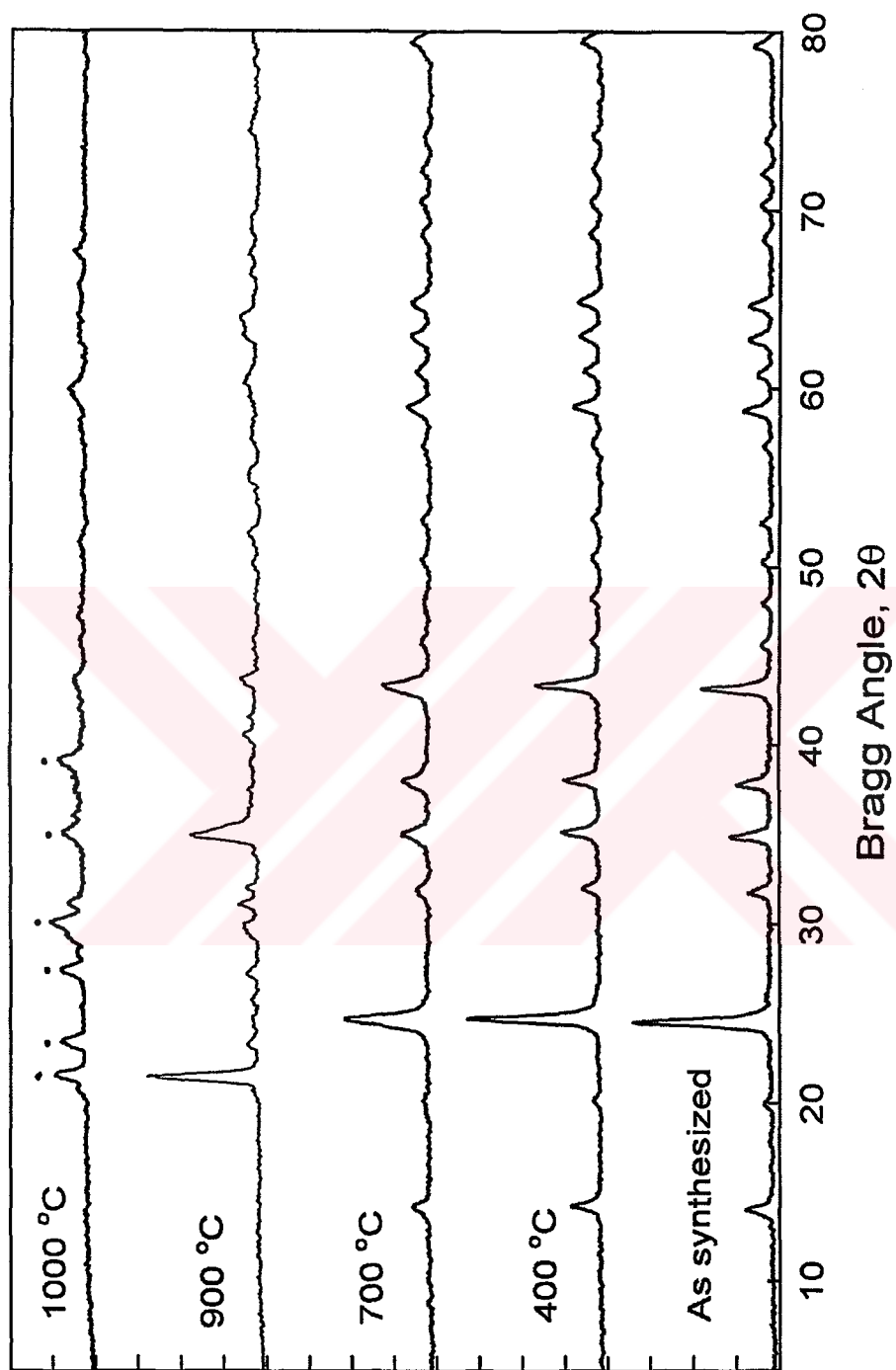


Figure C.5: High Temperature Decomposition Behavior of Chlorosodalite
Peaks indicating conversion into nepheline are marked with •'s.

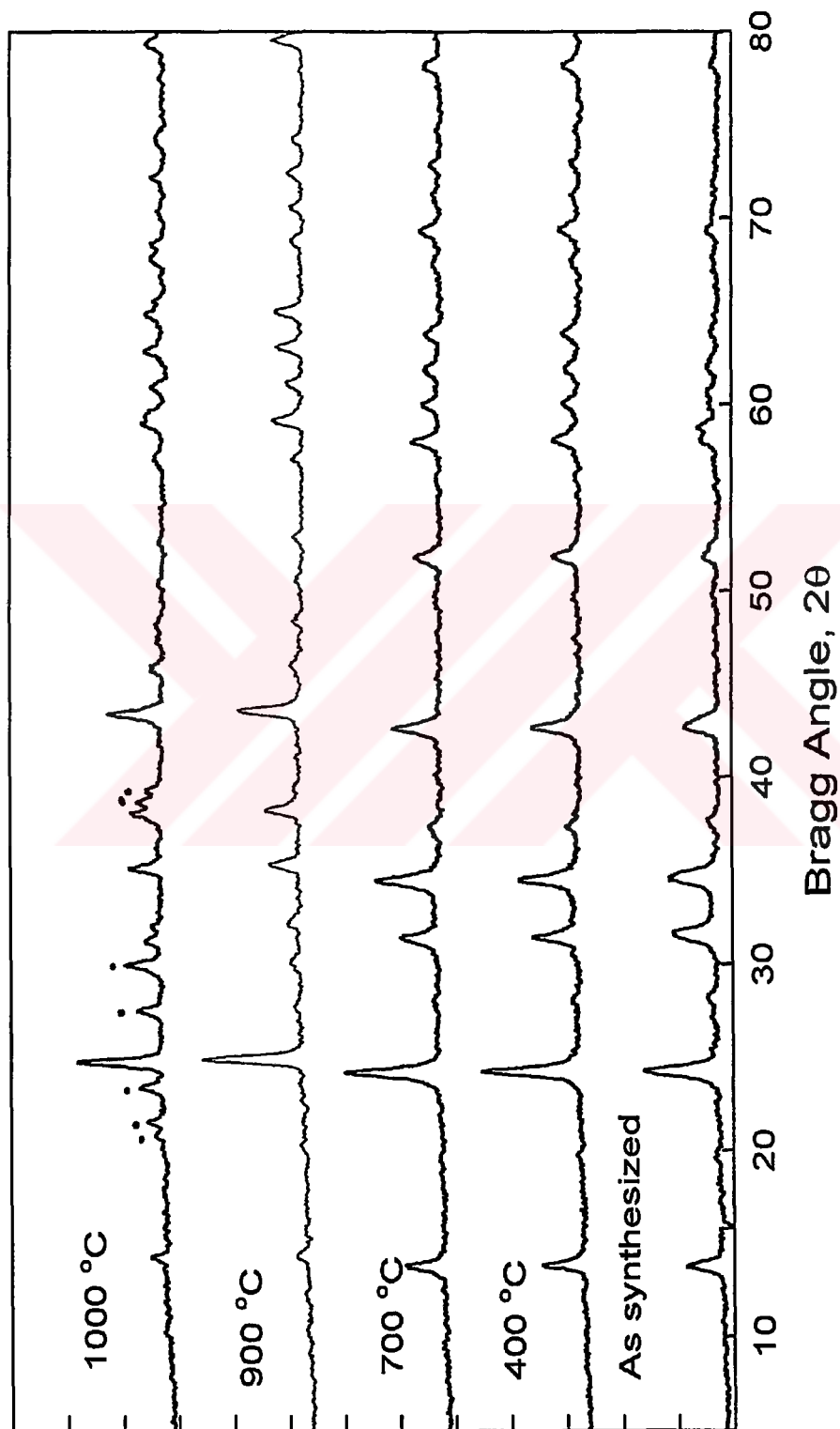


Figure C.6: High Temperature Decomposition Behavior of Basic Sodalite
 Peaks indicating conversion into nepheline are marked with •'s.

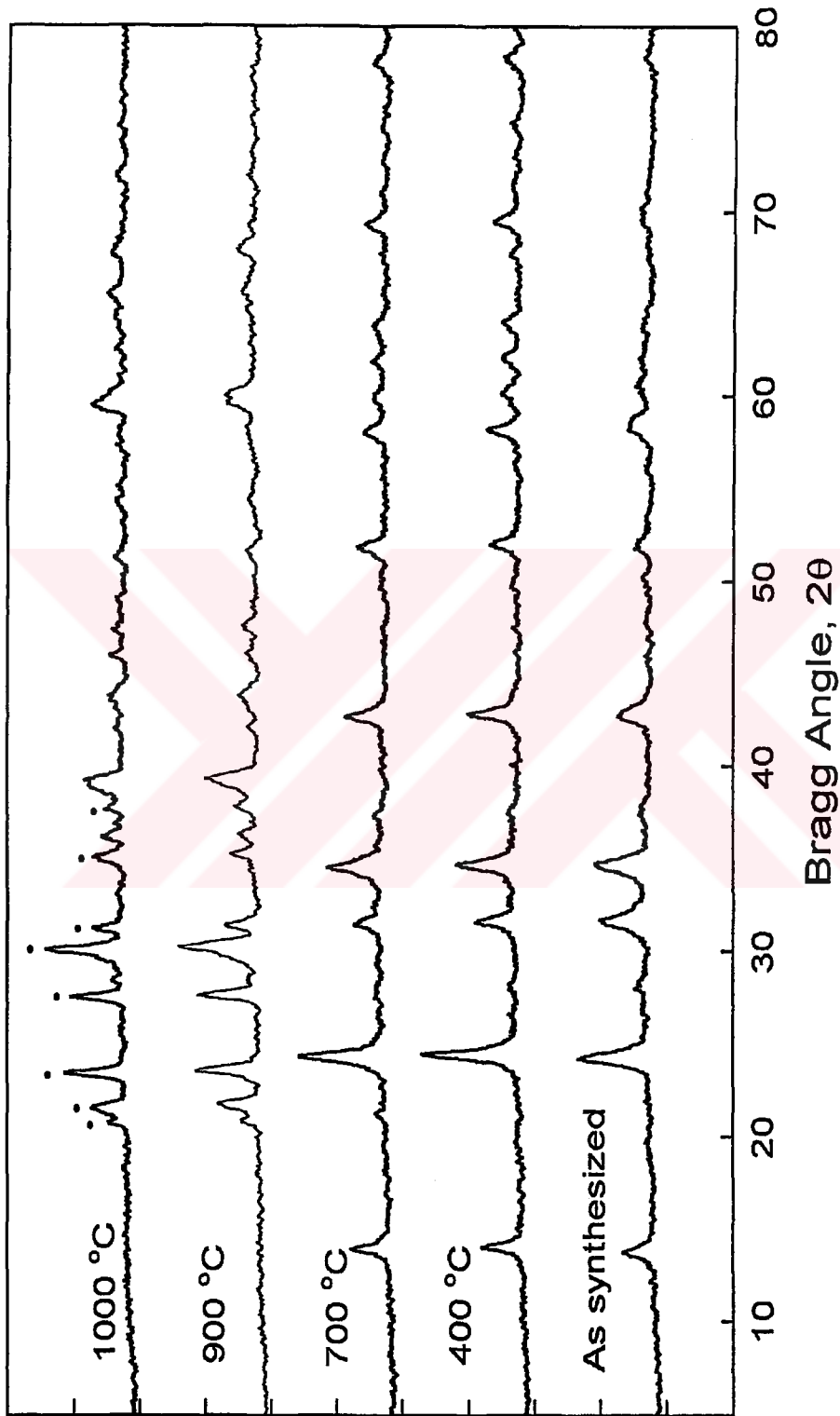


Figure C.7: High Temperature Decomposition Behavior of Oxalate Sodalite
 Peaks indicating conversion into nepheline are marked with •'s.

C.3 XRD Structure Determination

C.3.0.7 Calculation of Framework Oxygen Locations using Cell Edge

Derived equations for β -cages reported by Hassan and Grundy [4]:

$$\cos \varphi_{Si} = a/5.4020 - 0.7303 \quad (C.1)$$

$$\cos \varphi_{Al} = a/5.7420 - 0.6227 \quad (C.2)$$

$$x = \frac{1}{4} - 0.9863/a \quad y = \frac{1}{4} - 0.8938/a \quad (C.3)$$

$$z_{Si} = \frac{1}{2} - 1.3505(\sin \varphi_{Si}/a) \quad z_{Al} = \frac{1}{2} - 1.4355(\sin \varphi_{Al}/a) \quad (C.4)$$

where φ_{Al} and φ_{Si} are the Al and Si bond angles, z_{Al} and z_{Si} are the z coordinates of the oxygen atom with respect to Al or Si. x and y are the remaining coordinates of the oxygen atom and are fixed. φ_{Al} and φ_{Si} can be calculated from Eqns. C.1 and C.2 and substituted into Eqn. C.4. The values of z_{Al} and z_{Si} are generally similar and z is calculated from their mean.

Table C.1: Variation of Framework Oxygen Locations with Cell Edge

Unit Cell Edge (Å)	x	y	z	φ_{Si}	φ_{Al}	z_{Si}	z_{Al}
8.150	0.1290	0.1403	0.3948	0.679	0.649	0.3960	0.3935
8.200	0.1297	0.1410	0.3974	0.664	0.634	0.3985	0.3962
8.250	0.1304	0.1417	0.4000	0.649	0.620	0.4011	0.3989
8.300	0.1312	0.1423	0.4027	0.633	0.604	0.4037	0.4017
8.350	0.1319	0.1430	0.4054	0.617	0.589	0.4064	0.4045
8.400	0.1326	0.1436	0.4082	0.601	0.573	0.4091	0.4073
8.450	0.1333	0.1442	0.4110	0.585	0.557	0.4118	0.4102
8.500	0.1340	0.1448	0.4139	0.568	0.540	0.4146	0.4131
8.550	0.1346	0.1455	0.4168	0.550	0.523	0.4174	0.4161
8.600	0.1353	0.1461	0.4198	0.532	0.505	0.4203	0.4192
8.650	0.1360	0.1467	0.4228	0.514	0.487	0.4233	0.4223
8.700	0.1366	0.1473	0.4259	0.494	0.468	0.4263	0.4256
8.750	0.1373	0.1479	0.4292	0.475	0.448	0.4295	0.4289
8.800	0.1379	0.1484	0.4325	0.454	0.428	0.4327	0.4323
8.850	0.1386	0.1490	0.4360	0.432	0.406	0.4361	0.4359
8.900	0.1392	0.1496	0.4396	0.410	0.384	0.4396	0.4396
8.950	0.1398	0.1501	0.4434	0.386	0.360	0.4432	0.4435
9.000	0.1404	0.1507	0.4474	0.360	0.334	0.4471	0.4477
9.050	0.1410	0.1512	0.4517	0.333	0.306	0.4512	0.4521
9.100	0.1416	0.1518	0.4563	0.304	0.276	0.4556	0.4570
9.150	0.1422	0.1523	0.4614	0.271	0.242	0.4605	0.4624
9.200	0.1428	0.1528	0.4673	0.234	0.203	0.4660	0.4686
9.250	0.1434	0.1534	0.4744	0.190	0.154	0.4724	0.4763
9.300	0.1439	0.1539	0.4844	0.132	0.078	0.4809	0.4879

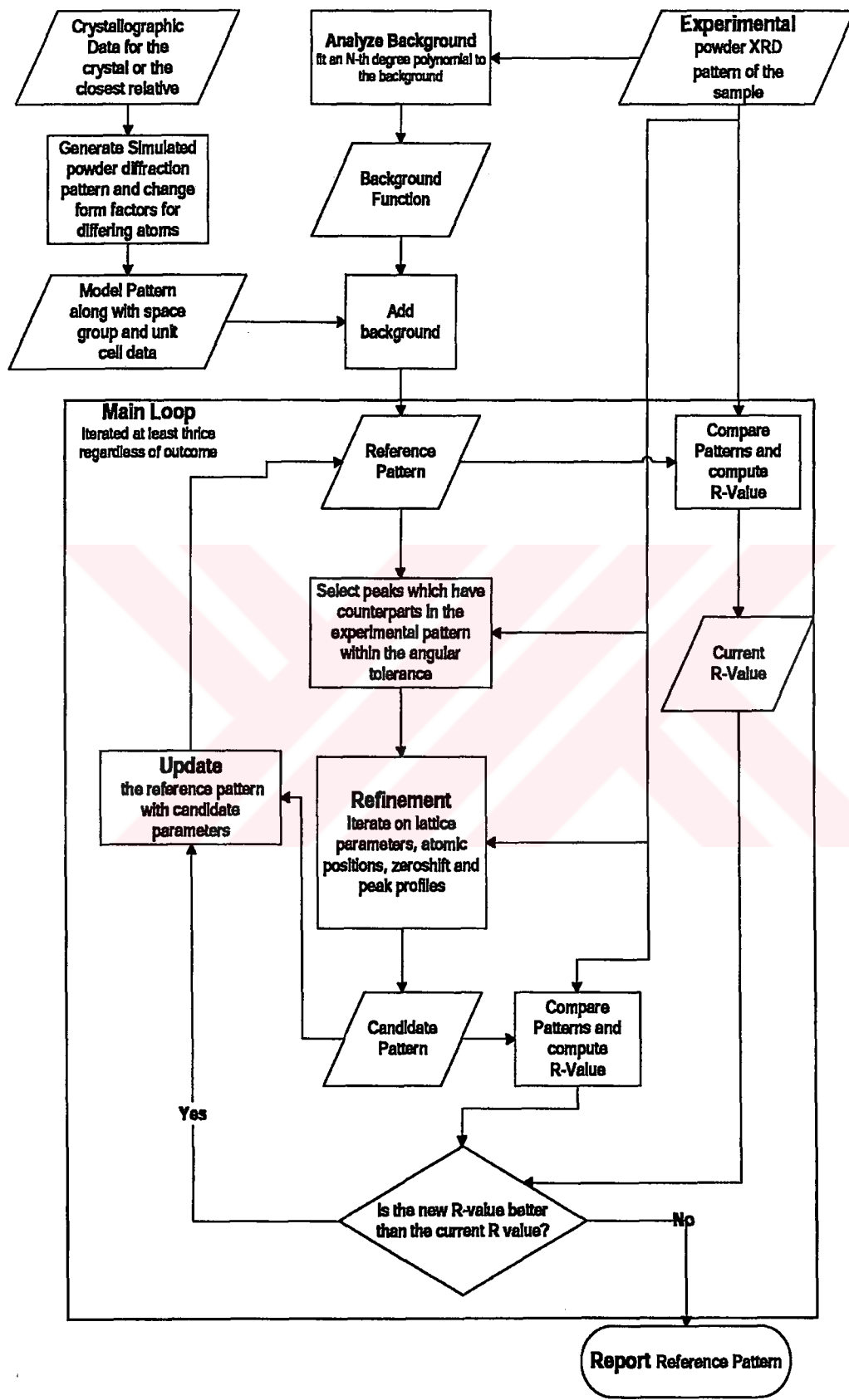


Figure C.8: Flowchart for Crystal Structure Determination Procedure

C.4 PDF Files

17-0476: QM:Star d:Diffractionmeter I:Diffractionmeter																			
Sodalite fas Al6 Si6 O24 Cl2		Specimen from Frazer Quarry, Tory Hill, Ontario, Canada. Blue. Microprobe analysis, average of twelve [wt %]: Na2 O 24.9, Al2 O3 31.7, Si O2 37.3, Cl 7.0. Unit cell refinements were carried out using a version of the least-squares procedure of Appleman and Evans (1973). To replace 20-1070.																	
Radiation: CuKα Calibration: Internal(Si) Ref: Keller, L., Rask, J., Buseck, P., Arizona State University, Tempe, Arizona, C:\JADK\PDF\JD-PDF.COM missing! (1986)		Lambda: 1.54178 Filter: Graph d-Cutoff: I/Ic(RIR):																	
System: Cubic() Cell Parameters= Ref: Ibid.		a= 8.878 8.878 8.878 b= 90.00 90.00 90.00 c= 90.00 Z= 1 mp=																	
Dx= 2.300 Dm=		Mwt= 969.21 Vol(RC)= 699.85 P(30)=223.7(.0037,36)																	
ea=		nvB=																	
Ref:		ey= Sign: 2V=																	
79 Reflections. Radiation: CU_1.540598. Strong lines: 3.62/λ 6.28/4 2.09/2 2.56/2 2.37/2 2.81/1 4.44/1 1.57/1 1.44/1																			
#	d(Å)	I(fix)	I(var)	h	k	l	2-Theta	Theta	1/(2θ)	#	d(Å)	I(fix)	I(var)	h	k	l	2-Theta	Theta	1/(2θ)
1>	6.2800	40	23	1	1	0	14.091	7.046	0.07962	41>	1.1276	2	6	7	3	2	86.178	43.089	0.44342
2>	4.4400	5	4	2	0	0	19.962	9.991	0.11261	42>	1.1098	1	3	8	0	0	87.909	43.955	0.45053
3>	3.9700	1	1	2	2	0	22.376	11.188	0.12594	43>	1.1013	1	1	8	8	0	88.765	44.383	0.45401
4>	3.6240	100	100	2	2	2	24.544	12.272	0.13797	44>	1.0928	1	1	1	8	8	89.641	44.820	0.45754
5>	2.8070	8	10	3	1	0	31.855	15.927	0.17813	45>	1.0846	1	1	3	9	0	90.505	45.252	0.46100
6>	2.6770	1	1	3	3	1	33.446	16.723	0.18678	46>	1.0766	1	1	3	9	3	91.367	45.684	0.46443
7>	2.5630	16	22	3	2	2	34.981	17.490	0.19508	47>	1.0689	1	1	3	9	3	92.216	46.108	0.46777
8>	2.3730	16	24	3	2	2	37.884	18.942	0.21070	48>	1.0611	1	1	3	9	3	93.095	46.547	0.47121
9>	2.2190	1	1	4	4	0	40.625	20.312	0.22533	49>	1.0463	1	1	4	6	6	94.820	47.410	0.47477
10>	2.0930	20	34	4	3	1	43.189	21.595	0.23889	50>	1.0321	1	1	4	6	6	96.549	48.274	0.48445
11>	1.9850	3	5	4	4	2	45.668	22.834	0.25189	51>	1.0252	1	1	4	6	6	97.417	48.709	0.48771
12>	1.8930	3	5	4	4	2	48.023	24.011	0.26413	52>	1.0184	1	1	4	6	6	98.292	49.146	0.49097
13>	1.8122	2	4	4	4	2	50.309	25.155	0.27591	53>	1.0118	1	1	4	6	6	99.161	49.580	0.49417
14>	1.7756	1	1	4	4	2	51.421	25.711	0.28159	54>	1.0052	1	1	4	6	6	100.048	50.024	0.49741
15>	1.7413	2	4	4	4	2	52.510	26.255	0.28714	55>	0.9927	1	1	4	6	6	101.785	50.892	0.50368
16>	1.6486	1	2	4	4	2	55.711	27.856	0.30329	56>	0.9865	1	1	4	6	6	102.675	51.338	0.50684
17>	1.6210	2	4	4	4	2	56.745	28.372	0.30845	57>	0.9805	1	1	4	6	6	103.556	51.778	0.50994
18>	1.5696	1	1	4	4	2	58.781	29.391	0.31855	58>	0.9687	1	1	4	6	6	105.346	52.673	0.51616
19>	1.5455	3	5	4	4	2	59.790	29.895	0.32352	59>	0.9630	1	1	4	6	6	106.240	53.120	0.51921
20>	1.5227	3	5	4	4	2	60.779	30.390	0.32836	60>	0.9574	1	1	4	6	6	107.138	53.569	0.52225
21>	1.5006	1	2	4	4	2	61.771	30.886	0.33320	61>	0.9464	1	1	4	6	6	108.962	54.481	0.52832
22>	1.4797	1	1	4	4	2	62.742	31.371	0.33791	62>	0.9411	1	1	4	6	6	109.872	54.936	0.53129
23>	1.4404	5	12	4	4	2	64.658	32.329	0.34713	63>	0.9359	1	1	4	6	6	110.784	55.392	0.53425
24>	1.4038	1	1	4	4	2	66.559	33.280	0.35618	64>	0.9307	1	1	4	6	6	111.717	55.859	0.53723
25>	1.3865	1	1	4	4	2	67.500	33.750	0.36062	65>	0.9257	1	1	4	6	6	114.537	57.268	0.54603
26>	1.3699	2	2	4	4	2	68.430	34.215	0.36499	66>	0.9062	1	1	4	6	6	116.430	58.215	0.55175
27>	1.3540	1	1	4	4	2	69.348	34.674	0.36928	67>	0.8968	1	1	4	6	6	118.396	59.198	0.55754
28>	1.3385	1	1	4	4	2	70.268	35.134	0.37355	68>	0.8923	1	1	4	6	6	119.372	59.686	0.56035
29>	1.3236	1	1	4	4	2	71.179	35.589	0.37776	69>	0.8791	1	1	4	6	6	122.383	61.192	0.56876
30>	1.3091	2	2	4	4	2	72.090	36.045	0.38194	70>	0.8664	1	1	4	6	6	125.516	62.758	0.57710
31>	1.2814	1	1	4	4	2	73.903	36.951	0.39020	71>	0.8624	1	1	4	6	6	126.557	63.279	0.57978
32>	1.2684	1	1	4	4	2	74.789	37.395	0.39420	72>	0.8583	1	1	4	6	6	127.655	63.828	0.58255
33>	1.2555	1	1	4	4	2	75.692	37.846	0.39825	73>	0.8543	1	1	4	6	6	128.758	64.379	0.58527
34>	1.2311	1	1	4	4	2	77.467	38.734	0.40614	74>	0.8504	1	1	4	6	6	129.865	64.932	0.58796
35>	1.2196	1	1	4	4	2	78.336	39.168	0.40997	75>	0.8466	1	1	4	6	6	130.976	65.488	0.59060
36>	1.2081	3	3	4	4	2	79.228	39.614	0.41387	76>	0.8315	1	1	4	6	6	135.760	67.880	0.60132
37>	1.1863	1	1	4	4	2	80.982	40.491	0.42148	77>	0.8279	1	1	4	6	6	137.002	68.501	0.60394
38>	1.1658	1	1	4	4	2	82.714	41.357	0.42889	78>	0.8243	1	1	4	6	6	138.291	69.146	0.60658
39>	1.1559	1	1	4	4	2	83.581	41.790	0.43256	79>	0.8208	1	1	4	6	6	139.593	69.797	0.60916
40>	1.1367	1	1	4	4	2	85.323	42.661	0.43987										

Figure C.9: PDF File for Sodium Chlorosodalite

42-0215: QM:Star g:Gunnar 1:Densitometer Reading

Sodium Aluminum Silicate Hydroxide Hydrate
Na8 [Al Si O4] 6 (O H) 2 12 H2 O

Radiation : CuKα1
Calibration: Internal (Si)
Ref: Sieger, P., Wiesecke, M., Engelhardt, G., Feische, J., Universität Konstanz, C:\JADG\PDF\JD-PDF.CDN missing! (1991)
Filter: I/ICRIR

System: Cubic() S.G.: P-43n (218)
Cell Parameters= 8.888 8.888 8.888 90.00 90.00 90.00 Z= 1
Ref: Hassan, I., Grundy, H. mp=
C:\JADG\PDF\JD-PDF.CDN missing!, 39 3 (1983)
Dx= 2.230 Dm= Nwt= 968.35 Vol(RC)= 703.12 F(30)=47.1 (.0130,49)

sa= nwb= ey= Sign: 2V=
Ref:

White, Hydrothermal from kaolinite in concentrated sodium hydroxide solution, 1.0 g kaolinite + 8 ml 16M NaOH in 10 ml Teflon coated steel autoclaves at 200 C under autogeneous pressure for 14 days, little washing. Pattern taken at room temperature. zeolite.

36 Reflections. Radiation: Cu1.540598. Strong Lines: 3.63/X 2.57/9 2.10/8 2.81/8 1.52/7 6.29/6 1.74/6 1.57/5 1.21/5										
#	d(A)	I(fix)	I(var)	h	k	l	2-Theta	Theta	1/(2θ)	1/(2θ)
1>	6.2850	58	21	1	1	0	7.040	32.314	0.4698	
2>	4.4440	5	2	2	0	0	9.982	33.247	0.35587	
3>	3.9750	2	1	2	1	0	11.174	34.184	0.35470	
4>	3.6290	100	62	2	1	1	12.255	35.089	0.37313	
5>	3.1420	78	14	2	2	0	14.191	36.016	0.38168	
6>	2.8100	78	63	3	1	0	15.910	36.898	0.38971	
7>	2.5660	87	77	2	2	2	17.469	37.793	0.39777	
8>	2.1770	42	40	3	2	1	18.925	38.700	0.40584	
9>	2.0950	83	90	3	3	0	21.573	39.579	0.41356	
10>	1.9870	11	12	4	2	0	22.810	40.421	0.42038	
11>	1.8930	5	6	3	3	2	23.985	41.305	0.42845	
12>	1.8140	37	46	4	2	2	25.128	43.022	0.44287	
13>	1.7430	58	75	5	1	0	26.228	43.895	0.45005	
14>	1.6500	2	2	5	2	1	27.830	44.758	0.45704	
15>	1.6220	7	9	5	2	1	28.353	45.607	0.46382	
16>	1.5710	47	68	4	4	0	29.362	47.368	0.47735	
17>	1.5240	67	100	5	3	0	30.361	48.219	0.48403	
18>	1.4810	33	50	6	0	0	31.340	49.107	0.49068	

Figure C.10: PDF File for Sodium Basic Sodalite

C.5 Peak Listings

Table C.2: Peak Listing for Silver Chlorosodalite

Radiation: $\text{CuK}\alpha$ System: Cubic Space Group: $\text{P}\bar{4}3\text{n}$ (218)

$a = 8.872 \text{ \AA}$ $b = 8.872 \text{ \AA}$ $c = 8.872 \text{ \AA}$

$\alpha = 90.00^\circ$ $\beta = 90.00^\circ$ $\gamma = 90.00^\circ$

51 Reflections

H	K	L	$2\theta/^\circ$	$d/\text{\AA}$	I(rel)	F(hkl)	μ	FWHM
1	1	0	14.106	6.2734	1	27.92	12	0.4382
2	0	0	20	4.43597	4	83.14	6	0.4109
2	1	0	22.39	3.96765	0	10.01	24	0.4036
2	1	1	24.558	3.62195	100	232.62	24	0.3991
2	2	0	28.432	3.1367	2	51.04	12	0.3964
3	1	0	31.872	2.80555	40	170.66	24	0.4001
2	2	2	35.007	2.56111	11	164.84	8	0.4086
3	2	0	36.486	2.46063	0	2.23	24	0.4143
3	2	1	37.915	2.37112	30	115.38	48	0.4208
4	0	0	40.644	2.21798	2	92	6	0.436
4	1	0	41.953	2.15176	0	2.87	24	0.4444
4	1	1	43.23	2.09113	45	219.97	24	0.4534
3	3	0	43.23	2.09113	52	333.38	12	0.4534
4	2	0	45.696	1.98382	11	110.89	24	0.4728
4	2	1	46.891	1.93601	0	2.76	48	0.4831
3	3	2	48.063	1.8915	4	70.04	24	0.4938
4	2	2	50.346	1.81098	28	189.64	24	0.5161
4	3	0	51.459	1.77439	0	2.35	24	0.5276
4	3	1	52.555	1.73993	3	45.26	48	0.5395
5	1	0	52.555	1.73993	3	61.77	24	0.5395
5	2	0	55.752	1.64748	0	4.66	24	0.5764
4	3	2	55.752	1.64748	0	8.39	48	0.5764
5	2	1	56.791	1.61979	26	140.32	48	0.5892
4	4	0	58.833	1.56835	13	201.73	12	0.6154
4	3	3	60.831	1.52152	15	158.08	24	0.6423
5	3	0	60.831	1.52152	11	136.46	24	0.6423
5	3	1	61.816	1.49963	0	5.65	48	0.656
6	0	0	62.791	1.47866	14	309.08	6	0.67
4	4	2	62.791	1.47866	19	181.48	24	0.67
6	1	0	63.759	1.45854	0	5.99	24	0.6841
6	1	1	64.718	1.43922	4	84.7	24	0.6983
5	3	2	64.718	1.43922	14	111.09	48	0.6983
6	2	0	66.614	1.40278	7	116.43	24	0.7275
6	2	1	67.552	1.38556	0	4.24	48	0.7423
5	4	0	67.552	1.38556	0	2.91	24	0.7423
5	4	1	68.483	1.36897	31	175.2	48	0.7573
6	2	2	70.329	1.33749	0	20.67	24	0.7878
6	3	0	71.244	1.32255	0	2.23	24	0.8034
5	4	2	71.244	1.32255	0	5.21	48	0.8034
6	3	1	72.154	1.3081	3	54.13	48	0.8192
4	4	4	73.96	1.28055	5	173.07	8	0.8513
6	3	2	74.857	1.26742	0	1.35	48	0.8676
5	5	0	75.75	1.25468	0	37.95	12	0.8842
7	1	0	75.75	1.25468	1	52.77	24	0.8842
5	4	3	75.75	1.25468	3	52.3	48	0.8842
6	4	0	77.526	1.23032	2	67.05	24	0.918
7	2	0	78.409	1.21865	0	2.15	24	0.9352
6	4	1	78.409	1.21865	0	5.92	48	0.9352
5	5	2	79.289	1.20732	4	90.42	24	0.9527
6	3	3	79.289	1.20732	29	257.8	24	0.9527
7	2	1	79.289	1.20732	20	148.69	48	0.9527

Table C.3: Peak Listing for Silver Basic Sodalite

Radiation: $\text{CuK}\alpha$ System: Cubic Space Group: $\text{P}\bar{4}3\text{n}$ (218)

$a = 8.956 \text{ \AA}$ $b = 8.956 \text{ \AA}$ $c = 8.956 \text{ \AA}$

$\alpha = 90.00^\circ$ $\beta = 90.00^\circ$ $\gamma = 90.00^\circ$

51 Reflections

H	K	L	$2\theta/^\circ$	d/ \AA	I(rel)	F(hkl)	μ	FWHM
1	1	0	13.895	6.36832	8	56	12	1.3066
2	0	0	19.699	4.50308	11	109.2	6	1.1309
2	1	0	22.052	4.02768	0	7.6	24	1.0608
2	1	1	24.187	3.67675	42	119.1	24	0.998
2	2	0	27.999	3.18416	4	57.4	12	0.8885
3	1	0	31.384	2.848	100	213.9	24	0.7956
2	2	2	34.469	2.59986	71	329.7	8	0.7166
3	2	0	35.924	2.49786	0	1.5	24	0.6819
3	2	1	37.329	2.407	30	91.8	48	0.6505
4	0	0	40.012	2.25154	0	6.7	6	0.5975
4	1	0	41.299	2.18432	0	1.2	24	0.5762
4	1	1	42.554	2.12277	60	200.5	24	0.5585
3	3	0	42.554	2.12277	36	218.8	12	0.5585
4	2	0	44.978	2.01384	1	21.8	24	0.5343
4	2	1	46.152	1.96531	0	1.3	48	0.528
3	3	2	47.303	1.92012	3	51.4	24	0.5256
4	2	2	49.544	1.83638	7	73	24	0.532
4	3	0	50.637	1.80123	0	2.8	24	0.5405
4	3	1	51.713	1.76625	7	55.3	48	0.5523
5	1	0	51.713	1.76625	7	76.9	24	0.5523
5	2	0	54.851	1.6724	0	13	24	0.6045
4	3	2	54.851	1.6724	1	22.5	48	0.6045
5	2	1	55.87	1.64429	4	41.8	48	0.6267
4	4	0	57.872	1.59208	26	229.4	12	0.6768
4	3	3	59.831	1.54455	7	85.9	24	0.7332
5	3	0	59.831	1.54455	26	166.1	24	0.7332
5	3	1	60.796	1.52232	0	8.1	48	0.7634
6	0	0	61.752	1.50103	7	175.2	6	0.7947
4	4	2	61.752	1.50103	17	136.4	24	0.7947
6	1	0	62.699	1.48061	0	6.6	24	0.827
6	1	1	63.639	1.46099	3	60	24	0.8603
5	3	2	63.639	1.46099	37	144.6	48	0.8603
6	2	0	65.495	1.424	4	67.8	24	0.9293
6	2	1	66.413	1.40653	0	2.8	48	0.965
5	4	0	66.413	1.40653	0	1.9	24	0.965
5	4	1	67.325	1.38968	12	83.8	48	1.0013
6	2	2	69.13	1.35773	5	80.4	24	1.0759
6	3	0	70.025	1.34256	0	1.3	24	1.1142
5	4	2	70.025	1.34256	0	2.9	48	1.1142
6	3	1	70.914	1.32789	2	39.4	48	1.153
4	4	4	72.679	1.29993	22	297.6	8	1.2323
6	3	2	73.555	1.2866	0	1.6	48	1.2728
5	5	0	74.427	1.27366	4	104.5	12	1.3138
7	1	0	74.427	1.27366	1	30.5	24	1.3138
5	4	3	74.427	1.27366	0	16.9	48	1.3138
6	4	0	76.161	1.24893	0	6.8	24	1.3976
7	2	0	77.023	1.23709	0	1.8	24	1.4403
6	4	1	77.023	1.23709	0	8.3	48	1.4403
5	5	2	77.881	1.22558	1	39	24	1.4835
6	3	3	77.881	1.22558	25	189.5	24	1.4835
7	2	1	77.881	1.22558	30	147.1	48	1.4835

UNIVERSITÄT WÜRZBURG
 INSTITUT FÜR ANORGANISCHE CHEMIE
 UNIVERSITÄT WÜRZBURG